A THESIS SUBMITTED IN FULFILLMENT OF THE REQUIREMENTS FOR THE DEGREE MAGISTER SCIENTIAE IN THE DEPARTMENT OF EARTH SCIENCE, UNIVERSITY OF THE WESTERN CAPE

Geological modeling of the offshore Orange Basin, west coast of South Africa

CURNELL CAMPHER
EARTH SCIENCE DEPARTMENT
UNIVERSITY OF THE WESTERN CAPE

SUPERVISOR: R. DOMONEY

CO-SUPERVISORS: G. KUHLMANN
R. DI PRIMIO
D. VAN DER SPUY

2009

ABSTRACT

Separation between the South American and African plate's occurred along the present day Atlantic margin during the Middle to Late Jurassic leading to the formation of a passive margin along the west coast of Southern Africa. The margin then later developed into the large Orange Basin flanking the west coasts of South Africa and Namibia. The Orange Basin on the west coast of South Africa covers an area of roughly 130 000 square kilometers relevant to the 200 m isobath and has roughly one well drilled for every 4000 square kilometers. The basin has proven hydrocarbon reserves and potential for further discoveries. The study area is located within South African exploration licencing blocks 3A/4A and 3B/4B and covers a region of roughly 97 km by 150 km. The study aims at understanding the geological processes responsible for the formation of the Orange Basin with a focus on the evolution of source rock maturity. The methodology involved utilizing the Petrel software for seismic interpretation and well correlation utilising two-dimensional seismic data and all the relevant well data including geological well logs, petrophysical well logs, well top data, check-shot data, borehole temperature data and geochemical well data such as Rock Eval and vitrinite reflectance data. PetroMod (IES, Version 10) was utilized to simulate the Orange Basin evolution and the affect on source rock maturity.

Seismic interpretation of the Post-Hauterivian succession shows a relative thickening of the sedimentary sequence westward as the basin evolves from the early drift to complete drift phase. Results from the petroleum system modeling indicate that the Barremian - Early Aptian source rock is at present overmature and producing mostly gas in the shelf areas whereas the potential for oil are most likely present in the deep water area of the basin where Tertiary progradation has resulted in renewed petroleum generation. Petroleum system modeling results indicate that the younger Cenomanian - Turonian source rock is less mature than the older Barremian - Early Aptian source rock as indicated by a lower transformation ratio and is mainly producing oil.

DECLARATION

I declare that "*Geological modeling of the offshore Orange Basin, west coast of South Africa*" is my own work, that it has not been submitted before for any degree or examination at any other university, and that all the sources I have used or quoted have been indicated and acknowledged as complete references.

Curnell John Campher October 2009

Signed: . . . . . .

ACKNOWLEDGEMENT

I hereby take the opportunity to thank everyone who has been involved in this project particularly the organisers of the Inkaba Ye Afrika initiative without whom this project would not have been possible. I would like to thank my supervisors and co-supervisor namely Dr. Geza Kuhlman and Dr. Rolando di Primio who assisted in helping to set up the basin model at the GeoForschungZentrum (GFZ) in Germany as well as Dave van der Spuy from the Petroleum Agency of South Africa and Reginald Domoney from the University of the Western Cape for his support throughout the study.

TABLE OF CONTENTS

LIST OF FIGURES

LIST OF TABLES

CHAPTER ONE

1. INTRODUCTION

1.1 THESIS OUTLINE

This thesis was put together with the aim of predicting the degree of maturity of two identified Cretaceous source rocks, within a south central study area covering a region of roughly 97 kilometers by 150 kilometers within the Orange Basin. The study utilizes key geological principals including seismic interpretation, petrophysical well log correlation and petroleum system modeling to determine the evolution of the Orange Basin post rift source rocks. The thesis is divided into six chapters each concerned with different aspects of the study.

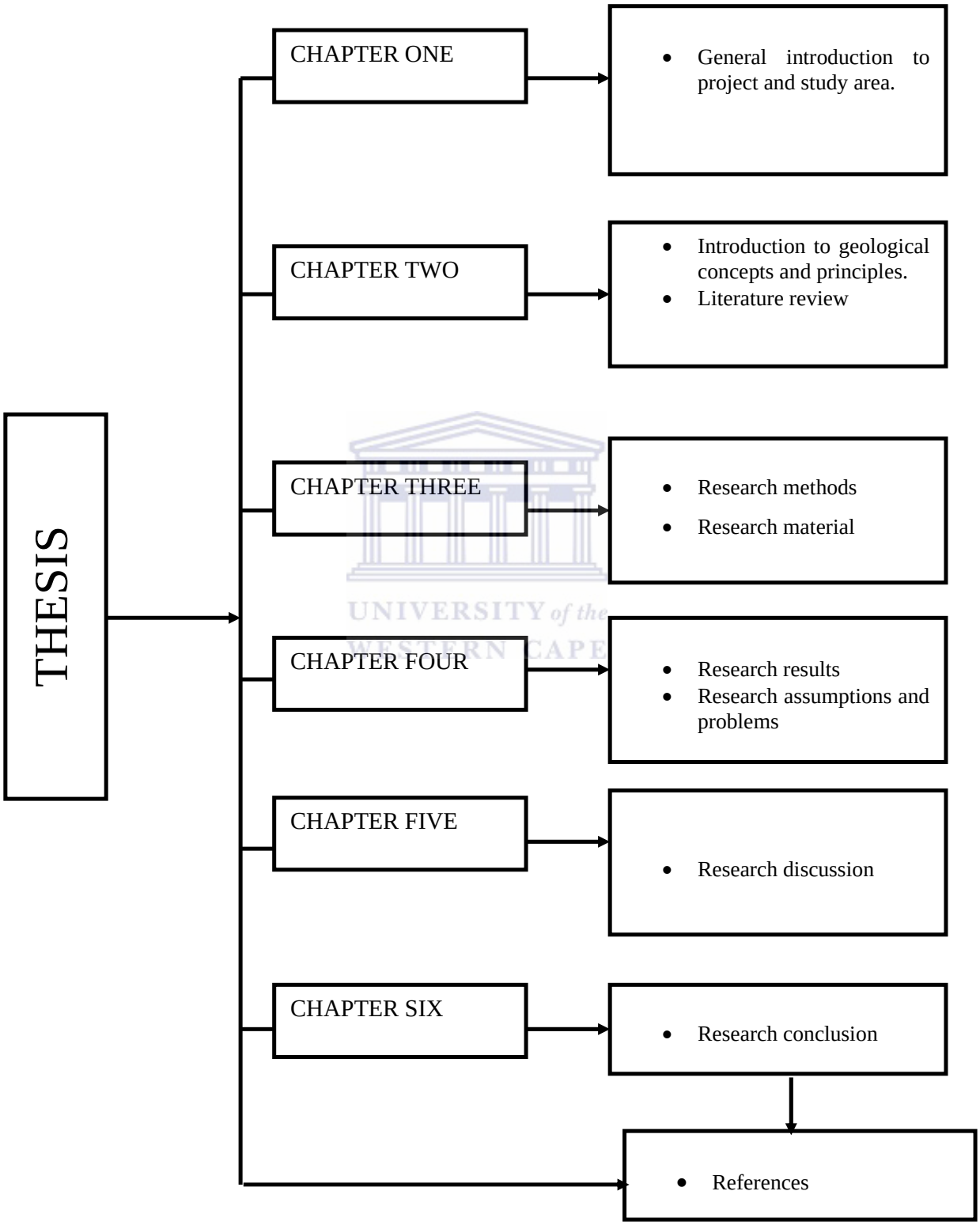

1.2 STUDY AREA

The study area is situated in the South African section of the offshore Orange Basin off the west coast of South Africa (Figure 1A) and has an aerial extent of 97 Kilometres by 150 kilometres, which includes part of the petroleum licence blocks 3A/4A and 3B/4B (Figure 1B). The area was chosen to assess the source rock maturity of the northern Orange basin in the South African section of the basin. The study makes use of thirty two 2-Dimensional seismic lines and five wells (A-A1, A-L1, A-I1 K-F1 and K-H1) (Figure 2).

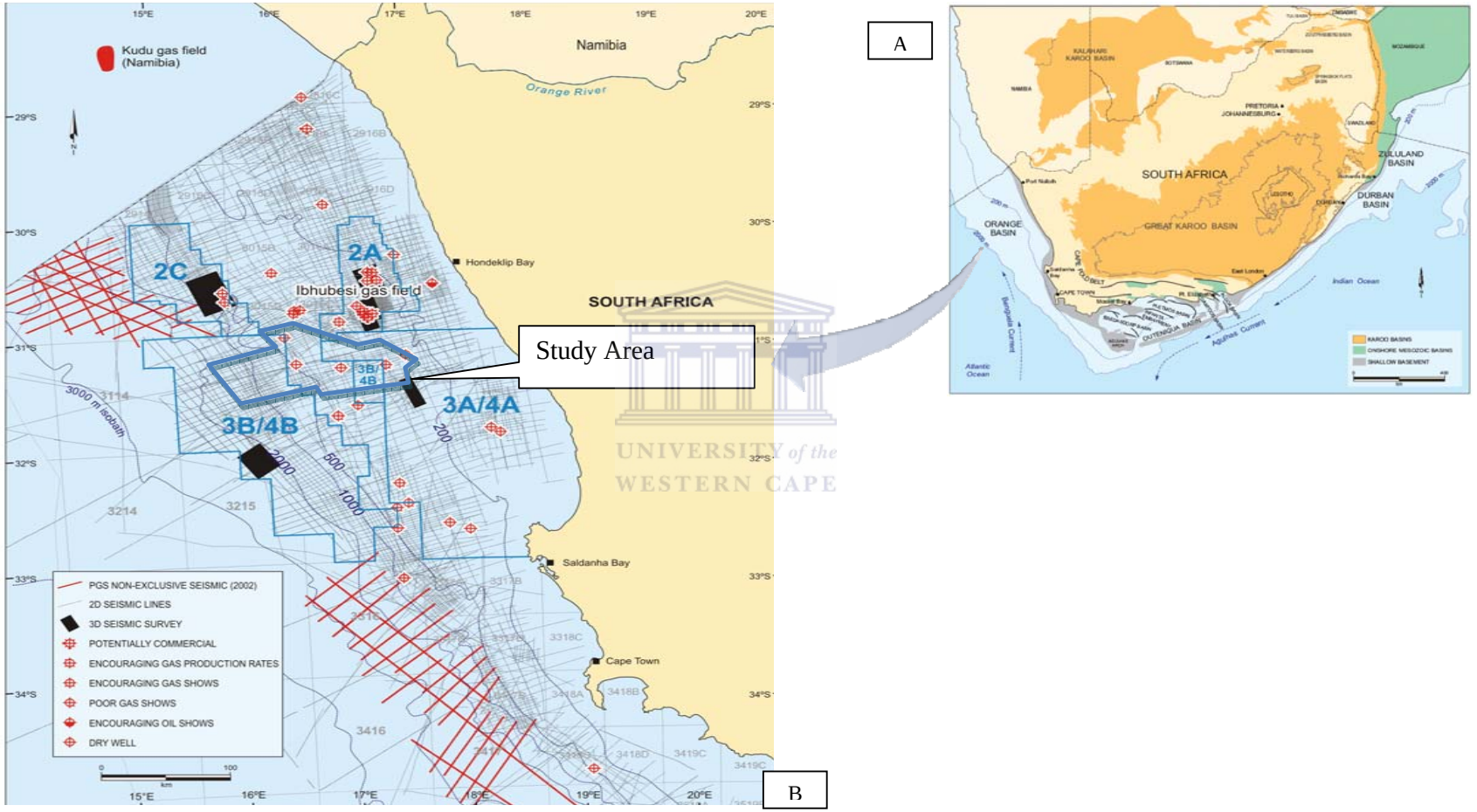

Figure 1. (A) Location of the Orange Basin (B) Location of the study area, South African petroleum licence blocks, well locations and seismic coverage of the Orange Basin. Promotional pamphlet, Petroleum Agency SA, 2007, Petroleum Exploration Information and Opportunities Brochure Figure 1A and 1B.

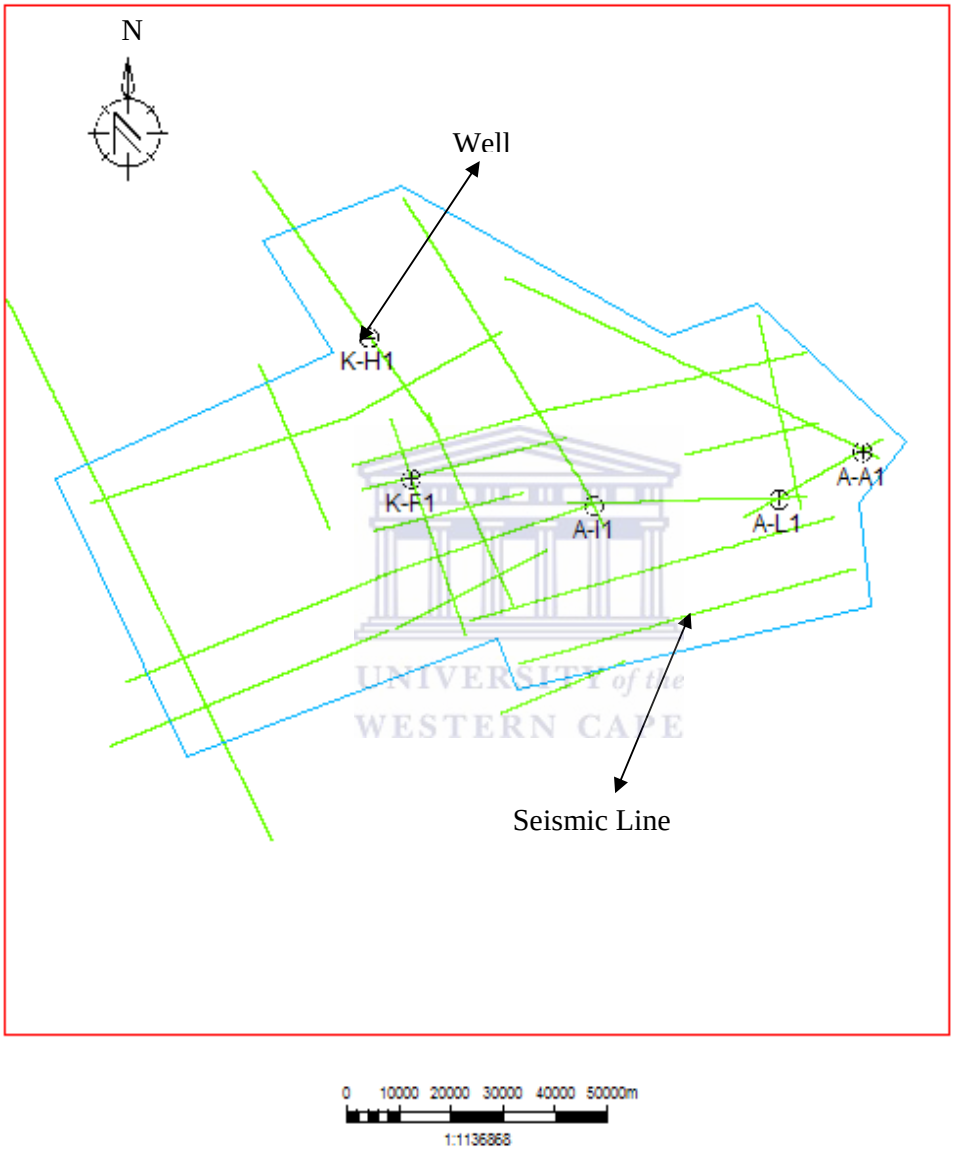

Figure 2. Map showing a close up view of the study area indicating the location of all the wells in black and 2D seismic lines in green.

1.3 DEVELOPING THE RESEARCH IDEA

It is postulated by various researchers including (Barton et al., 1993, Muntingh, 1993, Jungslager, 1999, van der Spuy, 2003) that there is potential for oil discoveries in the deep-water areas of the Orange Basin beyond the present day shelf area. This hypothesis is based on the perception that source rocks in the deeper areas are of much better quality than those on the shelf due to the deposition of predominantly marine organic matter with decreasing terrestrial influence. It is also hypothesised that these deepwater areas of interest are presently in the oil window. Substantiating this hypothesis led to the initiative of studying the maturity of the Orange Basin source rocks. This study was accomplished through a project within a joint venture between geological institutions of both South Africa and Germany referred to as the Inkaba Ye Africa project.

The Inkaba Ye Africa project aims to trace the geological history related to Southern Africa. The project is divided into three themes namely Heart of Africa, Margins of Africa and Living Africa. These three themes are further subdivided into various subprojects. This specific study is related to the theme “Living Africa” and contributes to the goal of linking sedimentation histories to tectonic evolution and the subsequent hydrocarbon generation potential.

1.4 AIMS AND OBJECTIVES

The research aims at understanding the various geological processes responsible for the formation of the Orange Basin with a focus on the maturity evolution of two post-rift source rocks in the Orange Basin. Understanding these geological processes and their influence on source rock maturity was accomplished though the construction of a geological model of the Orange Basin with the primary purpose of reconstructing the geological history including the basin formation, heat-flow regimes over time, sequence stratigraphy, depositional regimes and the subsequent maturity evolution of two identified post-rift source rocks in the Orange Basin. These include a Barremian - Early Aptian source rock found above the 13At1 unconformity (Figure 4). The second source rock under investigation includes the postulated Cenomanian - Turonian source rock developed above the 15At1 unconformity (Figure 4) (Barton et al., 1993).

The geological model is subdivided into two models: the geomodel concerned with constructing the basin architecture and sedimentation history, and the petroleum systems model concerned with determining the maturity history of post-rift source rocks of the Orange Basin. The steps followed to construct the first model were seismic interpretation of two-dimensional seismic data and the correlation of petrophysical wireline logs using Petrel software. The second model was constructed by integrating individual petroleum system elements using PetroMod (IES, Version 10) to calculate the evolution of the two source rocks in the Orange Basin.

1.5 GEOLOGICAL BACKGROUND

The break up of the Gondwana supercontinent can be described as the single greatest geological event affecting the southern hemisphere (Watkeys, 2006). This break-up event played a significant role in controlling the rift geometry and subsequent shape of the present continents as the development of the Indian and Atlantic oceans occurred. The break-up process includes various geological events that have been subdivided by Watkeys (2006) into five stages (Figure 3):

1. Stage one is marked by rifting but no real continental separation at the time of the Karoo volcanism between 180 and 175 Ma.

2. Stage two (175 – 155 Ma) marks a period of microplate rotation caused by strike slip movement along the Gastre Fault-Falkland-Aghulas Fracture Zone (GFFAFZ) linking the (Gastre Fault System) GFS and the AFFZ Agulhas Falkland Fracture Zone and stretching from the proto-Pacific ocean to the Lebombo region.

3. Stage three (155 – 135 Ma) marks the splitting of Gondwana into an east and west Gondwana as strike slip movement occurred along an interconnected fracture system propagating across Gondwana via the Mozambique Basin and the Weddell Sea. As the now east and west Gondwana plates slid past each other movement occurred along the GFFAFZ, which may well have been responsible for the development of an incipient northward propagating rift system along the western coast of Southern Africa, recorded by the development of the Orange and Walvis Basins separated by the Luderitz arch (Dingle et al., 1983).

4. During stage four between 135 and 155 Ma the main event in terms of the separation of Africa and South America was the positioning of the incipient continental rift zone over the Tristan da Cunha plume that developed under the South American Parana Basin (Turner et al., 1994). The Tristan da Cunha plume now lying under this weaker crust intruded and broken through the crust initiating seafloor spreading and subsequent continental break-up between South America and Africa.

5. During the final stage between 155 and 90 Ma the final split in the South Atlantic involved a triple junction jump to the southern continental part of the Agulhas Plateau which was intruded by oceanic crust at about 93 Ma (Tucholke et al., 1981). It was this breakup between the continental crusts of Africa and South America that enabling the whole Atlantic Ocean to become linked (Fairhead, 1988) and therefore resulting in the final separation of the African and South American continents.

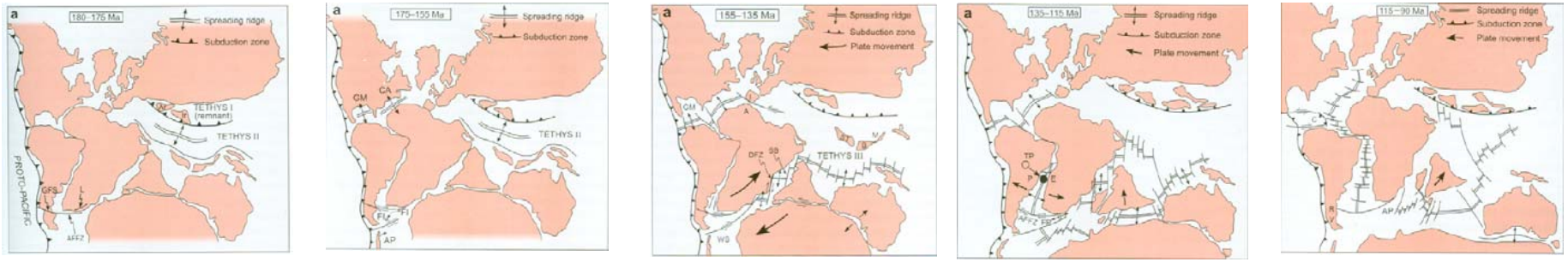

Stage 1 Stage 2 Stage 3 Stage 4 Stage 5

GONDWANA BREAK-UP

Stage one: AFFZ(Agulhas Falkland Fracture Zone); Ar(Armenian microplate); Ir(Iranian microplate; GFS(Gastre Fault System; L(Lebombo); AB(Agulhas Bank); AP(Agulhas Plateau); FI(Falkland Islands); MEB(Maurice Ewing Bank); MR(Mozambique Ridge); DML(Drönning Maud Land); EWM(Ellsworth Island). *Stage two*: AP(Antarctic Peninsula); CA(Central Atlantic); GM(Gulf of Mexico); FPB(Falkland Plateau Basin). *Stage three*: A(Atlas region); B(Burma); DFZ(Davies fracture Zone); I(Iberia); M(Malaya); S(Sumatra); SB(Somali Basin); ST(Southern Tibet microplate); WS(Weddel Sea); LA (Luderitz Arch); MCP(Mozambique coastal plain); OB(Orange River Basin); WB(Walvis Basin). *Stage four*: E(Etendeka Basalts); P(Parana Basalts); TP(Tristan Plume); NV(Natal Valley). Stage five: C(Caribbean); RV(Rocas Verdes).

GONDWANA BREAK-UP IN THE SOUTH AFRICAN PERSPECTIVE

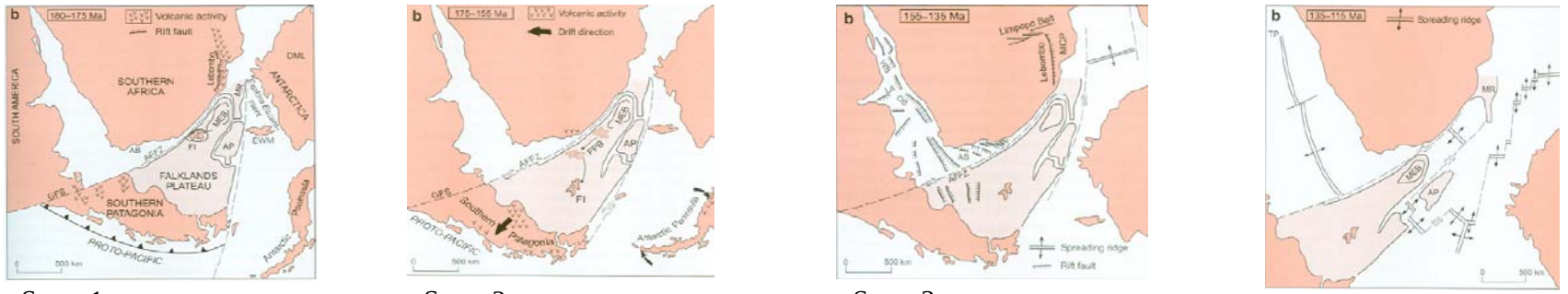

Stage 1 Stage 2 Stage 3 Stage 4

Figure 3. Tectonic plate reconstruction illustrating the break up process of Gondwana with reference to Southern Africa and the development of South Africa's western margin (modified from Watkeys, 2006).

Break-up around Southern Africa therefore first occurred along the eastern margin of South Africa during the Middle-Jurassic (Dingle et al., 1983). The dextral shear stress generated along the Agulhas Falkland Fracture Zone (AFFZ) resulted in the development of the Durban and Zululand rift basins along the east coast of South Africa. Through continued extension, coupled with the transform movement of the right-lateral strike-slip Agulhas Falkland Transform (Ben-Avraham et al., 1993), the offshore Outeniqua Basin on the south coast of South Africa was formed.

Pertinent to this specific study is the development of the western margin of Southern Africa referring to stage three and four of Watkeys (2006). The western margin of South Africa is classified as a rifted passive margin (Barton et al., 1993) which according to Bott, (1980) can be characterised by two main types of subsidence. An initial fault controlled graben subsidence followed by a second flexural downwarping subsidence expressed in four stages.

1. The first stage includes a rift valley stage, which is not necessarily always present with thermal uplift and subsequent graben formation before actual continental break-up.

2. Stage two is classified as a youthful stage lasting about 50 Ma after the initial splitting of the continents when the thermal effects of the split are strongly experienced in the form of pronounced thermal subsidence.

3. Stage three is classified as the mature stage and is characterised by passive development characteristic of the present Atlantic Margin.

4. The final stage is classified as “a fracture stage when subduction starts, terminating the history as a passive margin” (Bott, 1980).

The continental margin along the western coast of South Africa shares many of these characteristics mentioned above, such as initial rifting resulting in the formation of basement grabens and half-grabens, followed by a period of thermal sag as the deposition of the drift succession progressed.

The South African western continental margin includes a great part of the Orange Basin as defined by the extent and thickness of post-rift sedimentary succession. The basement graben and half-grabens underlying the Orange Basin are bounded by north-south striking normal faults that trend sub-parallel to the western coast of South Africa (Barton et al., 1993). These graben complexes are divided into an inner marginal zone and a central zone with horizon T as the rift onset unconformity (Muntingh, 1993). The inner graben complex is predominantly filled with land-derived coarse-grained clastics with a possible pre-rift unit inferred from onshore Karoo deposits (Muntingh, ibid). The central zone consists of a thick succession believed to be of a fluvial and lacustrine nature overlying a sequence of seaward-dipping reflectors interpreted to be the result of huge subaerial basaltic extrusion associated with continental breakup (Muntingh, ibid).

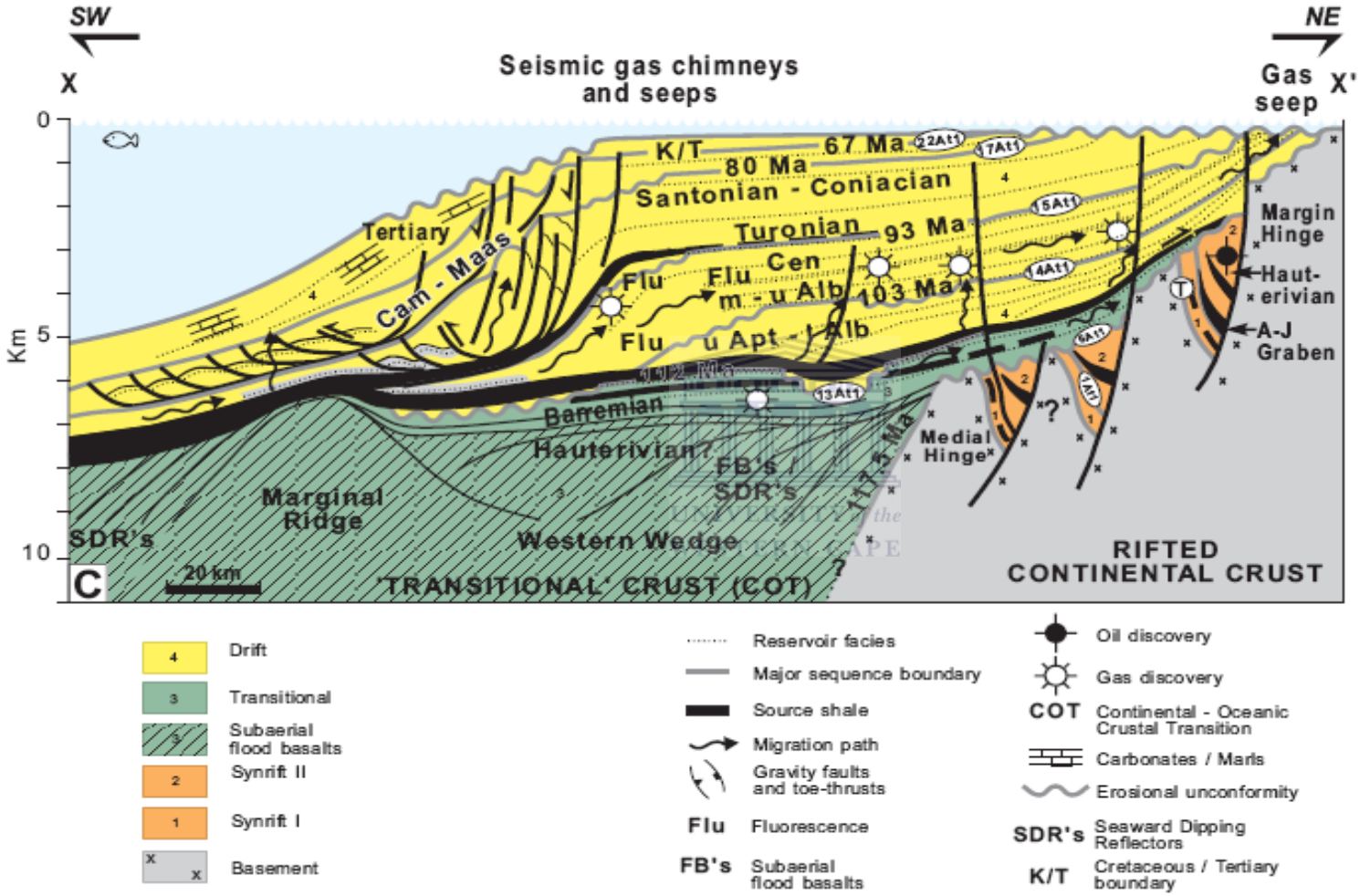

Figure 4. A profile across the central Orange Basin indicating the basin architecture, sedimentation sequence and style, structural features and the source rock intervals and all petroleum system elements (Jungslager, 1999).

These rift basins are offset by major continental transcurrent faults, which appear to be on the same trend as oceanic fracture zones and are responsible for separating the western margin into crustal segments (Broad et al., 2006). The rifting phase was terminated during the Late Hauterivian and marked by the 6At1 erosional unconformity, also referred to as the drift-onset unconformity (Figure 4) (Muntingh, 1993). True oceanic crust is believed to be present beyond the marginal ridge.

Subsequent to the active rifting phase, spreading along the Atlantic Mid-Oceanic Ridge started the onset of drift and thermal subsidence of the western margin as the early drift succession of the Orange Basin was deposited (Figure 4).

Dated between Hauterivian - Mid Aptian (Muntingh, 1993) the early drift succession reaches a maximum thickness of 2200m and is bound at the base by the 6At1 unconformity and at the top by the 13At1 unconformity (Brown et al., 1995). The sequence contains sediments ranging from continental red beds to restricted marine sediments deposited under alternating fluvial and marine dominated environments responding to alternating regressive and transgressive cycles (Muntingh, 1993).

Evaporites deposited during marine transgression represent a key element indicating that restricted marine conditions prevailed at the time of deposition and that the sequence was indeed deposited within a period of transition when restricted flow dominated the basin (Brown et al., 1995). The sequence is therefore referred to as an intermediate sequence displaying a ramp-like character as gradual transgressive regimes culminated in a flooding event during the Early Aptian (Jungslager, 1999). Lower Aptian shale deposited during periods of marine transgression form major source rocks and regional seals as well as cap-rocks to continental carrier beds (Jungslager, ibid). The early drift phase was terminated by the Mid Aptian 13At1 unconformity (Figure 4) (Muntingh, 1993) and succeeded by the deposition of generally prograding sequences and the development of a shelf edge leading to the establishment of open marine conditions (Broad et al., 2006).

Complete open marine conditions occurred along the proto-Atlantic ocean at around 112 Ma or Late Aptian / Early Albian (Brown et al., 1995) with the development of two major deltaic depocentres situated adjacent to two main sediment suppliers to the Orange Basin. These sediment suppliers were the Orange River in the north and the Olifants River to the south (Barton et al., 1993) supplying sediments of a mostly siliciclastic and deltaic nature to the Orange Basin.

A thick prograding drift succession, with the development of turbidites in the distal parts of the basin, evolved basin-ward (Brown et al., 1995). The extension of the drift sequences is used to define the aerial extent of the Orange Basin (Gerrard & Smith, 1982). "The basin thus defined covers an area of more or less 160 000 square kilometres to the 2000m isobath" (van der Spuy, 2007). The succession is interbedded with frequent erosional unconformities owing to continued changes in accommodation space controlled by relative regressive and transgressive cycles and has subsequently been defined by five super-sequences and 28 third-order sequences reaching a combined thickness of 5500m according to Muntingh (1993). These Supersequence are dealt with in more detail in the following chapter and is summarized here as follow, Supersequence 6-12 deposited between 117.5 and 112 Ma, Supersequence 13 deposited between 112 to 103 Ma, Supersequence 14 deposited between 104 to 93 Ma, Supersequence 15-16 deposited between 93 to 80 Ma, and Supersequence 17-20 deposited between 80 to 68 Ma.

The youngest of these supersequences includes the rift to drift transition sequence discussed above. The second supersequence referred to as supersequence 13 is characterised by an initial period during which relative sea level fall caused a decrease in accommodation space and extensive erosion of the Early Aptian unconformity (Brown et al., 1995).

This was followed by a period of regional flooding resulting in the deposition of a prograding sequence together with the Early Aptian source rock, which appears to be regionally developed (Brown et al., ibid). The sequence between the 14At1 and the 15At1 unconformity is characterised by alternating progradational and aggradational stacking patterns (Muntingh, 1993).

The sequences deposited between the 15At1, 16Dt1 and the 17At1 unconformities exhibit a predominantly aggradational stacking character (Muntingh, 1993). A period of reduced accommodation rates followed, characterised by a decrease in sediment supply and an increase in the rate of tectonic subsidence and/or a rise in sea level resulting in the deposition of a prograding sequence (Muntingh, ibid).

The 22At1 unconformity (Figure 4) marks the end of Cretaceous sedimentation and is overlain by the younger Cenozoic succession exhibiting a well-developed sedimentary wedge reaching a thickness of 1500m basinward (Muntingh, 1993). Structurally the full drift succession is largely featureless in the shelfal area. However with continued aggradational stacking along a steep depositional margin, particularly during the upper Cretaceous, the distal regions of the Orange Basin became increasingly unstable and ultimately collapsed resulting in the development of extensional growth faults, large slump structures and associated compressional toe-thrusts (Figure 4) (Brown et al., 1995). The full drift succession incorporating the early drift, Hauterivian to Mid Aptian succession reaches a maximum thickness of 7700m (Figure 4) and is bound to the north by the Kudu arch and to the south east by the Agulhas-Columbine arch (Muntingh, 1993).

1.6 EXPLORATION HISTORY OF THE ORANGE BASIN

South Africa's offshore Orange Basin covers an area of approximately 130 000 km^2 relevant to the 200m isobath (Gerrard and Smith, 1982) and extends into the neighbouring country of Namibia. The Orange Basin is the southernmost West African basin and the largest and youngest South African offshore basin. Despite the fact that the basin is under - explored with only one well drilled per 4000 km^2, numerous petroleum systems have been identified since exploration commenced in 1973 (Muntingh, 1993). Large gas fields have been discovered including the Kudu and Ibhubesi gas fields both discovered in 1973 and later confirmed by subsequent wells (Barton et al 1993). Both these fields have the potential of multi-trillion cubic feet of natural gas reserves (van der Spuy et al., 2003).

The only oil discovery in the Orange Basin was made when well A-J1 drilled within an isolated synrift graben sequence in the A-J graben (figure 4), encountered waxy oil trapped within lakeshore sandstones (Muntingh, 1993). The Orange Basin has confirmed hydrocarbon reserves apparently sourced from different source rocks at various stages of maturity. Understanding the basin evolution, maturity of potential source rocks within the Orange Basin can provide insight into the possibility of predicting future maturation trends.

CHAPTER TWO

2.1 SEQUENCE STRATIGRAPHY

2.1.1 SEQUENCE STRATIGRAPHY AND SEISMIC STRATIGRAPHY: DEFINITIONS

Sequence stratigraphy is the study relating to interpretation and delineation of sedimentary basin fill into relatively conformable successions of genetically related strata bounded by erosional (unconformities) or depositional surfaces (Brown et al., 1995). Seismic stratigraphy on the other hand involves the recognition of unconformities and various lapout surfaces as bounding surfaces of depositional sequences (Brown et al., ibid). The general geometry, reflection pattern, continuity and amplitude of these unconformities are critical in identifying depositional environments (Brown et al., ibid).

2.1.2 UNCONFORMITIES

Unconformities as defined by Van Wagoner et al. (1988) are “a surface separating younger from older strata along which there is evidence of subaerial erosion and truncation (and in some areas correlative submarine erosion) and subaerial exposure and along which a significant hiatus is indicated”. Two types of unconformities namely type 1 and type 2, are classified in Brown et al. (1995). Type 1 unconformities according to Vail (1987) are formed when a relatively fast sea level fall causes the equilibrium point of the shoreline depositional break to migrate basinward. Type 1 unconformities are recognized by intense subaerial and submarine erosion, submarine canyon incisions and a substantial basinward shift of facies ultimately resulting in the deposition of a lowstand systems tract Vail (ibid).

Type 2 unconformities also classified by Vail (1987) are formed by a relatively slow fall in sea level and subsequently no basinward migration of the equilibrium point (Brown et al., 1995). "These unconformities show signs of subaerial exposure, but no subaerial valley erosion, submarine canyon incision or the development of basin floor fans" (Brown et al., ibid). Type 1 unconformities are therefore more easily recognized in seismic profiles than type 2 unconformities and are also the most common in the post-rift Cretaceous rocks offshore South Africa (Brown et al., ibid).

2.1.3 ACCOMODATION SPACE

Accomodation space is defined as the amount of space available for sediment deposition (Jervey, 1988) and is controlled mainly by relative sea level rise and fall and tectonic processes (figure 5). A fall in sea level (regression) decreases the accommodation space and subsequently results in erosion while a rise in sea level (transgression) (Figure 6) increase the accommodation space and consequently increases the basin fill. The interplay of tectonics, eustatic and climatic conditions controls sediment supply and the degree to which the accommodation space is filled (Brown et al., 1995).

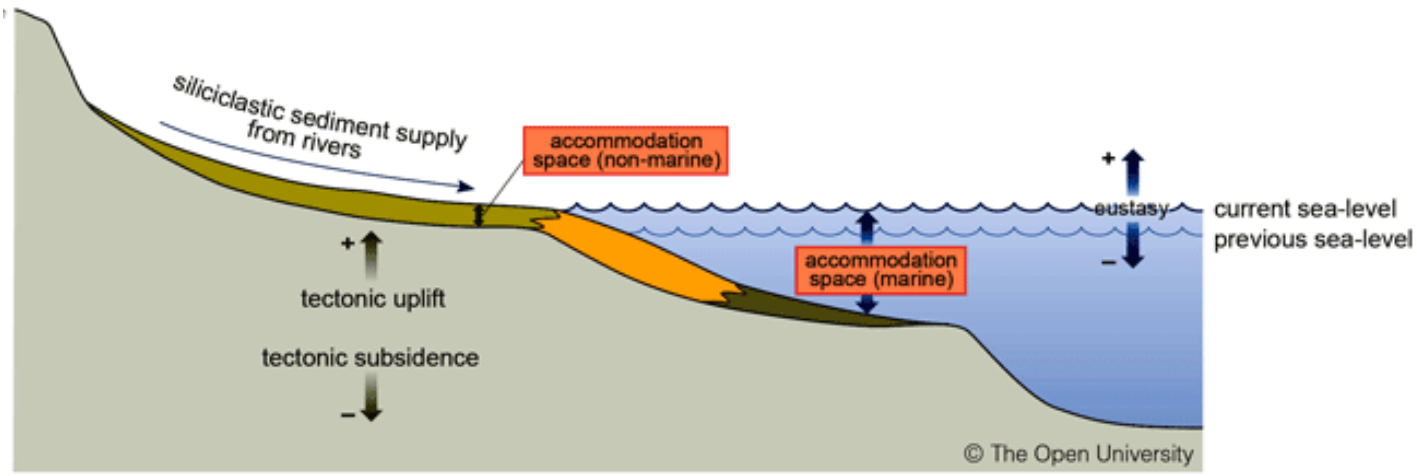

Figure 5. Development of accommodation space under the influence of tectonic uplift and eustasy.
http://strata.geol.sc.edu/terminology/accommodation.html

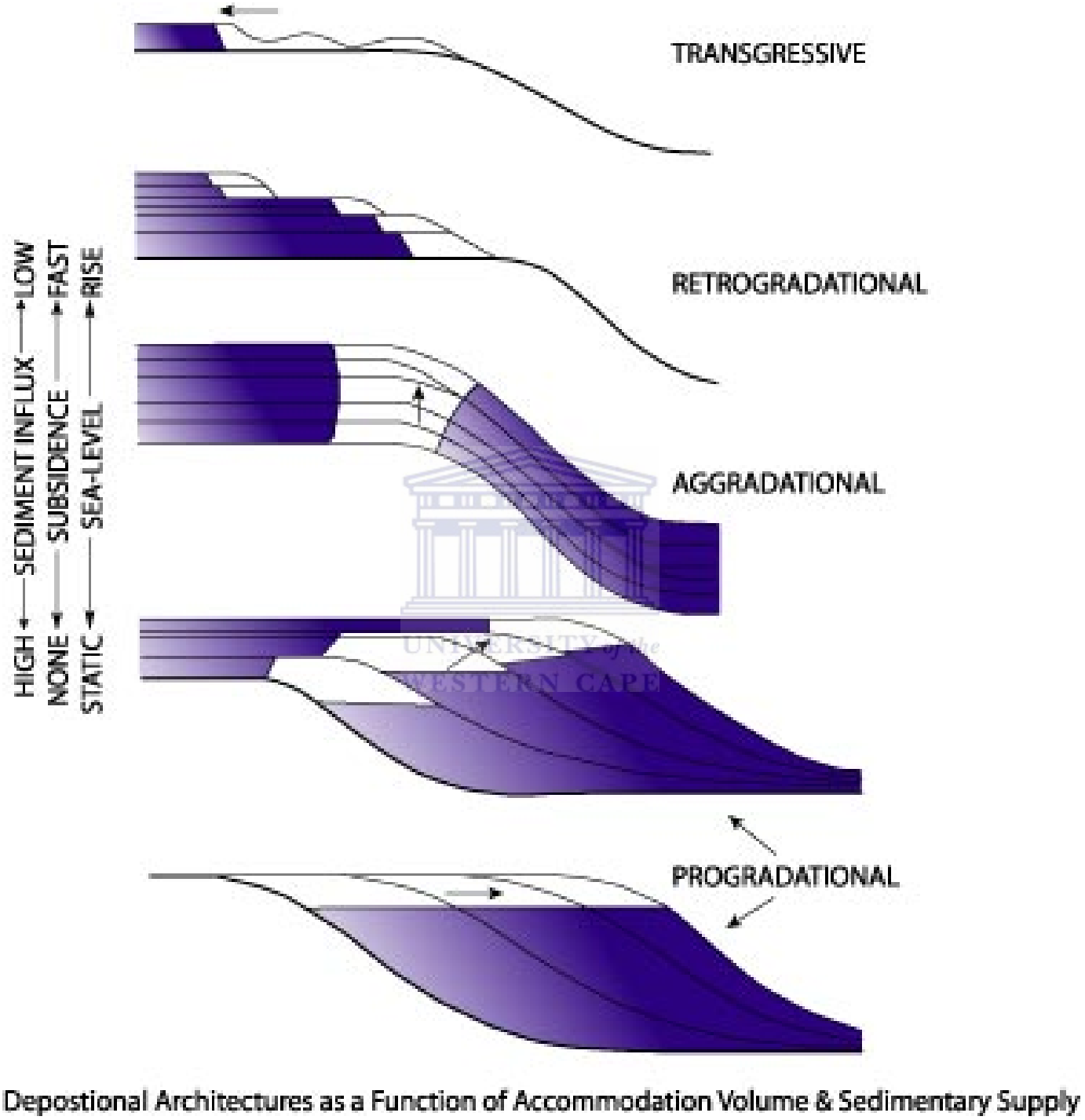

Figure 6. Different depositional sequences as a function of accommodation space and sediment supply.
http://strata.geol.sc.edu/terminology/accommodation.html

2.1.4 DEPOSITIONAL SEQUENCES

Depositional sequences are stratigraphic units composed of relatively conformable successions of genetically related strata bounded at the top and base by unconformities and the correlative conformities (Figure 6) (Mitchum et al., 1977). These sequences are deposited during one cycle of sea level rise and fall and therefore consist of vertical successions of a sequence boundary (basal unconformity), lowstand systems tract, transgressive surface, transgressive systems tract, maximum flooding surface, highstand systems tract and the next sequence boundary (top unconformity) (Brown et al., 1995).

2.1.5 PARASEQUENCES AND PARASEQUENCE SETS

Parasequences and Parasequence sets are relatively conformable, coarsening upward successions of genetically related beds and bedsets bounded by marine flooding surfaces or their correlative surfaces (Van Wagoner, 1985). Parasequence sets can display various stacking patterns which include (A) progradational patterns where the deposition of sediment exceeds the rate at which accommodation space is created (Figures 6 & 7(A)), (B) aggradational patterns whereby the sediment deposition equals that of the accommodation rate (Figures 6 & 7(B)) and lastly, (C) retrogradational patterns where the accommodation rate exceeds sediment deposition rate (Figures 6 & 7(C)) (Brown et al., 1995).

Parasequence sets are therefore controlled by the interaction of the rates of sediment supply and accommodation space (Van Wagoner et al., 1990). These parasequence sets are used in conjunction with their bounding surfaces and their position within a sequence to define systems tracts (Van Wagoner et al., ibid). Lowstand systems tracts are therefore characterised by progradational to aggradational parasequence sets, transgressive systems tracts are characterised by retrogradational parasequence sets and highstand systems tracts are characterised by aggradational to progradational parasequence sets (Brown et al., 1995) (Figures 8 (A)(B)(C)). Parasequences and parasequence sets therefore constitute the fundamental building blocks of sequences and their systems tracts (Brown et al., ibid).

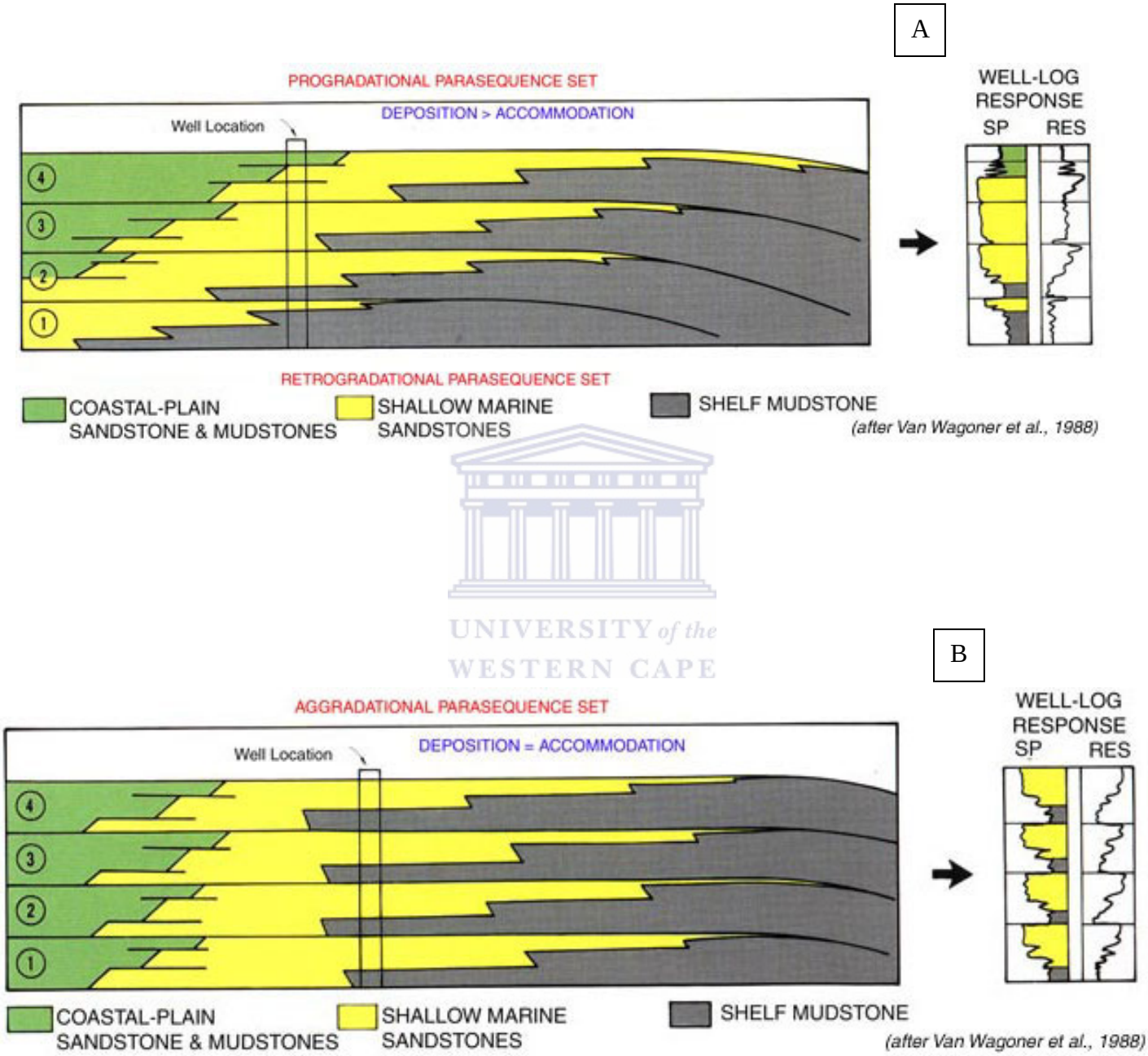

C

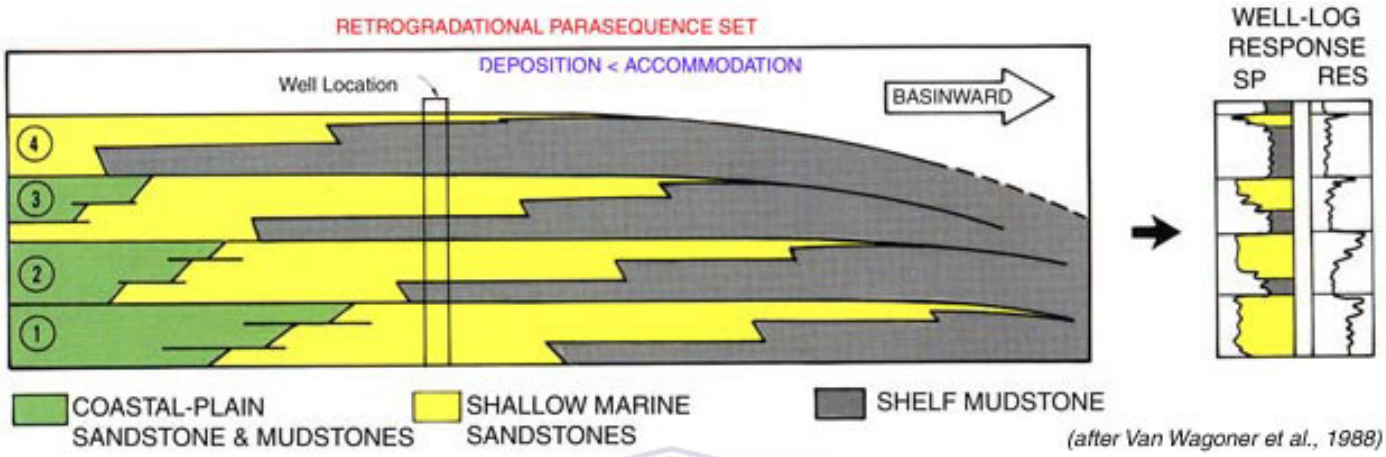

Figure 7 (A)(B)(C). Different parasequence sets (Van Wagoner et al., 1988)

<http://strata.geol.sc.edu/terminology/prog-para-set.html> (A)
<http://strata.geol.sc.edu/terminology/retro-para-set.html> (B)
<http://strata.geol.sc.edu/terminology/aggr-para-set.html> (C)

2.1.6 DEPOSITIONAL SYSTEMS TRACT

A depositional system can be defined as “a three dimensional assemblage of lithofacies, genetically linked by active (modern) or inferred (ancient) processes and environments” (after Fisher and McGowen, 1967) where a systems tract as defined by Brown and Fisher (1977) is a” linkage of these contemporaneous depositional systems”. “A depositional systems tract is therefore composed of one or more contemporaneous depositional systems” (Brown and Fisher ibid; Brown et al., 1990).

There are three depositional systems tracts known and they include a lowstand systems tract, a transgressive systems tract and a high stand systems tract (Vail, 1987) (Figure 8 (A) (B) (C)) each characteristic of a different time of relative sea level rise and fall. These systems tracts are recognized and defined based on the nature of their boundaries and their internal geometries (Vail et al., 1989).

2.1.7 LOWSTAND SYSTEMS TRACT

The following information in this section was taken mainly from (Emery and Myers, 1996). A lowstand systems tract (Figure 8(A)) is stratigraphically defined as the oldest systems tract deposited at the base of a type 1 depositional sequence and generally on a type 1 erosional surface. These lowstand systems tracts are deposited during periods of relative sea level fall (Vail, 1987; Posamentier and Vail, 1988), causing river systems to incise into previously deposited alluvial, coastal plain as well as shelf deposits of the previous sequence as the river profile adjusts to a lowered base level. With a lowering base level rivers are now less likely to avulse and sediment filled channels are focused, causing deposition at a single point on the slope. This leads to sediment instability and ultimately slope failure and the deposition of lowstand submarine fans in the deep basin.

Two types of lowstand submarine fans are known, an initial basin floor fan unit that is detached from the foot of the slope and a subsequent slope fan unit (slope front fill) that is in contact with the slope (Figure 8(A)) (Emery and Myers, 1996). These fan units together form the base upon which the second section of the lowstand systems tract, the lowstand prograding wedge is deposited.

The lowstand prograding wedge is normally composed of more sand material than the preceding highstand wedges due to recycling of sand from the highstand topsets. The tract is deposited during periods of accelerated sea level rise and is initially confined to the areas around the mouths of the incised rivers.

A progressive or abrupt rise in sea level leading to extensive flooding terminates the deposition of the lowstand systems tract and initiates the deposition of the transgressive systems tract as the system begins to backfill and a retrogradational sequence is deposited (Brown et al., 1995). The lowstand systems tract therefore consists of two components, a unit of submarine fans deposited during falling sea level and an initially progradational becoming aggradational topset/clinoform system deposited with a rise in sea level (Figure 8 (A)) (Emery and Myers, 1996).

2.1.8 LOWSTAND SYSTEMS TRACTS IN THE ORANGE BASIN

Lowstand systems tracts of the Orange basin (Figure 9) are thickest directly basinward of the previous highstand offlap break and generally thin to beyond seismic resolution downdip and pinch out near the relict shelf edge or offlap (Muntingh and Brown, 1993). Basin floor fans and prograding deltaic wedges in sequences 14B, 14C, 14D, 15B and 15C are generally visible on seismic profile downdip of where major incised river systems can be documented (Brown et al., 1995). Downdip, prograding wedges such as those found in sequence 15B generally downlap basinward onto either slope fans, basin floor fans or type 1 surfaces while updip the wedges typically exhibit marine and coastal onlaps onto type 1 surfaces (Muntingh and Brown, 1993). “Maps of lowstand systems tracts in the Orange Basin typically exhibit incised valley fills that grade basinward into submarine canyons containing prograding coastal wedges and slope fans” (Muntingh and Brown, ibid).

2.1.9 TRANSGRESSIVE SYSTEMS TRACT

Following deposition of the lowstand systems tract the transgressive systems tract (Figure 8(B)) forms the middle system tract overlain by the top highstand systems tract. As sea levels continue to rise and if the rate at which accommodation space is created is faster then the rate of sediment supply (Emery and Myers, 1996) into the basin, a backstepping of the sediment column occurs resulting in the development of a retrogradational sequence (transgressive systems tract) (Figure 8(B)). This subsequently leads to a starvation of the deeper basin and the development of distal glauconitic, organic rich or phosphatic shales (condensed sections) as less sediment is transported to the deeper parts of the basin (Emery and Myers, ibid).

The thickness of a trangressive systems tract is normally dependent on the balance between the amount of sediment supply and free accommodation space (Brown et al., 1995). "Transgressive systems tracts in the South African offshore basins are usually thin possibly due to the general low rate of sediment supply and more importantly the rapid rise in sea level and subsequent flooding of the shelves" (Brown et al., ibid).

The deposition of the transgressive systems tract is terminated when the rate of topset accommodation volume matches sediment supply and progradation occurs (Emery and Myers, 1996). This initial prograding sequence is deposited on a maximum flooding surface created as rising sea levels limit shorelines to their ultimate landward position (Loutit et al., 1988) forming the top of the transgressive systems tract.

2.1.10 TRANSGRESSIVE SYSTEMS TRACTS IN THE ORANGE BASIN

The following information was taken mainly from (Muntingh and Brown, 1993). “Transgressive systems tracts of the Orange Basin (Figure 9) are typically thin and rarely seismically resolved”. Those that can be seismically resolved are found in sequences 13A, 15A and 16A with the trangressive systems tract and maximum flooding surface of the 15A sequence recording a major flooding event in the Orange Basin. “Normally the thin, transgressive tracts coincide with strong reflections generated by marine condensed sections”. These condensed sections are composed of black shales and thin limestone beds in the deeper sections of the basin and thin glauconitic sandstone on the shelf. “Well developed marine condensed sections in the Orange Basin are found superimposed on well developed seismically resolvable transgressive systems tracts at 111 Ma (13A mfs), 91.5 Ma (15A mfs) and 89 Ma (16A mfs)”. Source rock within the thin, fining upward, retrogradational parasequences typically exhibits an increase in kerogen quality upward in the sequence.

2.1.11 HIGHSTAND SYSTEMS TRACT

"The highstand systems tract (Figure 8 (C)) is deposited when sufficient sediment supply exists to fill the accommodation space generated by the decelerating relative rise of sea level" (Vail, 1987; Posamentier and Vail, 1988). The Highstand systems tract is composed of three parts namely the early highstand, late highstand prograding complex and the late highstand subaerail complex "The systems tract gradually evolves from a sigmoidal aggradational parasequence stacking pattern to an oblique progradational parasequence stacking pattern as the rate of sea level rise decreases through time" (Brown et al., 1995).

The systems tract is bounded at its base by a downlap surface associated with a condensed section referred to as a maximum flooding surface (mfs) and either a type 1 or type 2 unconformity at the top (Muntingh and Brown, 1993).

2.1.12 HIGHSTAND SYSTEMS TRACTS OF THE ORANGE BASIN

The highstand systems tracts of the Orange Basin (Figure 9) are thick and generally extend proximally from the basin margin to beyond seismic control distally (Muntingh and Brown, 1993). These tracts are bounded at the base by marine condensed sections and at the top by a type one unconformity and have an internal upward coarsening and thickening character as recognized on well logs (Muntingh and Brown, ibid).

A

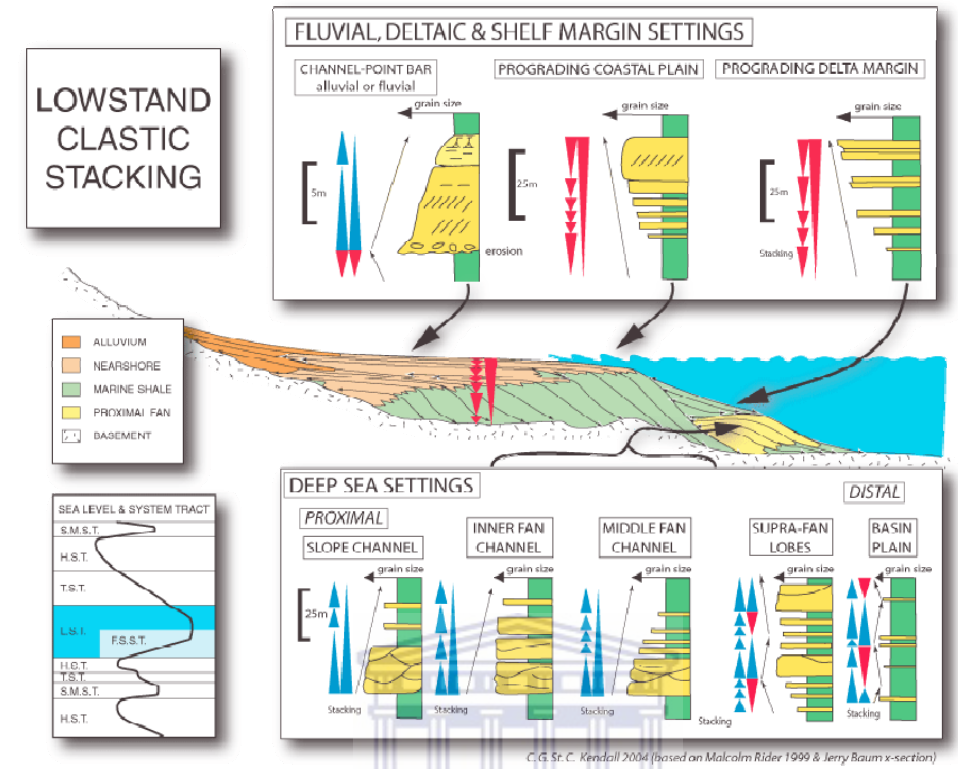

B

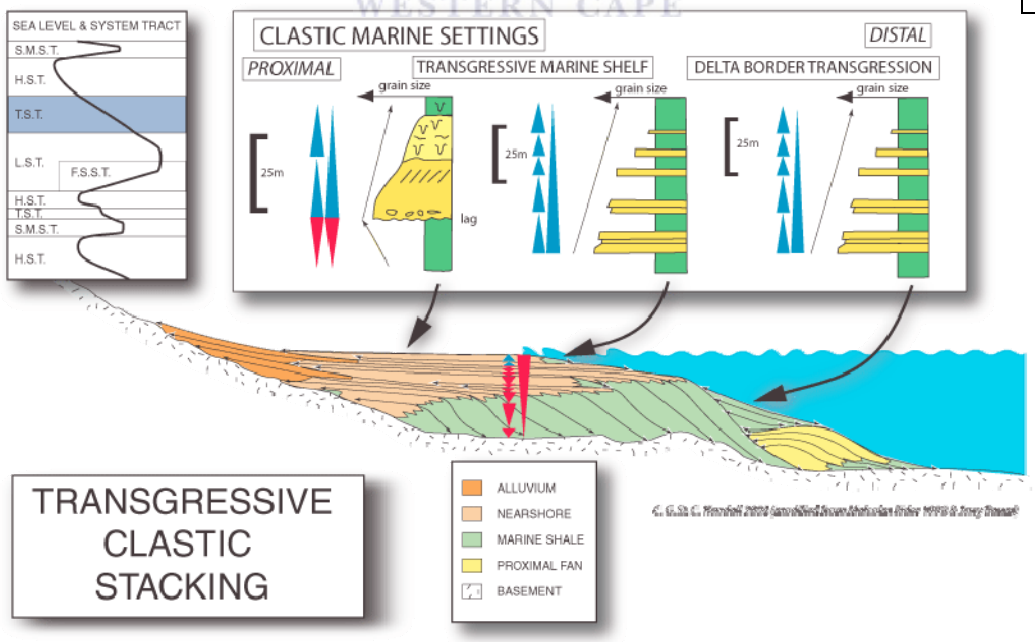

C

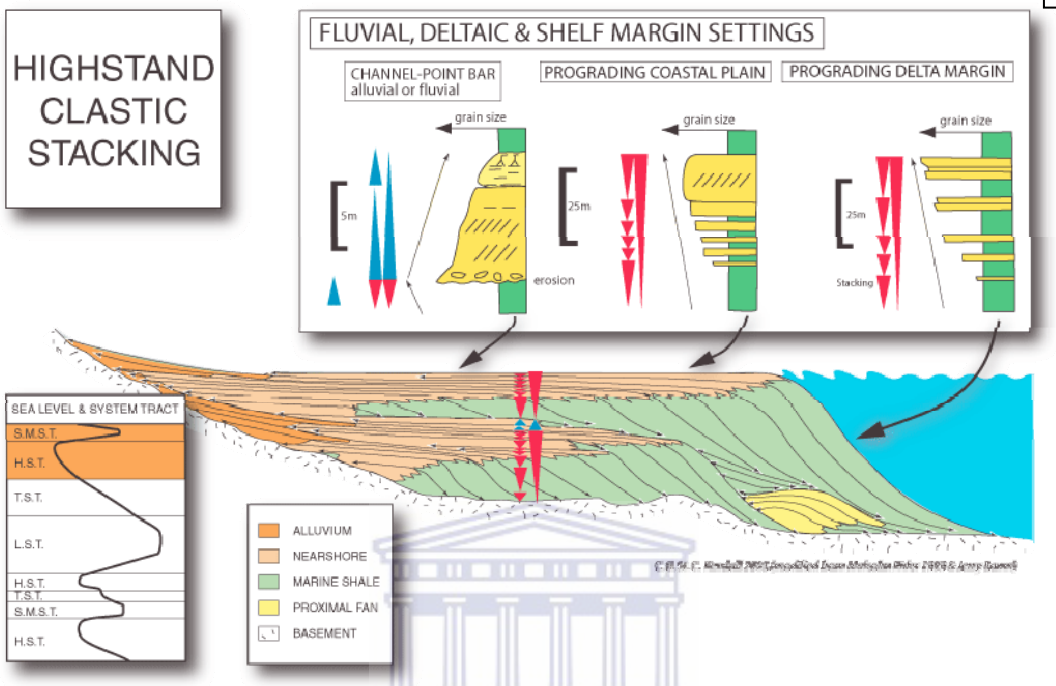

Figure 8 (A)(B)(C). Depositional systems tracks with the characteristic parasequence stacks.
(A) General progradation associated with lowstand systems track, (B) Retrogradation associated with the transgressive systems track (C) Aggradation to progradation associated with the highstand systems track.
USC Sequence Stratigraphy Web, 2005, University of South Carolina, Geology Department, http://strata.geol.sc.edu/log-stacking.html
(A) C.G. St. C. Kendall, 2004
(B) C.G. St. C. Kendall, 2004
(C) C.G. St. C. Kendall, 2003

2.1.13 MARINE CONDENSED SECTIONS AND MAXIMUM FLOODING SURFACES

Maximum flooding surfaces occur within a marine condensed section and develop when rising sea levels reach their maximum landward position (Loutit et al., 1988). "The surface also acts as a boundary between the transgressive retrogradational parasequence set and the overlying regressive progradational parasequence set "(Emery and Myers, 1996). The surface is present within an aggradational parasequence set towards the proximal end and evolves to a shelfal and basinal condensed section towards the distal end (Emery and Myers, ibid).

2.1.14 MARINE CONDENSED SECTIONS OF THE ORANGE BASIN

Marine condensed sections in the Orange Basin are typically found to be a few metes thick composed mostly of black shale and some thin limestone beds in the distal sections and thin glauconitic sandstone on the relict shelf (Muntingh and Brown, 1993). Well developed marine condensed sections in the Orange Basin are superposed on well developed transgressive systems tracks at 111 Ma (13A mfs), 91.5 Ma (15A mfs), and 89 Ma (16A mfs) with the marine condensed section and maximum flooding surface at 91.5 Ma correlating with a major anoxic event in the Orange Basin (Schlanger and Jenkyns, 1976, Muntingh and Brown, 1993).

2.2 SEQUENCE STRATIGRAPHY OF THE ORANGE BASIN

2.2.1 SEQUENCE STRATIGRAPHIC NOMENCLATURE

Classifying the drift succession of the Orange Basin required a detailed sequence-stratigraphic study, identifying and marking stratigraphically significant marker horizons (unconformities) used to subdivide the post-rift succession into various sedimentary packages. The sequence stratigraphy of the Orange Basin is described in much detail by Muntingh and Brown (1993) and (Brown et al., 1995) and will therefore be the main source of information in summarizing the sequence stratigraphy of the Orange Basin.

The Orange Basin sequence has been classified using an alphanumeric nomenclature system. The system operates through applying numerical symbols ranging from 1 to 22 in stratigraphic succession to seismically-distinctive, unconformity-bound sequences or sequence sets. Other less defined sequences typically found within the larger more distinctive numerically designated sequences and sequence sets are classified in stratigraphic succession by alphabetical symbols ranging from A to E.

Most sequences are classified based on the symbol annotated to their basal unconformities which in turn are classified as are either type 1 or type 2 sequence boundaries for example the basal unconformity of third order fundamental sequence 13A is 13At1. "Sequences consisting of basal type one unconformities are classified as type one sequences" (Brown et al., 1995) which are the most common in the post rift Cretaceous successions in the offshore basins of South African.

Other stratigraphic surfaces such as marine condensed sections (mcs) and maximum flooding surfaces (mfs) present within sequences are also designated by the symbol of the sequence which contain them, for example 15A mcs.

2.2.2 SEQUENCE STRATIGRAPHY OF THE ORANGE BASIN

The post-rift succession deposited above the 6At1 unconformity has been estimated to reach a maximum thickness of roughly 7700m and to consist of five Super Sequences each of which lasted more or less 10 million years (Brown et al., 1995) (Figure 9). "The supersequences are bounded by second order type one unconformities and are characterised by major transgressive and regressive cycles reflected by component third-order sequence sets" (Brown et al., ibid). These supersequences record the various paleo-depositional environments that dominated during the deposition of the post-rift sequences of the Orange Basin.

The following description outlines the main events during each of the five supersequence phases (Muntingh and Brown, 1993, Brown et al., 1995).

- The first of the supersequences, referred to as Supersequence 6-12, was deposited between 117.5 and 112 million years (Figure 9) and records a period of transgression brought about by the initial drift-onset flooding followed by a period of aggradation and progradation of third-order sequences. These events indicate that tectonic subsidence and eustatic accommodation rates decreased while sediment supply rates increased.

- Supersequence 13 deposited between 112 and 103 million years (Figure 9) records a major relative sea level fall following uplift and intense subaerial and submarine erosion, transgression and regional flooding of second order type1 unconformity 13At1 third order sequences. This period of regional flooding resulting in the deposition of mostly progradational and some aggradational third order sequences in areas where the 13At lowstand systems track did not occur. The geometry of the third order sequence sets indicates a low but slowly accelerating tectonic subsidence and possible eustatic accommodation rates.

- Supersequence 14 deposited between 104 and 93 million years (Figure 9) records a moderate relative sea level fall as uplift continued, resulting in moderate erosion, transgression and regional flooding of second order type 1 unconformity 14At1 third- and fourth-order sequences. The geometry of the third order sequence sets indicate that an accelerated rise in sea level possibly due to both tectonic and eustatic processes was balanced by a relative increase in sediment supply.

- Supersequence 15-16 deposited between 93 and 80 million years (Figure 9) also records a moderate sea level fall following minor uplift, resulting in minor erosion, major transgression, and regional flooding of second-order type 1 unconformity 15At1 third- and fourth order sequences of highly aggradational developing into slightly progradational nature. The geometry of the third order sequence sets indicate that a high but slowly decelerating rise in sea level was balanced by a high, continued sediment supply rate. Subsequent to a high rate of aggradation along a steep depositional margin, gravity faulting resulted in the development of a complex zone of slumps, rollover anticlines and tilted fault blocks posing as potential hydrocarbon traps.

- The final Supersequence 17-20 deposited between 80 and 68 million years (Figure 9) records another major relative sea level fall and minor transgression which was followed by regional flooding of second- order type 1 unconformity 17At1 third- order sequences highly progradation, becoming slightly aggradational were deposited. The geometry of the third-order sequence sets indicate that a major se level fall followed by a slow sea level rise coincided with moderate to high continued sediment supply rates.

Supersequences 13, 14 and 15-16 (Figure 9) can be described as a Supersequence set as described by Greenlee and Moore (1988) and Vail et al. (1991) whose ideas led to the conclusion by Brown et al. (1995) that the supersequence set is essentially a 32 million - year composite sequence comprising three 10 million - year supersequence systems tracts each comprising of third order sequence sets.

Following the above description the post-rift succession of the Orange Basin would resemble from oldest to youngest a lowstand supersystems tract in the central parts of the basin being the main depocentre area (supersequence 13), a transgressive retrogradational supersytems tract (supersequence 14), an early and late highstand supersystems tract (supersequence 15-16) and a lowstand supersystems tract (supersequence 17-20) (Brown et al., 1995).

Comprising the youngest of the Orange Basin sediments the Cenozoic succession consists of sequences lying mostly basinward of the youngest Cretaceous offlap break and reaches a maximum thickness of more or less 1500 meters (Muntingh and Brown, 1993). Younger episodes of gravity faulting in the Cenozoic sequence are evident beyond the Cretaceous shelf break.

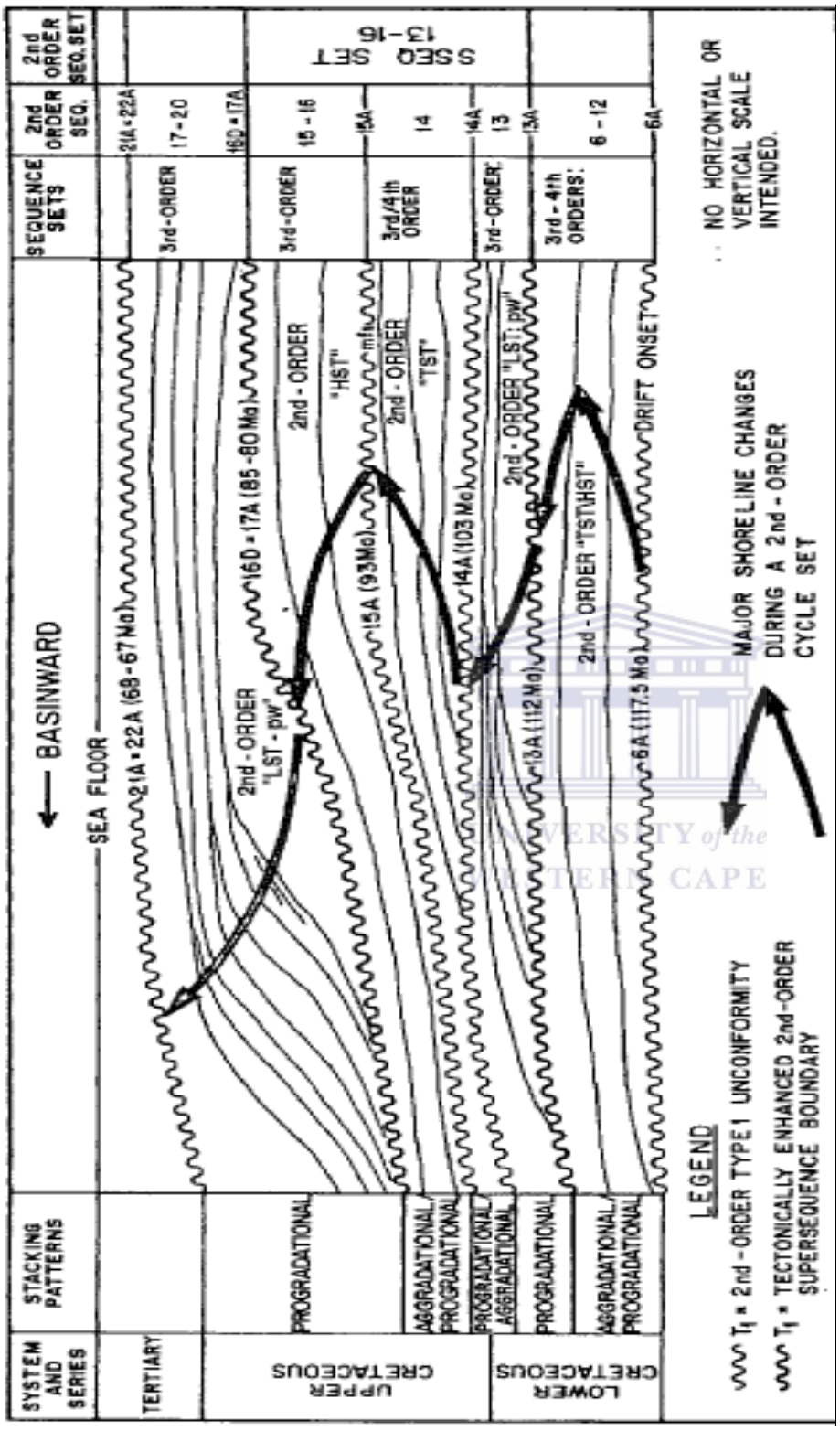

Figure 9. Various drift Super Sequences and whether it is prograding or aggradating with the bounding second order type 1 unconformities.
(Muntingh., and Brown, 1993)

2.3 PETROLEUM SYSTEM ELEMENTS

Petroleum systems comprise various petroleum system elements interacting with each other to ultimately result in the commercial accumulation of hydrocarbons. The five main petroleum system elements include the initial source rock, carrier bed, reservoir, trap and a seal with time, maturation and migration acting as secondary but equally important petroleum elements.

2.3.1 SOURCE ROCK

A source rock is defined as an organic-rich fine-grained sedimentary rock containing sufficient organic matter that could be converted to oil or gas if buried to a certain depth and/or heated to a specific temperature (Chapman, 1976). The organic matter found within the fine-grained sedimentary rock can vary in origin thus influencing the type of petroleum generated. The quality of the source rock is thus determined by the nature of the organic matter (Kerogen type) constituting the source rock, whether it is mostly land derived, marine or a mixture of both land and marine derived organic matter. These organic matter types are related to the three groups of kerogen types, including type one kerogen which is essentially algal in origin (Figure 10) with higher hydrogen to oxygen ratio in relation to the other groups (Tissot and Welte, 1978).

Type two kerogen (Figure 10) is of intermediate composition with a mixture of both algal material and material derived from zooplankton and phytoplankton (Figure 10) (Selley, 1985). The type three kerogen (Figure 10) is low in aliphatic compounds but predominantly rich in aromatic compounds. This humic kerogen is derived mainly from the lignin of the higher woody terrestrial plants (Figure 10) and tends to produce mainly gas and little to no oil (Selley, ibid).

Marine derived organic matter, mainly phytoplankton, bacteria, algae and zooplankton played a dominant role in providing source material for petroleum generation during the Cambrian to the Devonian after which terrestrially derived organic matter provided an alternative source (Tissot and Welte, 1978).

Maturing these source rocks with their varied compositions to produce hydrocarbons is credited to the temperatures and depths to with the source rocks are exposed (Figure 11). The generalized trend for the maturation of source rock starts with the process of diagenesis (Figure 11) which is defined as a process through which the system tends approach equilibrium under conditions of shallow burial and though which the sediments normally become consolidated from the mixture of large amounts of water, dead organic material and minerals initially deposited in subaquatic environments (Tissot and Welte, 1978). The depth interval under the process of diagenesis is generally a few hundred meters where increases in temperature and pressure are generally small and hydrocarbon transformation moderate. (Tissot and Welte, ibid).

With continued burial and subsequent increase in temperate and pressure the system are now entering the stage of catagenesis (Figure 11). Temperatures in this stage generally range from 50 to 150 degrees Celsius (Figure 11) (Tissot and Welte, 1978) with the organic matter entering the phase of hydrocarbon generation starting with liquid petroleum and evolving to wet gas during the later stages of catagenesis. A generalized temperature dependent interval found between approximately 60 and 120 degrees Celsius is refer to as the oil window/oil zone (Figure 11) and acts as the window within which oil is generally generated and expelled from the source rock (Pedersen, 2007).

The last stage in the evolutionary trend of organic matter before which metamorphisms occurs is referred to as metagenesis (Figure 11). This stage is reached when the system is subjected to even deeper burial and higher temperature and pressures compared to the stage of catagenesis. Limited amount of methane but no petroleum is generated within this stage (Tissot and Welte, 1978).

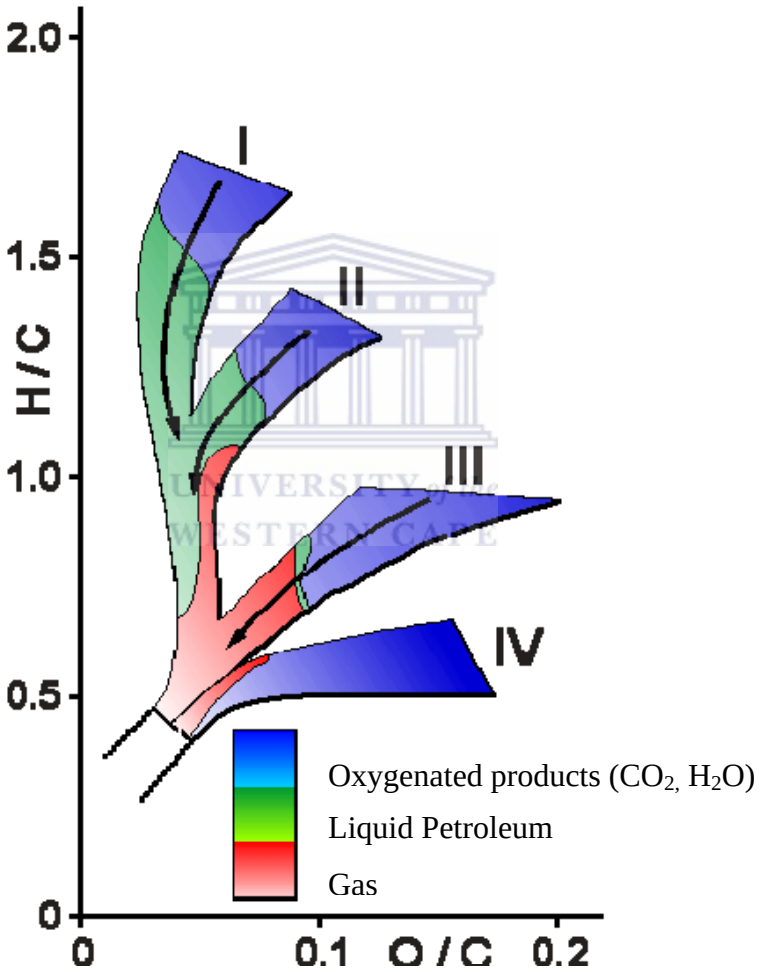

Figure 10. Van Krevelen diagram indicating the various kerogen types and their evolutionary paths with increased burial/temperature. (Beardsmore and Cull, 2001) (http://www.geosci.monash.edu.au/heatflow/chapter5.html)

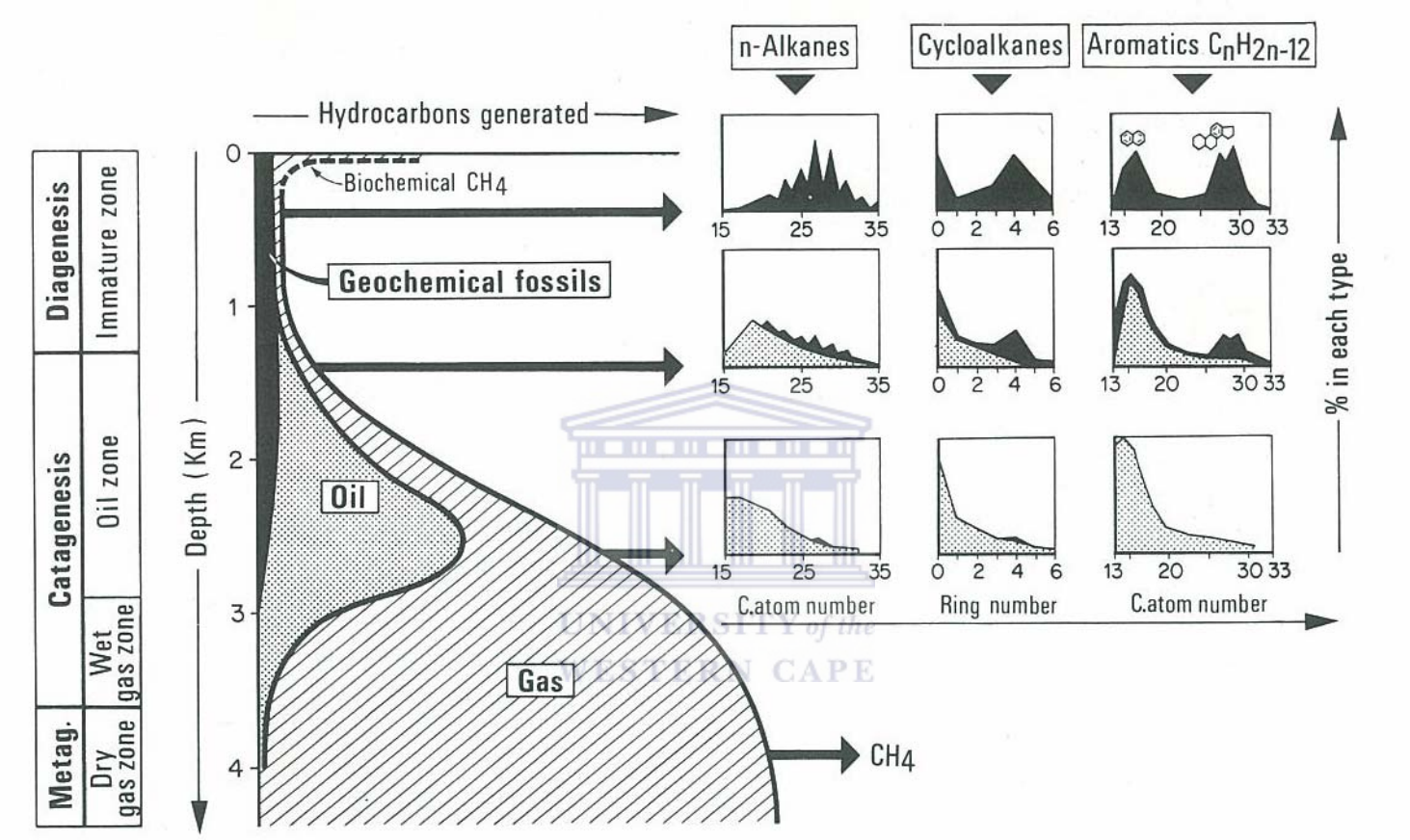

Figure 11. Showing the generalized evolution of hydrocarbons with increased temperature and depth. Pedersen.
(Tissot and Welte, 1978)

2.3.2 RESERVOIR

Any rock may act as a reservoir provided sufficient porosity and permeability is present (Selley, 1985) but in general a reservoir rock is defined as a coarse-grained porous and permeable rock usually sandstone, containing little to no insoluble organic matter (Tissot and Welte, 1978). The two most essential requirements for a reservoir are porosity (Ø) expressed as the ratio of pore spaces or voids to solid rock, and permeability (K) which is the ability of the rock to transmit fluids through interconnected pore spaces (Selley, 1985). These two essential elements are primarily affected by the sediment texture, which includes grain size, shape, sorting, packing, orientation and secondarily through diagenesis in the form of compaction, cementation and dissolution (Selley, ibid).

Reservoir sandstones in the Orange Basin occur throughout the stratigaphic column and comprise fluvio-deltaic, lacustrine sandstones and conglomerates within the graben units (Muntingh, 1993). Post rift reservoir units range from fluvio-deltaic to marine sandstones (Muntingh, ibid).

2.3.3 TRAP AND SEAL

“A trap is defined as a geological feature enabling migrated petroleum to accumulate and be preserved for a certain time interval” (Tissot and Welte, 1978). Traps come in various shapes and sizes and are formed through tectonic processes (structural traps), depositional processes (stratigraphic traps) or a combination of both (combination traps) (Selley, 1985). The seal is defined as any impermeable rock layer overlaying the trap closure and preventing any migration of oil or gas out of the closure.

2.4 LITERATURE REVIEW

2.4.1 PREVIOUS BASIN MODELING STUDIES IN THE ORANGE BASIN

The Orange Basin has been proven to contain two main source rock units the first of which include the older oil-prone Late Hauterivian synrift source rocks, which were deposited during active rifting when lacustrine environments dominated the west coast of South Africa. The source rocks reach a maximum thickness of approximately 60 meters (Barton et.al., 1993) to 100 meters (van der Spuy, 2007) and is postulated by Muntingh (1993) to have expelled large amounts of oil throughout the burial history of the Orange Basin to be trapped in overlying structures.

Basin modeling conducted by Jungslager (1999) in the A-J graben indicate that the Late Hauterivian synrift source rock has only entered the top of the oil window, mainly as a result of the low geothermal gradient (2.5ºC 100 m $^{-1}$) while maturation modeling conducted by Paton et. al. (2007) using the PetroMod modeling software, reveals that the entire syn-rift source interval is completely matured with a 100% transformation ratio indicating complete kerogen conversion. However in this study only the proven Barremian - Early Aptian and the postulated Cenomanian - Turonian source rocks will be investigated.

Source rock modeling conducted by Barton et al. (1993) as well as Muntingh. (1993) reveals that the Barremian - Early Aptian source rock reaches maturity for gas generation over the central and western shelf area. The source rock also reaches oil-window maturity west of the shelf because sediment thinning results in lower temperatures. Thermal modeling conducted by Jungslager (1999) corroborates the findings of Barton et al. (1993) and Muntingh (1993) supporting evidence that the Barremian - Early Aptian source rocks has a centrally gas-mature region and a distal oil-mature area. Bray et.al. (1998) predicted maturity for the Barremian - Early Aptian source rock and the Cenomanian - Turonian source rock further north in the basins along the Namibian offshore margins (Figure 12).

Bray et al. (1998) shows that the Barremian - Early Aptian source rock “is early or mid-mature for oil over the length of the Namibian offshore, increasing to late mature for oil over areas of the Walvis and Lűderitz Basins and into the main gas generation window in parts of the Namibia and Orange Basin” (Figure 12) (Bray et al., 1998). Maturation modeling towards the south of the Orange Basin conducted by van der Spuy (2003) using BasinMod software reveals the Barremian - Early Aptian source rock to be presently in the oil window at this position in the distal areas of the basin. The modeling utilised maturity and temperature data from well O-A1 and a pseudo-well west of the borehole K-F1 incorporating data from this well K-F1, which is included in the present study.

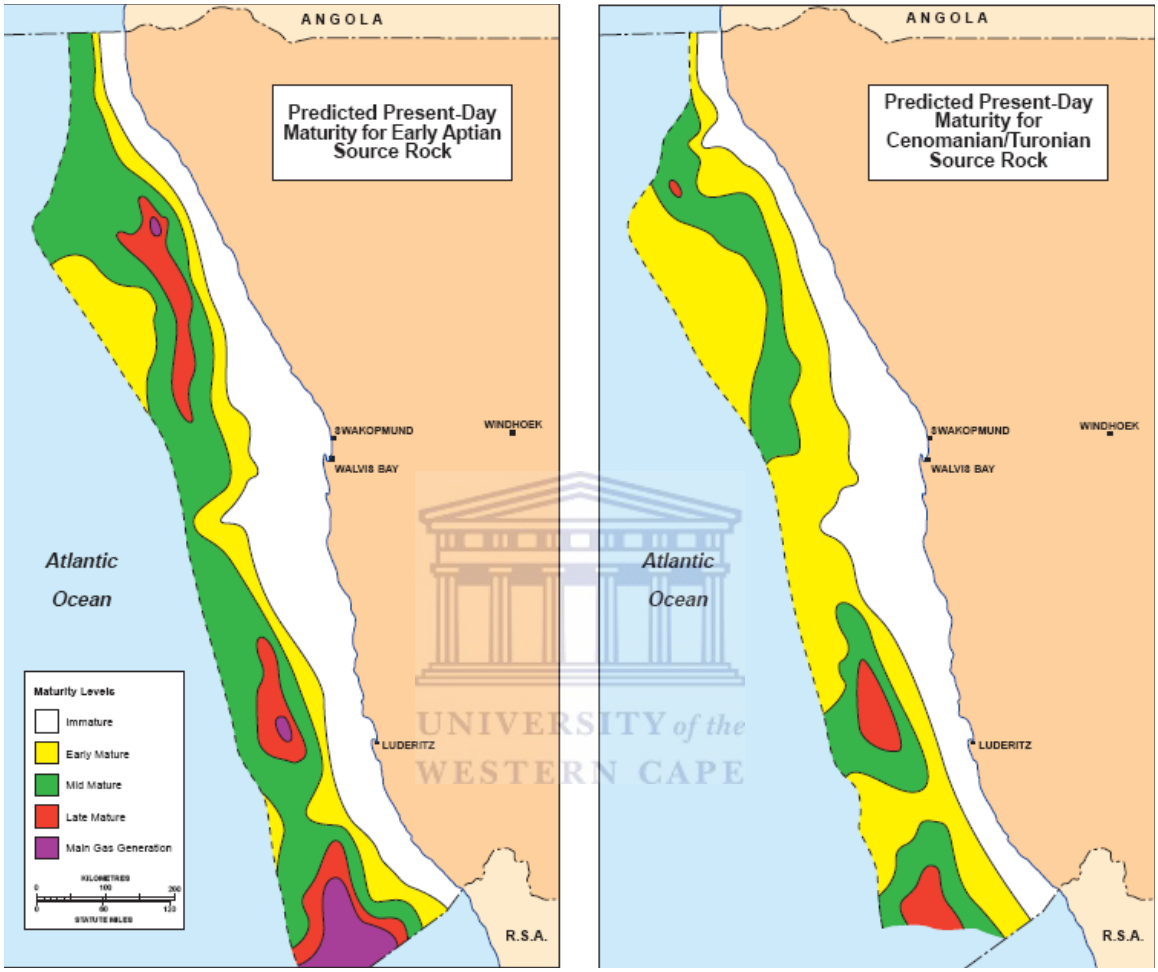

Figure 12: Maturity maps for the Barremian - Early Aptian source rock and the Cenomanian - Turonian source rock. (Bray et al., 1998)

Maturation modeling done by Paton et al. (2007) of the Barremian - Early Aptian source rock reveal that this source rock has variable extents of conversion at present, supporting Paton's theory that the overburden sediment thickness is not the principal main control on the degree of transformation but erosional events also played a critical role. The main parameters of this model included kinetic models assigned to source rock units based on the source rock facies. Heat flow values were modeled using a McKenzie type lithospheric stretching model (McKenzie, 1978) with stretching factors ranging from 1.5 to 2.5. The model also assumes a 10 million year rifting event starting at 130 million year followed by a period of thermal decay over 70 million year after which a constant rate of heat flow continues to present (Paton et al, op cit).

The heat flow model incorporated in the basin model of Paton et al. (2007) was calibrated using vitrinite reflectance data the maturation of which was modelled using the kinetics for vitrinite reflectance of (Sweeny and Burnham, 1990). As the wells are situated in the middle shelf, estimations had to be made about the heat flow of the remainder of the shelf. Paleo-water depth in the middle and inner shelf were constrained by palaeontological data from Petroleum Agency SA and was inferred for the outer shelf. Sea surface temperatures were calculated based on paleo-latitude as defined by Wygrala (1989).

Source rock modeling on a third regionally developed source rock above the 15At1 unconformity, associated with the global Cenomanian - Turonian oceanic anoxic is predicted by Barton et al. (1993) to be immature over the shelf area becoming more oil prone westward as the source rock quality improves from east to west.

(Bray et al., 1998) predict that the “the Cenomanian - Turonian source reaches the mid mature window over areas of the Namibia, Walvis, Lűderitz and Orange Basin, increasing to late mature in the Lűderitz and Orange Basin depocentres and over restricted parts of the Namibe Basin” (Figure 12). (Aldrich et al., 2003) describe the Cenomanian - Turonian source rock as a marine, oil prone source presently in the oil window.

CHAPTER THREE

RESEARCH DESIGN, RESEARCH MATERIALS AND METHODOLOGY

3.1 RESEARCH DESIGN

The study area covers parts of blocks 3A/4A and 3B/4B in the Orange Basin (Figure 1(A) (B)). The data comprises a grid of 2 D seismic data and five wells A-A1, A-L1, A-I1, K-F1 and K-H1 (Figure 2) located in an east-west transect.

The study focuses on the maturity of the post-rift source rocks of the Orange Basin. By utilizing various data sets, which include 2 D seismic data, well data comprising geological well logs, petrophysical well logs, well top data, check-shot data, and borehole temperature data as well as geochemical well data such as Rock Eval and vitrinite reflectance data (Figure 13), the model was able to demonstrate likely maturity conditions of the post rift source rocks of the Orange Basin.

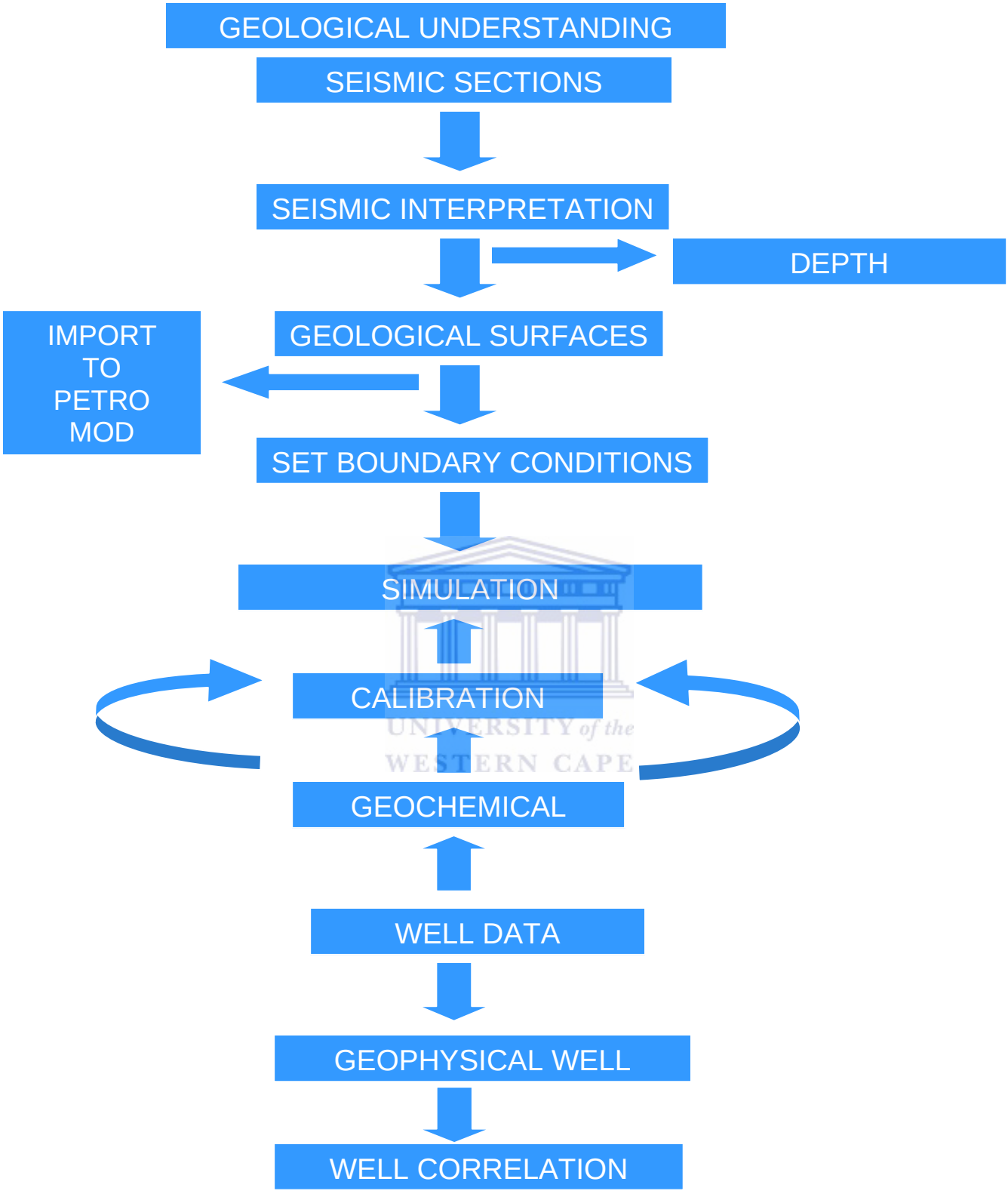

Figure 13. Sequence of methods followed during the study.

3.2 RESEARCH MATERIAL

Throughout the study different data material and equipment was used to assist in compiling, interpreting and displaying data for the purpose of a better comprehension and presentation of the study. The data material used, form part of the data archive of the Petroleum Agency SA and was made available for the purpose of the study. The data used included (a) seismic data of different vintages, (b) well data and (c) geochemical data. These data sets consist of various different supporting data sets which include well tops, checkshot data, biostratigraphy data, geophysical well logs, geological well reports, well logs, geochemical well reports, vitrinite reflectance data and Rock Eval pyrolysis data. The various data sets will be described in more detail below.

3.2.1 SEISMIC DATA

2 D seismic sections were purposefully selected in a north-south (long axes) and east west (short axes) direction creating a grid network covering the study area (Figure 14). A list of the seismic data used is listed below (Table 1).

Seismic line Names in Working Area	
E – W Lines	N – S lines
A76-10	K91-410
K91-415	A78-013
K89-019	A81-67
K92-119	A81-67A
K89-016	A81-67B
A87-027	A81-67C
A87-026	A81-67D
A76-008	A81-67E
A76-001	K92-134
K89-015	K89-023
A84-023	K89-011
K89-013	K89-021
K89-012	A88-083
A81-028	
K92-113	
K89-010	

Table 1: List of seismic lines used during the study

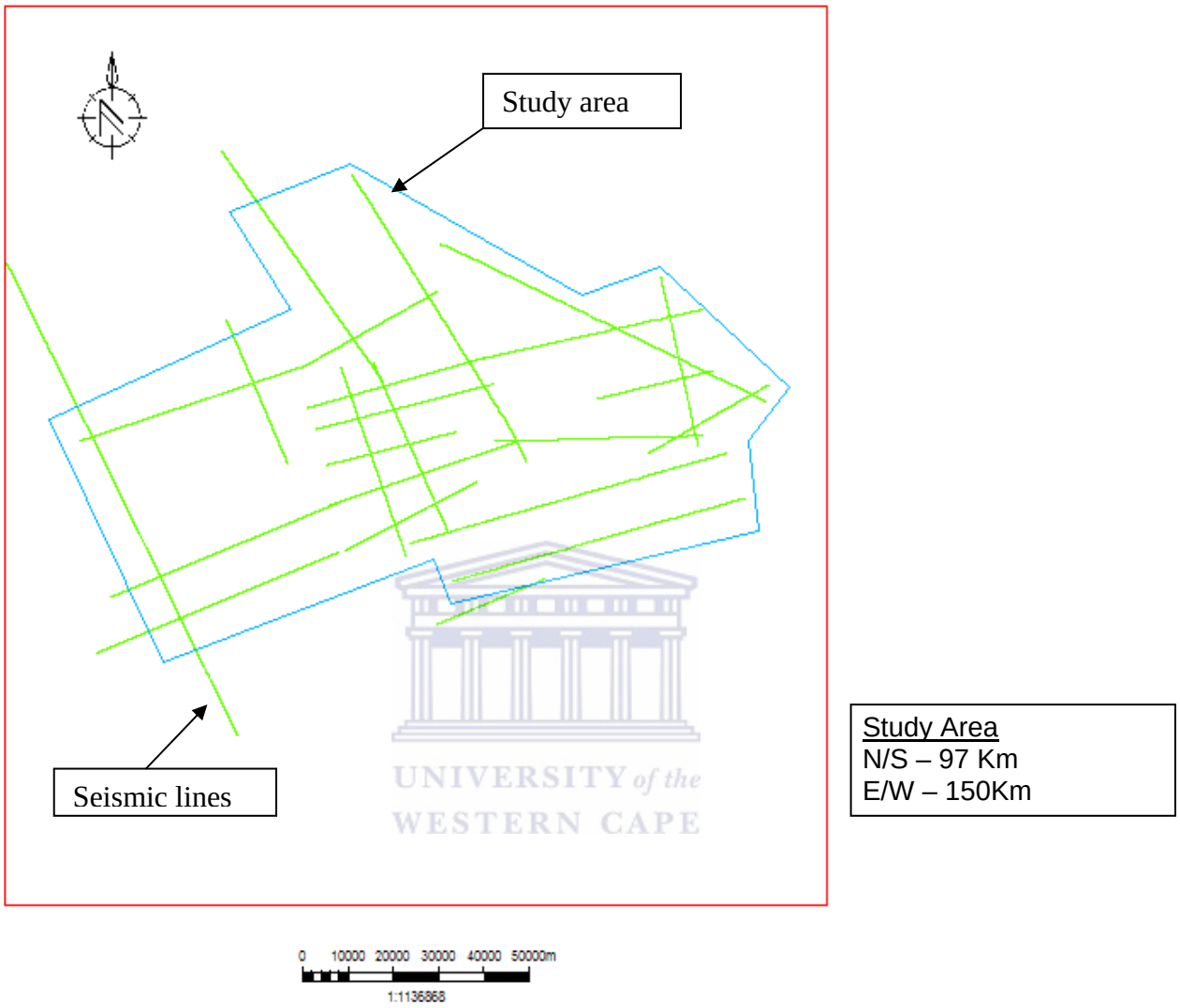

Figure 14: The spatial relationship of the seismic sections within the outlined study area.

3.2.2 WELL DATA

The following data sets are all included in the well data:

- Geological well reports
- Geological well logs
- Well tops
- Checkshot data
- Temperature data
- Geophysical well log

The wells were selected in an approximately east to west transect to better track the evolution of the post-rift prograding system of the Orange Basin.

3.2.2.1 GENERAL WELL INFORMATION

PROXIMAL

DISTAL

WELL NAME	X COORDINATE	Y COORDINATE	KB (m)	TOP DEPTH (m)	BOTTOM DEPTH (m)	WATER DEPTH (m)
A-A1	682923.00	6544478.00	29.9	235.3	3805	235.3
A-L1	666842.00	6535656.00	25	263	3277	263
A-I1	631290.00	6534527.00	25	371	4254	371
K-F1	596082.00	6539477.00	22	484	3798	484
K-H1	588028.00	6565654.00	25	342	4260	342

Table 2: General well information from well reports.

3.2.2.2 GEOLOGICAL SUMMARY OF WELL (Table 2, Figure 28)

Well A-A1

Trapping mechanism: Structural

Chief lithology: Predominantly sandstones, siltstones, shale and mudstones with occasional thin limestone present in the upper succession and thin beds of lignite occurring in the deeper succession.

Status: Dry well

No hydrocarbons were encountered in the well although reservoir quality was good within sandstones developed above 1800 meters but most of the shale's above 1800 meters would not make adequate cap rocks. The petroleum system can therefore not hold any hydrocarbons.

Well A-I1

Trapping mechanism: Roughly north-south trending elongated anticlinal structure with stacked multidomal closure.

Chief lithology: Predominantly sandstones

Status: Dry well

At this well location the reason for a dry well is based on the fact that no potential source rock was intersected.

Well A-L1

Trapping mechanism: Structural fault compartment with stacked fault closure.

Chief lithology: Predominantly sandstones

Status: Dry well with poor gas shows

Poor development and quality of the source rock in this vicinity is given as the main reason for having a dry well with poor gas shows. This poorly developed source rock could be attributed to the presence of numerous Cretaceous to early Tertiary intrusions playing a role in maturing source rocks to the gas phase as well as breaching traps that might have been filled with hydrocarbons prior to the intrusions.

Well K-F1

Trapping mechanism: Structural and stratigraphic trapping within a lowstand wedge in 15C sequence and within the sequence 15B basin floor fan 3 mounded complex.

Chief lithology: Sequence consists of mainly claystone with minor sandstone development.

Status: Dry well

Poor reservoir (sandstone) quality is the given as the main reason why the well is dry.

Well K-H1

Trapping mechanism: Stratigraphic traps in prograding lowstand systems tracks

Chief lithology: Predominantly argillaceous sediments with minor sandstone development.

Status: Dry well

At well location K-H1 the reason for a dry well is attributed to the poor development of source rocks as well as reservoir sandstones.

3.2.2.3 WELL TOPS

The well-top data used indicated the estimated depth of the various sequence boundaries. The table below (Table 3) indicates the well top data in both depth and two-way time of all the mapped surfaces for all the wells.

Well name	Surfaces	X	Y	Z (m)	TWT
A-A1	22At1	682923.00	6544478.00	-350	
A-A1	16At1	682923.00	6544478.00	-790	805.9
A-A1	15At1	682923.00	6544478.00	-1244	1116.8
A-A1	14At1	682923.00	6544478.00	-2624	1875.1
A-A1	13At1	682923.00	6544478.00	-3380	2203.3
A-A1	6At1	682923.00	6544478.00	-3790	2361.2
A-L1	22At1	666842.00	6535656.00	-316	
A-L1	16At1	666842.00	6535656.00	-1156	
A-L1	15At1	666842.00	6535656.00	-1634	1409.5
A-L1	14At1	666842.00	6535656.00	-3105	2192.6
A-I1	18At1	631290.00	6534527.00	-520	
A-I1	17At1	631290.00	6534527.00	-685	
A-I1	16At1	631290.00	6534527.00	-1852	1757.6
A-I1	15At1	631290.00	6534527.00	-2250	2016.4
A-I1	14At1	631290.00	6534527.00	-3825	2865.9
K-F1	16At1	596082.00	6539477.00	-1753	1838.6
K-F1	15At1	596082.00	6539477.00	-3396	2960.0
K-H1	22At1	588028.00	6565654.00	-572	1938.8
K-H1	16At1	588028.00	6565654.00	-2018	2029.7
K-H1	15At1	588028.00	6565654.00	-2660	

Table 3: Well top data for all the wells.

3.2.2.4 CHECKSHOT DATA

The check shot data represents the velocities at which sound travels through the sediments at various depths within the wells (Table 4), and is used to tie the seismic data to the measured geophysical data of the wells.

WELL NAME	X	Y	MD (m)	TWT
A-A1	682923.00	6544478.00	575	628
A-A1	682923.00	6544478.00	1190	1072
A-A1	682923.00	6544478.00	1400	1204
A-A1	682923.00	6544478.00	1790	348.6
A-A1	682923.00	6544478.00	1990	1537
A-A1	682923.00	6544478.00	2200	1639
A-A1	682923.00	6544478.00	2400	1752
A-A1	682923.00	6544478.00	2595	1824
A-L1	666842.00	6535656.00	1000	988
A-L1	666842.00	6535656.00	1150	1092
A-L1	666842.00	6535656.00	1249	1158
A-L1	666842.00	6535656.00	1349	1224
A-L1	666842.00	6535656.00	1450	1288
A-L1	666842.00	6535656.00	1550	1348
A-L1	666842.00	6535656.00	1646	1408
A-L1	666842.00	6535656.00	1750	1472
A-L1	666842.00	6535656.00	1850	1524
A-L1	666842.00	6535656.00	1949	1584
A-L1	666842.00	6535656.00	2050	1636
A-L1	666842.00	6535656.00	2150	1688
A-L1	666842.00	6535656.00	2249	1738
A-L1	666842.00	6535656.00	2349	1796
A-L1	666842.00	6535656.00	2450	1848
A-L1	666842.00	6535656.00	2550	1902

A-L1	666842.00	6535656.00	2650	1952
A-L1	666842.00	6535656.00	2750	2004
A-L1	666842.00	6535656.00	2849	2056
A-I1	631290.00	6534527.00	1000	1078
A-I1	631290.00	6534527.00	1300	1330
A-I1	631290.00	6534527.00	1600	1570
A-I1	631290.00	6534527.00	1900	1782
A-I1	631290.00	6534527.00	2200	1978
A-I1	631290.00	6534527.00	2400	2108
A-I1	631290.00	6534527.00	2600	2222
A-I1	631290.00	6534527.00	2800	2328
A-I1	631290.00	6534527.00	2900	2366
A-I1	631290.00	6534527.00	3093	2472
A-I1	631290.00	6534527.00	3202	2532
A-I1	631290.00	6534527.00	3300	2582
A-I1	631290.00	6534527.00	3400	2632
A-I1	631290.00	6534527.00	3502	2682
A-I1	631290.00	6534527.00	3599	2734
A-I1	631290.00	6534527.00	3703	2790
A-I1	631290.00	6534527.00	3798	2840
A-I1	631290.00	6534527.00	3902	2898
A-I1	631290.00	6534527.00	4000	2948
A-I1	631290.00	6534527.00	4100	2994
A-I1	631290.00	6534527.00	4200	3044
K-F1	596082.00	6539477.00	1791	1890
K-F1	596082.00	6539477.00	1913	1976
K-F1	596082.00	6539477.00	2028	2078
K-F1	596082.00	6539477.00	2128	2145
K-F1	596082.00	6539477.00	2218	2211
K-F1	596082.00	6539477.00	2323	2283
K-F1	596082.00	6539477.00	2418	2347

K-F1	596082.00	6539477.00	2518	2415
K-F1	596082.00	6539477.00	2588	2465
K-F1	596082.00	6539477.00	2743	2565
K-F1	596082.00	6539477.00	2828	2623
K-F1	596082.00	6539477.00	2908	2677
K-F1	596082.00	6539477.00	3008	2741
K-F1	596082.00	6539477.00	3128	2815
K-F1	596082.00	6539477.00	3213	2861
K-F1	596082.00	6539477.00	3278	2897
K-F1	596082.00	6539477.00	3353	2947
K-F1	596082.00	6539477.00	3424	2989
K-F1	596082.00	6539477.00	3503	3033
K-F1	596082.00	6539477.00	3578	3079
K-F1	596082.00	6539477.00	3653	3121
K-H1	588028.00	6565654.00	1875	1850
K-H1	588028.00	6565654.00	2075	1992
K-H1	588028.00	6565654.00	2275	2132
K-H1	588028.00	6565654.00	2475	2260
K-H1	588028.00	6565654.00	2675	2388
K-H1	588028.00	6565654.00	2875	2510
K-H1	588028.00	6565654.00	3075	2628
K-H1	588028.00	6565654.00	3175	2688
K-H1	588028.00	6565654.00	3275	2746
K-H1	588028.00	6565654.00	3375	2802
K-H1	588028.00	6565654.00	3475	2856
K-H1	588028.00	6565654.00	3575	2917
K-H1	588028.00	6565654.00	3675	2977
K-H1	588028.00	6565654.00	3775	3033
K-H1	588028.00	6565654.00	3875	3089
K-H1	588028.00	6565654.00	3975	3201
K-H1	588028.00	6565654.00	4175	3255

Table 4: Checkshot data for all the wells.

3.2.2.5 BOREHOLE TEMPERATURE DATA

The borehole temperature data represented below (Table 5) indicate temperature measurements taken at various depths with the five wells.

Well name	Depth (m)	Borehole Temperature °C
A-A1	1116	39
A-A1	2587	71
A-A1	3352	101
A-A1	3802	104
A-A1	2804	121
A-A1	3802	118
A-L1	3277	127
A-I1	2947.5	80
A-I1	4254	127
K-F1	3152	92.8
K-F1	3750	120.3
K-H1	4239	140.83

Table 5: Borehole temperature data for all the wells.

3.2.3 GEOCHEMICAL DATA

The following data sets were consulted:

- Geochemical reports
- Rock eval data
- Vitrinite reflectance data

3.2.3.1 GEOCHEMICAL WELL REPORTS

The geochemical well reports generally include a source rock summary tables, source rock summary interpretation notes, source rock summary logs, interpretation tables, vitrinite reflectance plots and Rock Eval (T-max) plots. The source rock summary table indicates the approximate depth and quality of the source rock at the specific well location. The source rock summary interpretation notes indicate the data used and the interpretations made to determine the maturity and the quality of the source interval. The source rock summary log indicates the various log responses at the source rock intervals. The interpretation table indicates the total generation potential, hydrocarbon potential and organic matter types, maturation and bulk maturation potential data that were used in doing the source rock interpretation. The vitrinite reflectance plot indicates the vitrinite reflectance plotted against depth. The T-max plots were also plotted against depth indicating regions in the oil or gas window.

3.2.3.2 ROCK EVAL DATA

This data is accomplished through the process of Rock Eval pyrolysis. Rock Eval pyrolysis is a process whereby source rock samples are analysed and evaluated to determine the organic matter type as well as the degree of maturity. The method consists of a pulverized source rock sample placed in an inert atmosphere where it is progressively heated (Tissot and Welte, 1978). The process results in the release of free hydrocarbons which are already present in the rock under moderate temperatures and is graphically represented as a peak referred to as the S1 peak (Figure 15) (Tissot and Welte, ibid).

The temperature is then further increased resulting in the thermal cracking of the nonvolatile organic matter graphically represented as the S2 peak of which the peak is referred to as the Tmax (Figure 15) representing the stage where peak hydrocarbon generation has been reached during pyrolysis. (http://wwwodp.tamu.edu/publications/tnotes/tn30/tn3011.htm).

The last measurement is illustrated as the S3 peak (Figure 15) represents the amount of carbon dioxide produced during the pyrolysis of the kerogen giving an indication of the amount of oxygen within the kerogen (http://wwwodp.tamu.edu/publications/tnotes/tn30/tn30 11.htm)

These three measurements together with the total organic carbon measurement of the source rock are used to calculate the Hydrogen Index as well as the Oxygen Index which is subsequently used to determine the original source of the organic matter (Kerogen type) whether it is land or marine derived (Tissot and Welte, 1978).

Tmax data can also be used as a maturation indicator that could be correlated with vitrinite reflectance. The approximate maturity boundaries for oil generation is less then 435 degrees Celsius (immature), 435 to 460 degrees Celsius (mature) and more then 460 degrees Celsius (post mature) (Miles, 1994). Tmax measurement has however got some limitations such as being dependent on the type of organic matter, whether the oil had been migrated or whether samples has been contaminated through mud additives. Organic samples with a small S2 peak of less then 0.2 mg HC / g TOC also provide a limiting factor for the Tmax as these measurements are not reliable (Peters, 1986). Tmax values are lowered due to contamination of oil and water based mud additives as well as oil that have been migrated.The pitfalls in calibrating Tmax with vitrinite reflectance comes about when variations in Tmax of up to 10% occurs due to low maturity source intervals with lower vitrinite reflectance values are dominated by recycled organic matter (Peters, 1986). Tmax values also vary at the threshold of oil generation amongst different source rocks (Peters, 1986). The calibration of Tmax with vitrinite reflectance is also limited when a marceral called resinite is present in the organic matter. Typically found in land derived sediments with a lower then 0.6 % vitrinite reflectance the marceral causes a high Tmax values (Peters, 1986).

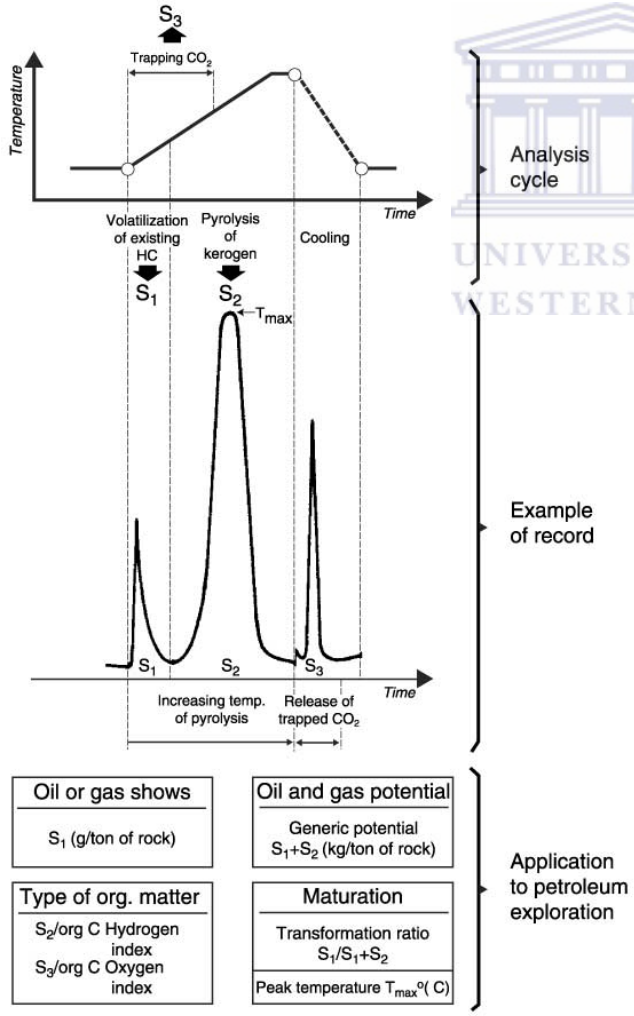

Figure 15: Rock Eval pyrolyses diagram. (Tissot and Welte, 1978)

Raw Rock Eval data for all the wells included:

- T-max values in degree Celsius at various depths for all the wells in the study area
- S1, S2 and S3 values at various depths for all the wells in the study area
- Total Organic Carbon (TOC) values at various depths for all the wells in the study area.
- Calcite and dolomite percentages at various depths for all the wells in the study area.

CALCULATING HYDROGEN INDEX (HI) AND OXYGEN INDEX (OI)

S1 = Fraction of original genetic potential which has been effectively transformed into hydrogen (Tissot and Welte, 1978).

S2 = Residual potential which has not yet been used to generate hydrocarbon (Tissot and Welte, ibid).

S3 = Represents the amount of carbon dioxide produced during the pyrolysis of kerogens indicating the amount of oxygen in the kerogen. Used to calculate the Oxygen Index (OI)
(Pimmel and Claypool, 2001)
http://www-odp.tamu.edu/publications/tnotes/tn30/tn30

S1 + S2 expressed in Kg hydrocarbons per ton of rock is therefore an evaluation of the genetic potential of the hydrocarbons (Tissot and Welte, ibid).

Hydrogen Index = (HI = (S_2 x TOC/100)

The HI is used to characterize the origin of organic matter. Marine derived organic matter, containing marine organisms are generally composed of lipid- and protein-rich organic matter where the ratio of H to C is higher compared to land derived organic matter containing land plants that is carbohydrate-rich and the H to C ratio is lower than marine derived organic matter.
(Pimmel and Claypool, 2001)
http://www-odp.tamu.edu/publications/tnotes/tn30/tn30

Oxygen Index = (OI = (S_3 x TOC/100)

The OI is used to compare the ratio of Oxygen to Carbon, which is high for land derived organic matter (land plants).
(Pimmel and Claypool, 2001)
http://www-odp.tamu.edu/publications/tnotes/tn30/tn30

3.2.3.3 VITRINITE AND VITRINITE REFLECTANCE DATA

Vitrinite forms part of three main groups of macerals (original organic source material) namely Liptinite, Vitrinite and Inertinite that makes up kerogen in organic rich rocks (source rocks) (Tissot and Welte, 1978). Kerogen refers to the insoluble compounds of organic matter in organic rich sedimentary rocks (Tissot and Welte, 1978). The macerals groups mentioned above is listed in the order of increasing reflectance. These kerogen types can be identified based on the optical properties such as color, fluorescence and reflectance (Gluyas and Swarbrick, 2004). The oil prone liptinite is derived mainly from algal material and has high hydrogen to carbon and low oxygen to carbon ratio (Gluyas and Swarbrick, 2004). Liptinite fluoresces under ultraviolet light. Vitrinite is primarily sourced from higher plant debris and mainly generate gas.

Vitrinite has a low ratio of hydrogen and high ratio of oxygen relative to carbon and does not fluoresce under ultravoiler light (Gluyas and Swarbrick, 2004). However it is increasingly reflective with increasing maturity. It is this property that allows for vitrinite reflectance to be used as a likely maturity indicator. Four stages of maturity are identified with reference to the general values of vitrinite reflectance. Tissot and Welte, 1978 classified the following,

Diagenesis stage: The source rock is still immature and vitrinite reflectance is from 0.5 to 0.7%.

Catagensis stage: Main zone of oil generation with a vitrinite reflectance is more then 0.5 to 0.7 and less then 1.3% and a wet gas and condensate zone with a vitrinite reflectance of more then 1.3% but less then 2%

Metagenisis stage: Dry gas zone where vitrinite reflectance is more the 2%

Although widely used, the vitrinite reflectance technique has some limitation and is outlined as follows. Vitrinite is abundant in type III Kerogen where is can be use as a maturity indicator, as the vitrinite marceral has a comparable composition to that of the type III kerogen and could therefore be said to have a similar reaction to increasing temperature (Tissot and Welte, 1978). Vitrinite is not so abundantly found in Type I and II kerogens and could even be absent in Type I source rock (Tissot and Welte, 1978) making the technique ineffective in determining all kerogen types. The vitrinite reflectance values should also not be used directly as a maturity indicator due to the fact that different source rocks could have undergone the same thermal history and would therefore have reached the same vitrinite reflectance but not necessarily the same maturity in terms of oil and gas generation (Tissot and Welte, 1978). This is due to vitrinite marcerals having similar composition to Type III kerogen and therefore following a similar trend and rate of transformation with increasing temperature while vitrinite in Type I and II kerogens follow a different rate of transformation.

3.2.4 GEOPHYSICAL WELL LOGS

The geophysical logs used in the study include the gamma ray, spontaneous potential, porosity, density, deep resistivity and sonic log.

3.2.4.1 INTRODUCTION TO PETROPHYSICAL WELL LOGS

The following well log descriptions are taken from Rider (1996).

Caliper log

The caliper tool measures the variation in borehole diameter with depth. The measurements are made by two arms linked to a cursor of variable resistance pushing against the borehole wall. Any movement of the caliper arms is translated into movement of the cursor and a subsequent variation in electrical output, which is translated into diameter variations. The response of the formation to drilling can indicate the lithological properties of the formation, for example a borehole with a larger diameter than the drill bit used is referred to as washed out or caved and indicates relatively soft and unconsolidated sediment usually shale, organic rich shales and coals. A decrease in borehole diameter is usually associated with a build-up of mud cake, which in turn is an indicator of good permeability. The zone of apparent decrease in the borehole size can therefore be used to indicate the limits of a potential reservoir zone.

Sonic log

The sonic log measures the capacity of the formation (which varies with lithology and rock texture) to transmit sound waves. The sonic tool consists of a transmitter and receivers placed at a known distance from each other. Transmitters translate an electric signal into an ultrasonic vibration and receivers convert the pressure waves into electromagnetic signals, amplified to provide the logging signal.

“Quantitatively the log is used to evaluate porosity in liquid filled holes” (Rider, 1996) and can also be used as an aid to seismic interpretation providing interval velocities and velocity profiles. Qualitatively the sonic log assists in identifying lithology and in indicating source rocks as the log is sensitive to slight changes in texture such as porosity in both sand and shale.

Resistivity log

The resistivity log is a measure of the resistance of the formation to a passing electric current. The basic arrangement of the resistivity tool involves passing a current between two electrodes in the earth and measuring the drop between them which provides the resistivity of the formation. As the resistivity of the formation is mostly dependent on the type of fluid in the pore spaces the use of the resistivity log is principally to identify hydrocarbons within the pores. Hydrocarbons are very resistive while salt water shows a low resistivity; this distinction can be used to identify hydrocarbon-bearing sands in the subsurface. Qualitatively the resistivity log can be used to relate to sediment textures for example, if the porosity of a formation increases or decreases so does the amount of fluid present and thus the subsequent degree of resistance in the formation. A decrease in porosity normally results in an increase in resistivity.

Gamma ray (GR) logs

The gamma ray log recorded by the gamma ray tool measures the natural radiation originating from the naturally occurring uranium, thorium and potassium found in most igneous, metamorphic and to some extent sedimentary rocks (mostly in shale). Quantitatively the gamma ray log is used to derive the shale volume and for well-to-well bed correlation when interpreting facies change and sequences.

Density log

The density log allows derivation of the overall density of the formation, which includes both the density of the solid matrix and the density of the fluids within the pores. "The density log is quantitatively used to calculate porosity and indirectly hydrocarbon density while it is qualitatively useful as a lithology indicator" (Rider, 1996). The tool operates by bombarding the formation with gamma rays and measures the decrease between the source and detector of the density tool. The degree of scattering of the gamma ray is related to the amount of electrons present within the formation (electron density), which is related to the overall density of the formation.

Neutron porosity

The neutron tool consists of a neutron source, which bombards the formation with neutrons with two detectors measuring the loss of energy as the neutrons pass though the formation. The log is quoted in terms of neutron porosity units, which are related to the formation's hydrogen index, which in geological terms are supplied by water. Quantitatively the neutron log is used to measure the porosity and qualitatively it is used as an excellent discrimination between oil and gas.

Spontaneous potential (SP) log

The SP tool measures the natural potential difference between two electrodes placed in the borehole and at the surface. A current is created when solutions of different salinity concentrations are in contact by two principal electrochemical effects, diffusion (liquid junction potential) and shale potential. Diffusion potential occurs when solutions of different salinity are in contact through a porous medium (possibly sands). These two solutions mix by ionic diffusion where the smaller and more mobile Cl^- ions mix faster than the slower larger Na^+ creating a charge separation as the ions mix at unequal rates.

“A potential is created between the negatively charged dilute solution with excess Cl^- and the positively charged concentrated solution with excess Na^+ “ (Rider, 1996). The shale potential occurs when the same solution are in contact through a semi-permeable membrane normally shales. The negatively charged clay minerals within the shale act as a semi-permeable membrane preventing the negatively charged Cl^- from entering the dilute solution while the positively charged Na^+ are allowed to diffuse into the dilute solution creating a positive charge with a corresponding negative charge in the concentrate solution. Therefore in a situation where the mud filtrate is less saline than the formation water the mud filtrate will become negatively charged as a result of the diffusion potential across a sandstone bed acting as a permeable membrane while across a semi-permeable membrane (shale) the mud filtrate will become positively charged through the shale potential. The main use of the SP log is to calculate the formation water resistivity and to indicate permeability.

3.3 METHODOLOGY

Subsequent to reviewing the data, the first method was the seismic interpretation of all major erosional unconformities based on the sequence stratigraphic classification of Brown et al. (1995) and recognizing the structural features of the post rift Orange Basin succession. Well-top data was used to indicate the depth of the various sequence boundaries while the check shot data was used to create a velocity model allowing for depth conversion of the various horizons. The wells used include well A-A1, A-L1, A-I1, K-F1 and K-H1, respectively named from proximal to distal and selected in approximately an east to west transect. The geophysical logs of each well was used to characterize the borehole rock properties and include the gamma ray logs, spontaneous potential logs, porosity logs, density logs, deep resistivity logs and sonic logs. The borehole temperature and vitrinite reflectance data were used as calibration parameters in the petroleum system modeling of the Orange Basin. Both the seismic interpretation and well correlations were done using the Petrel software package. Subsequent to the seismic interpretation and well correlation the three-dimensional petroleum system modeling was conducted using the PetroMod 3D software package.

3.3.1 CONCEPTUAL MODEL

The following steps will be outlined in point form:

The Petrel software package is a fully integrated geological, geophysical and reservoir engineering software package allowing for the integration of all these data. In this study the geological and geophysical domains of Petrel were utilized for interpretation and visualisation of the seismic data and for the correlation of geological units. The workflow was as follow:

SEISMIC INTERPRETATION

Import seismic data in ASCII format.

- Create a new Petrel project.
- Import seg-y data into project.
- Cross-check seismic line location with old seismic maps to see that lines plot in correct position.

Import well locations

- Importing well coordinates and general well information.
  - Well name.
  - Geographic coordinates.
  - Start and total depth.
  - Meters below Kelly bushing.
- Choose correct well top data to develop a working well top data set.
- Importing well top data to their various well locations.

Seismic interpretation

- Interpretation of all the major post rift unconformities (6At1 to seafloor).
- Correct for misties through bulk shifting and reinterpretation.
- Complete the interpretation of all the major seismic horizons

Surface creation

- Created horizon surfaces over the study area through interpolating between seismic interpretations for all the interpreted post-rift unconformities and seafloor.

Velocity model

- Filtered all the errors from the checkshot data.
- Created a database of all the correct checkshot data of all the wells.
- Importing the interval velocities into Petrel.
- Creating a velocity model using the velocity model tool of Petrel.

Depth conversion

- Depth converted surfaces using the interval velocities from the velocity model.
- The depth-converted surfaces were then converted using the “convert to separate surface” function from Petrel to allow for modification of the surfaces.
- Surfaces were then exported as Irap classic grids (Binary and Z-map+grid ASCII) files.

WELL CORRELATION

Quality control of raw well log data.

- Select the relevant logs used in the study (Gamma Ray (GR) log, Density log, Sonic log, Resistivity log and Spontaneous Potential (SP) logs).
- Select the most complete logs (Logs that run the deepest) for each of the wells.
- Create database in Excel of all the wells plotted, for example the GR logs of all the wells which in some cases are separated and therefore found at different depths, to examine and remove any overlapping or defective data.
- Create a database containing the complete and corrected data.
- Then the Excel sheet was saved as a text file and imported into Petrel.
- This process was followed for all the logs used.

Importing well logs into Petrel

- Well locations were first loaded using the coordinates provided from the well reports, thus placing the wells in their correct geographic locations.
- Imported the petrophysical well logs (gamma ray, density, sonic and resistivity and spontaneous potential) as ASCII files to their relevant wells.
- Created a lithological database for all the wells, containing all the lithologies and their relevant depths using information from the well reports and the comparison of the main prognosed features and actual drilling results logs.
- Source rock which was only identified in three of the wells namely A-L1, K-F1 and K-H1 was represented on the well logs.
- Used this information to create lithology panels in Petrel.

- Created a time-stratigraphic panel based on the International Commission on Stratigraphy (ICS) 2001 providing the geological time scale.
- Used the paleontological summary logs and biostratigraphy tables to adjust the time-stratigraphy to fit the relative depths and ages of the Orange Basin unconformities.
- Commenced with the well log correlation.

Well log correlation

- Plot the well tops over the well log data identifying upliftment and erosional events.
- Study the well logs, particularly the GR log, and identify major sequences.
- Colour-filled the logs with their respective lithologies based on the log signal and the geological well logs.
- Correlating these sequences to each other.
- Cross-plotted strategic well logs to identify certain characteristics of the sequences for example cross-plotting the gamma ray and the neutron porosity log which indicate if the sequence is either a coarsening or fining upward sequence.

3.3.2 GEODYNAMIC MODEL

PetroMod is fully integrated, 1D, 2D and 3D petroleum system modeling software a product of Integrated Exploration Systems (IES). The software is a basin modeling tool, allowing professionals to reconstruct basins and the evolution of their petroleum systems thus helping to better understand the factors controlling hydrocarbon generation, migration and accumulation thereby reducing risk in petroleum exploration and production. This study conducted two separate models testing two different heat flows and include a rift-drift heat flow heat flow model (Figure 44 (A) (B)) and a constant heat flow model (Figure 45 (A) (B)). In the rift to drift model the assumption is made that there was a heat flow spike at the stage of rifting after which the heat flow decayed. The second model assumed a constant heat flow during the entire basin evolution.

INPUT DATA:

Importing/editing Surfaces

- Create a directory to save all the files of the PetroMod data.
- Link PetroMod to the file directory.
- Create a new 3D model.
- Personalize the newly created PetroMod project.
- Import the surfaces produced from Petrel into PetroMod as DAT files.
- Smoothing of the horizons (surfaces) in PetroMod SeisStrat.
    - Select each individual horizon and apply a smoothing factor to the entire horizon.
    - Larger artifacts were removed individually by selecting these areas and applying smoothing factors to those specific areas.
    - Export the smoothed surfaces as z-map ASCII files to the PetroMod data file.
    - Import the horizons in the project with the smoothed surfaces (Figure 16).

- Splitting horizon to differentiate source rock units.
    - o Split the 6At1 horizon at the base and top to include the Barremian Early Aptian source rock unit
    - o Split the 15At1 at the base of the horizon to include the Cenomanian - Turonian source rock unit.

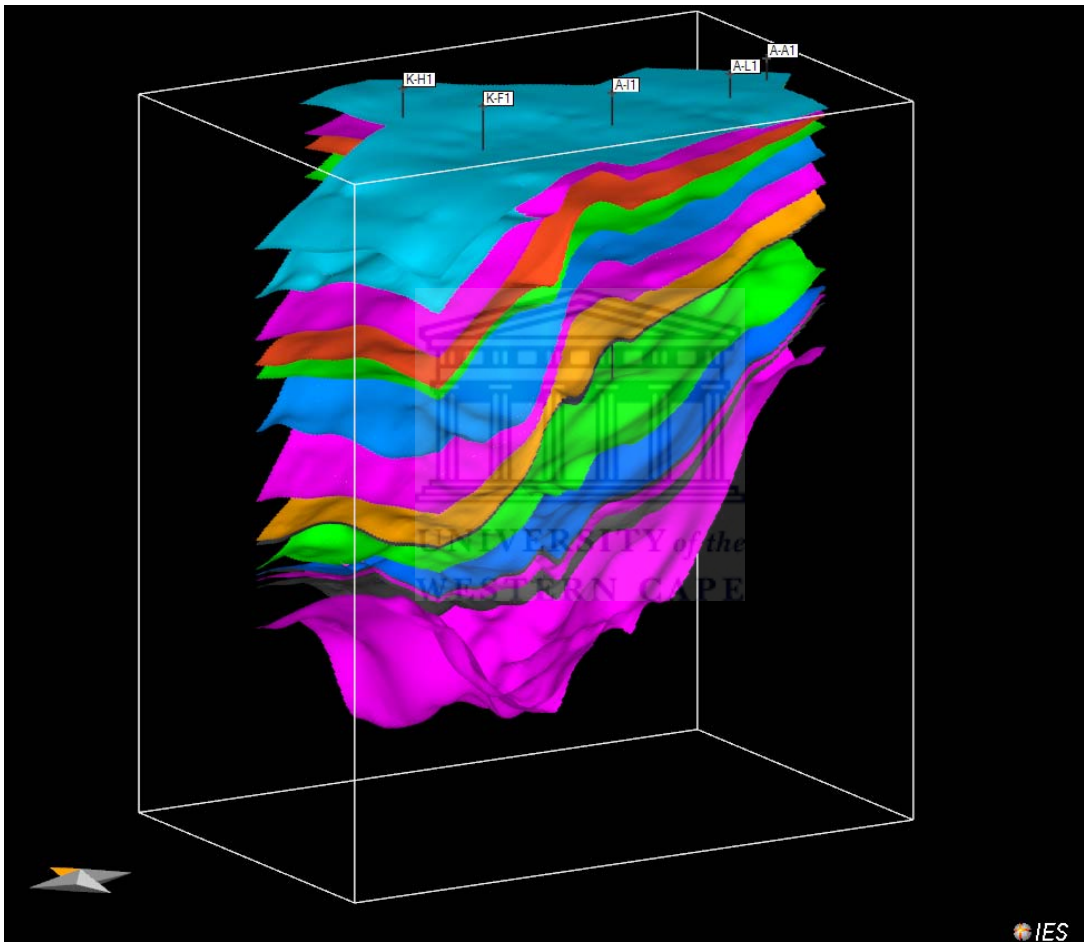

Figure 16: 3-Dimensional representation of imported surfaces in PetroMod IES version 10.

CALIBRATION OF DATA

- Entered the relevant data into PetroMod well editor:
  - Well name.
  - Well location (X - Y coordinates).
  - The meters below Kelly bushing.
  - Starting depth and ending depth.
  - Well tops.
- Saved the information and uploaded it into PetroMod Seistrat
- Entered the calibration data
  - Vitrinite reflectance data (from the vitrinite data sheets)
  - Borehole temperature data (from the geological well reports)

PETROMOD BASIN MODELING PARAMETERS (Figure 17)

- Age assignment
    - Assigned ages to the different horizons (Table 6) based on biostratigraphic and chronostratigraphic data taken from geological well reports and the geological time scale from (Gradstein et al., 2004).

- Facies assignment
    - Assigned facies to the horizons based on the information gathered from well reports, petrophysical well logs and geological well logs.

- Stretching (Beta factor)
    - A stretching factor of 1.5 was used based on the McKenzie-type lithospheric stretching model.

- Heat flow assignment
    - Assigned a heat flow distribution decaying from rifting 80mW to a present day 45mW. (after Welte et al., 1997)

- Sediment Water Interface Temperature (SWIT)
    - The SWIT was assigned automatically using PetroMod's built in global mean surface temperature.

- Erosional events

    - Identification of erosional events were based on Orange Basin literature in particular Brown et al. (1995) and the geological information gathered from the interpreted geological cross section where sections closer to shore were partially or completely removed due to erosion.
        - Two major erosional events were identified from the above source (Figure 17) (Table 6):
            - The first erosional event eroded down to the 17A sequence indicated by the 17A and 18A erosion maps, eroding a combined thickness of 960 meters off the 17 and 18A sequences.
            - The second erosional event indicated by 22A erosion map, eroded a thickness of approximately 421 meters off the 22A sequence
        - A set of maps was generated showing the extent and degree of erosion (eroded thickness in meters)
          (Figure 27 (A) (B) (C)).

Base of Sequence Unit	Source Rock	Deposition from (Ma)	Deposition to (Ma)	Erosional Event from (Ma)	Erosional even to (Ma)	Erosional Thickness (m)
Intra Tertiary		14.00	0.00			
Erosional event				20.00	14.00	421
22At1		55.00	20.00			
Erosional event				60.00	55.00	783
18At1		77.50	75.00			
Erosional event				60.00	55.00	178
17At1		80.00	77.50			
16Dt1		85.00	80.00			
16At1		89.00	85.00			
15At1		92.00	90.00			
Cenomonian - Turonian Source	Source Rock	92.70	92.00			
14At1		103.00	95.00			
13At1		110.65	103.00			
Upper Aptian Source	Source Rock	112.00	110.65			
6At1		112.50	112.00			
Lower Aptian Source	Source Rock	113.04	112.55			
6At1		117.50	113.04			

Table 6: Ages assigned to the mapped intervals and erosional events.

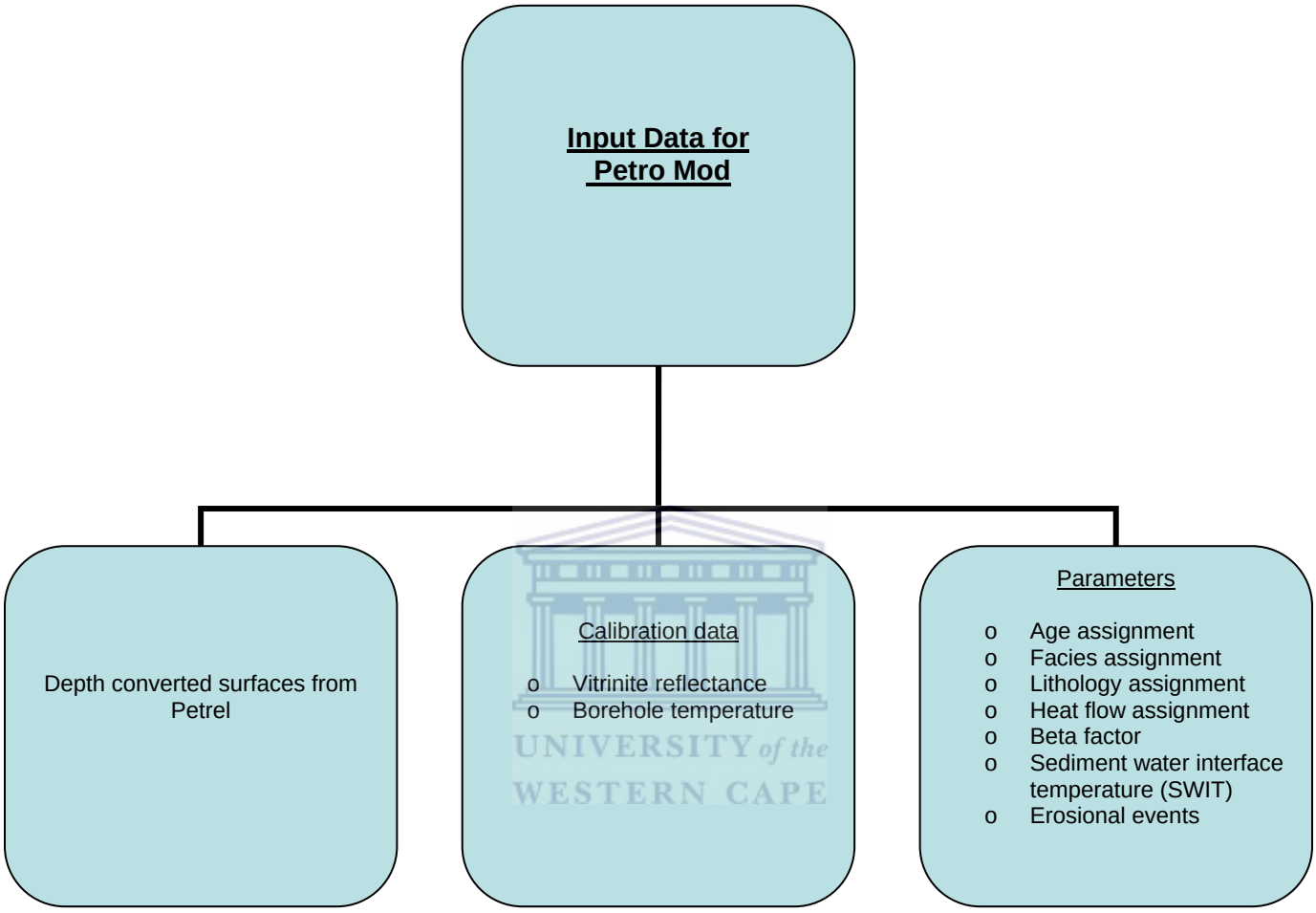

Figure 17: Summary of input data for the basin modeling PetroMod software.

OUTPUT DATA (Figure 18)

POST-EROSION MAPS

Post erosional maps were generated after the various erosional events were incorporated into the simulation modeling. These modeled units indicate the geometry of the sequences after erosion.

MAP OVERLAY FOR THE SOURCE ROCKS:

Several maps were generated based on the simulated results and include:

- Temperature Maps
    - The temperature overlay maps indicate areas of higher temperature and subsequent higher maturity, and areas of lower temperature and subsequent immature areas.

- Source Rock calibration overlay (Sweeney and Burnham, 1990)
    - Overlaying the vitrinite reflectance data and compartmentalizing the source rock into early oil/gas, main oil/gas and late oil/gas producing regions.

- Source Rock properties
    - This overlay incorporates the geochemical information given such as the HI, TOC values and the kinetic processes to divide the source rock into stages of transformation. The higher the transformation percentage the more mature the source rock and the lower the ratio the more immature the source rock.

3D MODEL

The final product was a fully integrated petroleum system model indicating the basin architecture and the predicted present day maturity of the source rocks.

The results and conclusions drawn from the study will provide more insight into the maturity of source rocks within the Orange Basin.

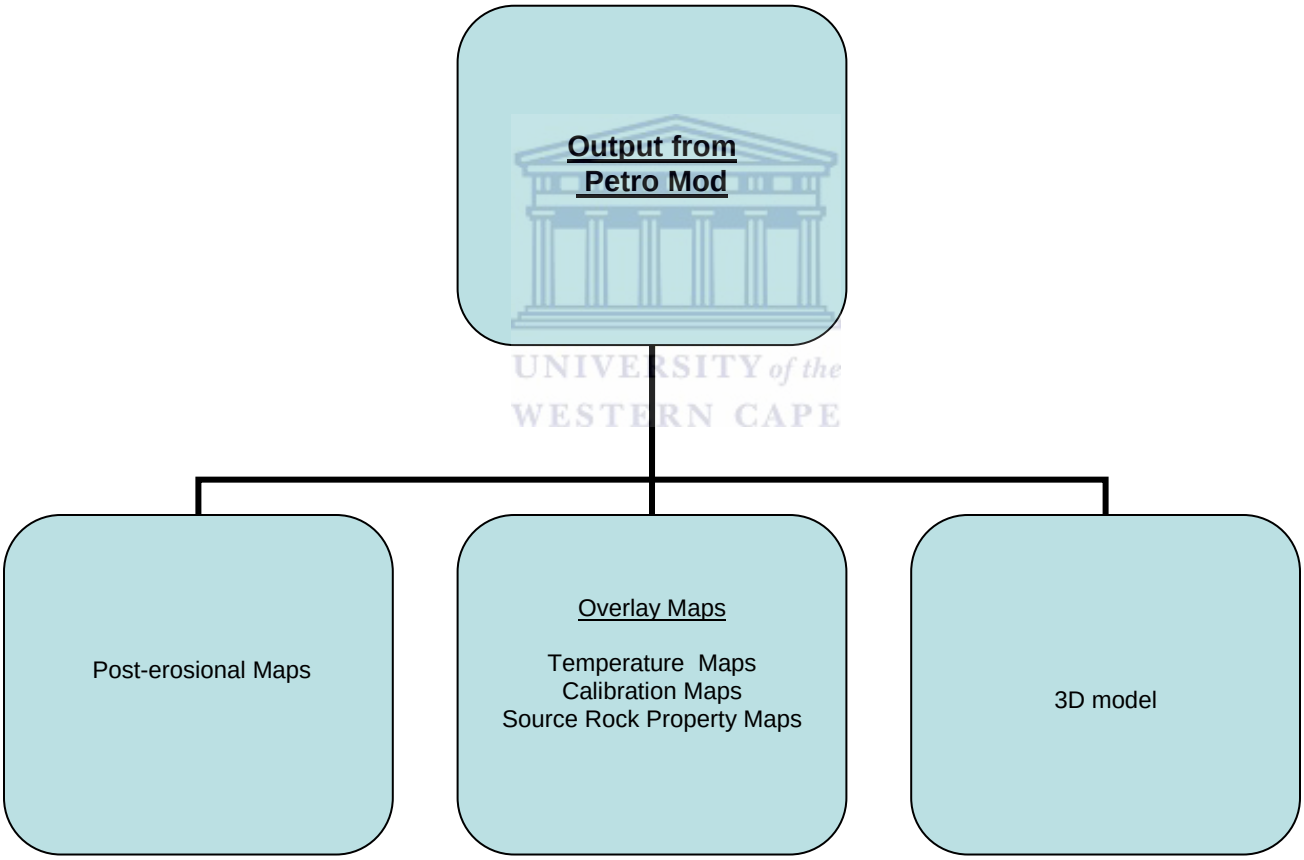

Figure 18: Summary of the output data for the basin modeling PetroMod software.

CHAPTER FOUR

4. RESULTS AND INTERPRETATION

This chapter outlines and illustrates the results attained throughout the study. The first section describes building the geological model through the processes of seismic interpretation and well correlation. The second section shows the results obtained from the basin modeling studies and source rock maturity simulations.

4.1 CONCEPTUAL MODEL

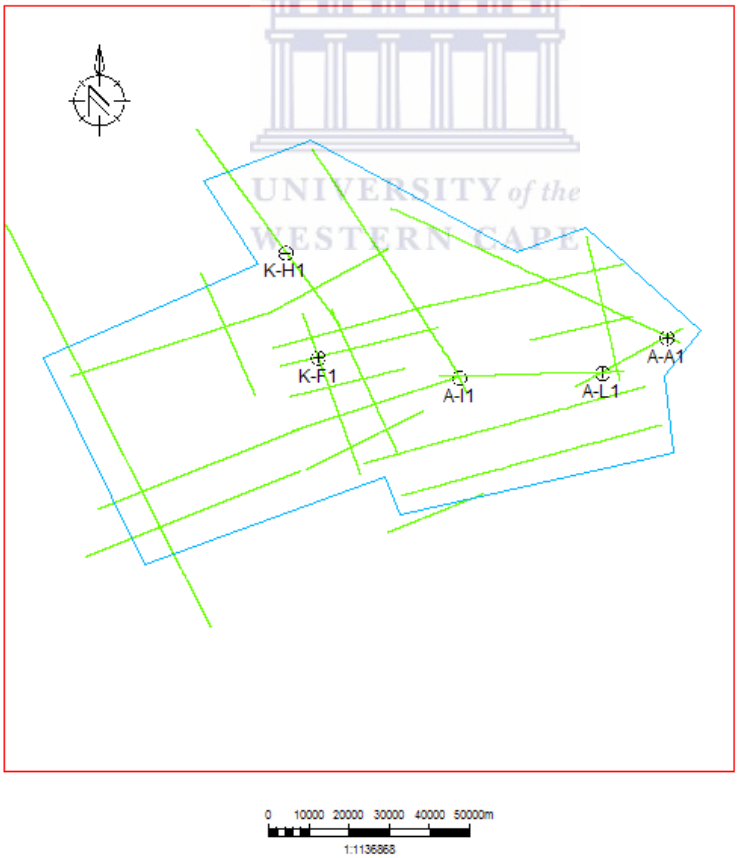

Figure 19. Location of wells and orientation of seismic lines in the study area

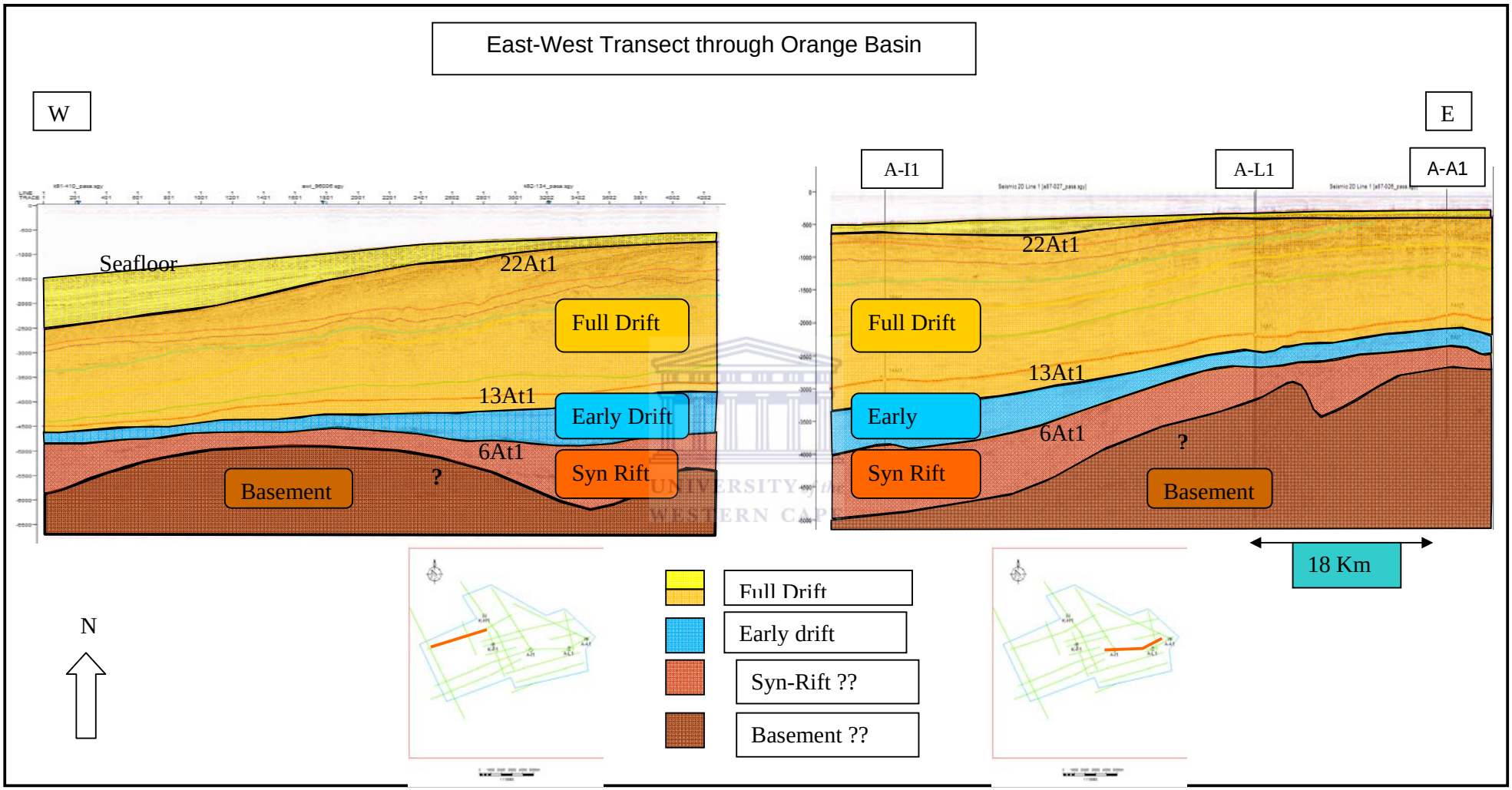

Figure 20. Geological interpretation of two 2 D seismic lines in an east west cross section through the Orange Basin to illustrate all the major unconformities mapped throughout the study area with well locations and well tops at the respective depths.

4.1.1 SEISMIC INTERPRETATION

Figure 21. Seismic line through well A-A1, A-L1 and A-I1 indicating the termination of the 17At1 and 18At1 unconformities against the 22At1 unconformity.

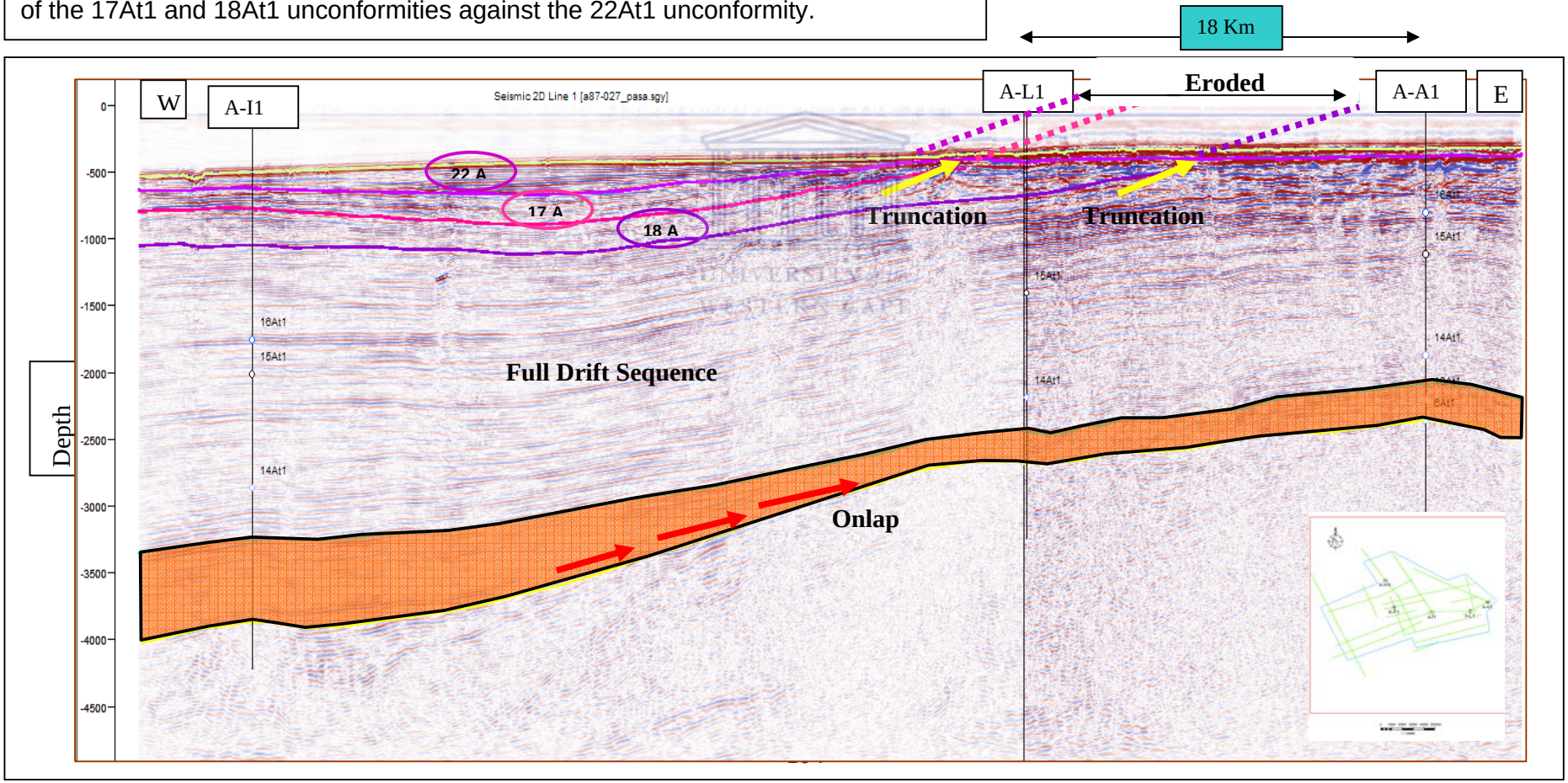

Figure 22. Inline K89-012 to illustrate the fault development along the shelf break and prograding sequences above 13At1.

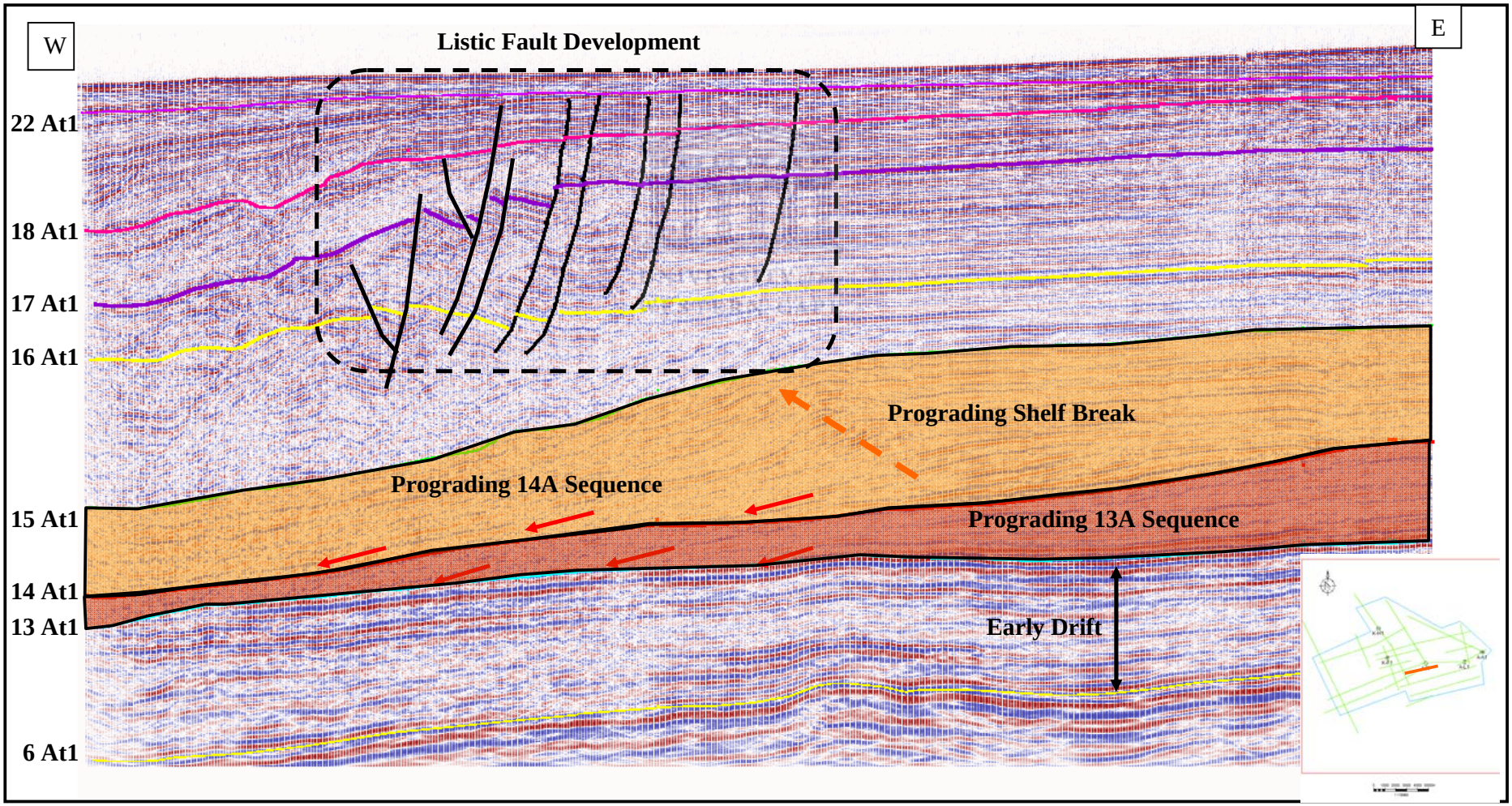

Figure 23. Inline K92-113 demonstrating the prograding packages of the Late Cretaceous pre 22At1 interval.

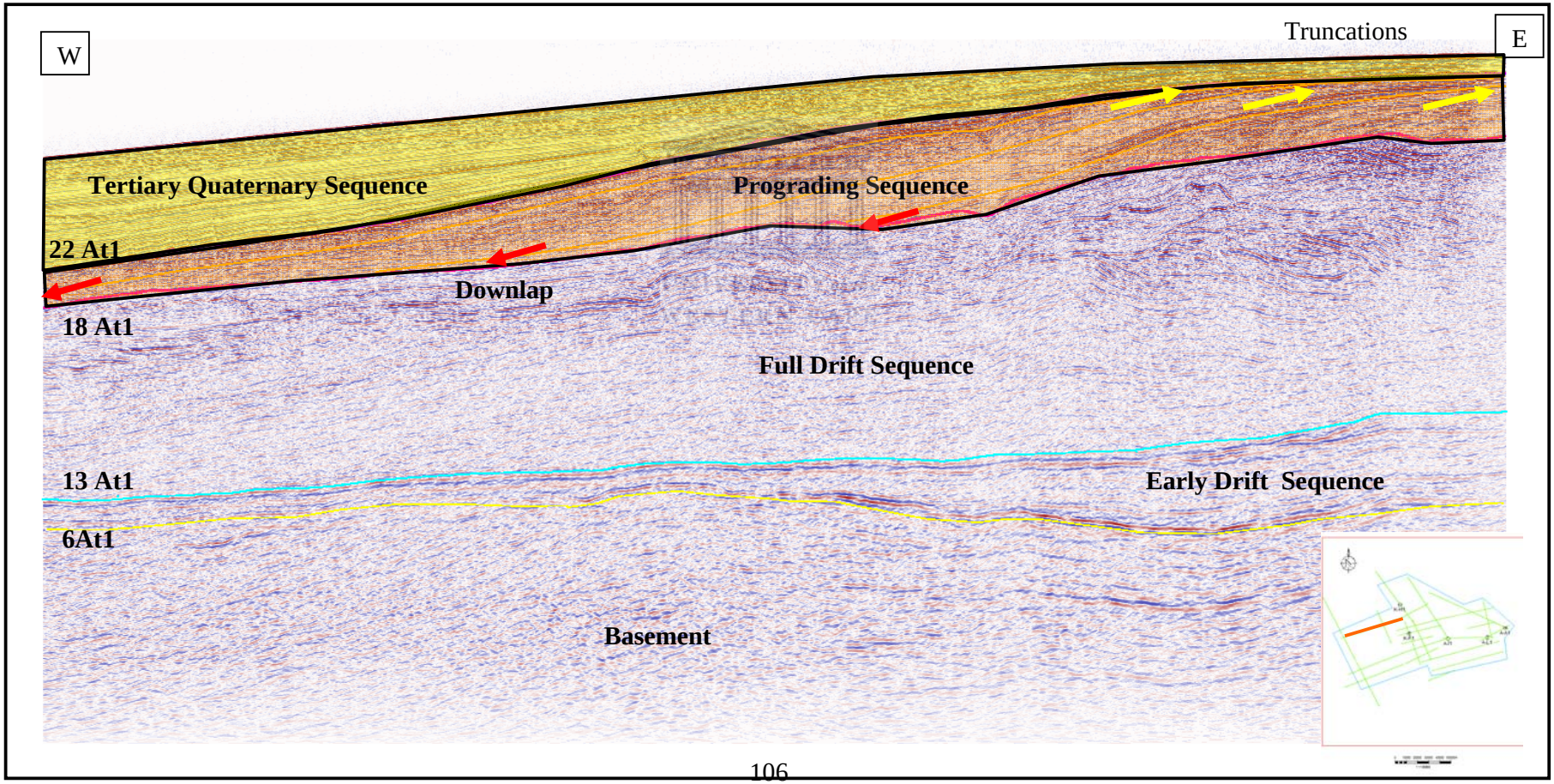

Seismic interpretation was conducted on a grid of 2D data, which ties all five wells together (Figure 19). The interpretation was done utilising the stratigraphic classification and unconformity terminology given by (Brown et al., 1995). This study concentrated only on the post-rift succession of the Orange basin.

Broadly examining the interpreted seismic sections of the Post-Hauterivian successions of the Orange Basin a few observations are made. The entire sequence can be classified as a sedimentary wedge thinning to each sides east and west with a thick depocentre in the mid section of the study area (Figure 20). A strong, highly erosive unconformity at the base of the section appears to be basin wide and is interpreted as the Hauterivian rift-drift unconformity (6At1) (Figure 20). An overlying strong reflector, which appear to follow the geometry of the 6At1 unconformity but thins further basinward is indentified as the 13 At1 early Aptian full drift-onset unconformity (Figure 20). These two unconformities respectively form the base and the top of the early transitional drift succession of the Orange Basin which was deposited between the Hauterivian and Aptian.

The succession is generally transgressive as indicated by the progressive onlapping landward (Figure 21) as a sudden rise in sea level and subsequent flooding of the shelf occurred (Brown et al., 1995). Rising sea level causes river systems to regress and build the succession landward, thus starving the distal sections of the basin. The geometric character of the intermediate sequence is indicated by the thinning of the sequence basinward (Figure 20) as the two unconformities come closer together in the distal part of the basin and the landward building of the sequence. Generally the intermediate sequence ranges in thickness from 380 meters at well location A-A1 (proximal shelf) to 1700 meters at well location K-H1 (distal shelf).

Studying the GR log of well A-A1 an initial fining upward followed by a sligh corasening upward sequence can be observed (Figure 30), further strengthening the proposal of a marine incursion as the sequence evolved from a more distal depositional environment to a more proximal depositional environment.

Another prominent feature on the seismic data following the early drift succession is the large predominantly prograding sequences above the 13At1 unconformity (Figure 22). The drift succession was deposited from the Aptian to present day and is postulated to attain a maximum thickness of 8000 meters (proposed by van der Spuy et al., 2003). The succession can broadly be described as a thick sedimentary wedge building basinward (west) as the basin evolved from early drift to complete drift environment (Barton, 1993). The sequence is interrupted by frequent erosional unconformities as seen in the cross section (Figure 20), separating the succession into five super sequences of which the intermediate sequence is the oldest (Brown et al., 1995). The second sequence referred to as Supersequence 13 is characterized by progradational and aggradational third order sequences (Figure 22) (Brown et al., ibid).

Following the deposition of the prograding Supersequence 13, sea level dropped from the early Albian (14At1) to the Maastrichtian (22At1) (Brown et al., 1995). Third and fourth order prograding sequences characterize supersequences 14 (Figure 22) and 15-16 with supersequence 15-16 as a highly aggradational becoming slightly progradational sequence. The last supersequence 17-20 consists of mainly highly progradational (Figure 23) becoming slightly aggradational third order sequences (Brown et al., ibid). The younger Tertiary and Quaternary succession is a generally thin succession and is well-developed basinward west of the Cretaceous shelf break (Figure 23).

Erosional truncations of various unconformities against the 22At1 unconformity are apparent on seismic data (Figure 21). Relevant to the study area the 16At1, 17At1 and 18At1 unconformities are all truncated against the 22At1 unconformity implying that major erosion must have occurred before the deposition of the distal Tertiary-Quaternary Sequence. The study assumed two periods of erosion based on the methods of extrapolating the sequences landward and consulting literature in the study area.

The technique involved extrapolating sequences landward and calculating the amount of sediments removed from the true thickness of the sequence basinward. This process allowed for the calculation of the amount of sediments removed. The first erosional event therefore occurred during the Early Paleogene from approximately 60 to 55 million years lasting 5 million years and eroding a total thickness of 961 meters, 178 meters off the 17A sequence and 783 meters off the 18A sequence (Figure 25 (A) (B) (C) and Table 6). The second erosional event during the Early Miocene lasted for approximately 6 million years and occurred eroded an estimated thickness of approximately 421 meters of the 22A sequence (Figure 25 (A) (B) (C) and Table 6).

4.1.2 ORANGE BASIN POST - RIFT SEDIMENTATION (THICKNESS MAPS) AND EROSION MAPS

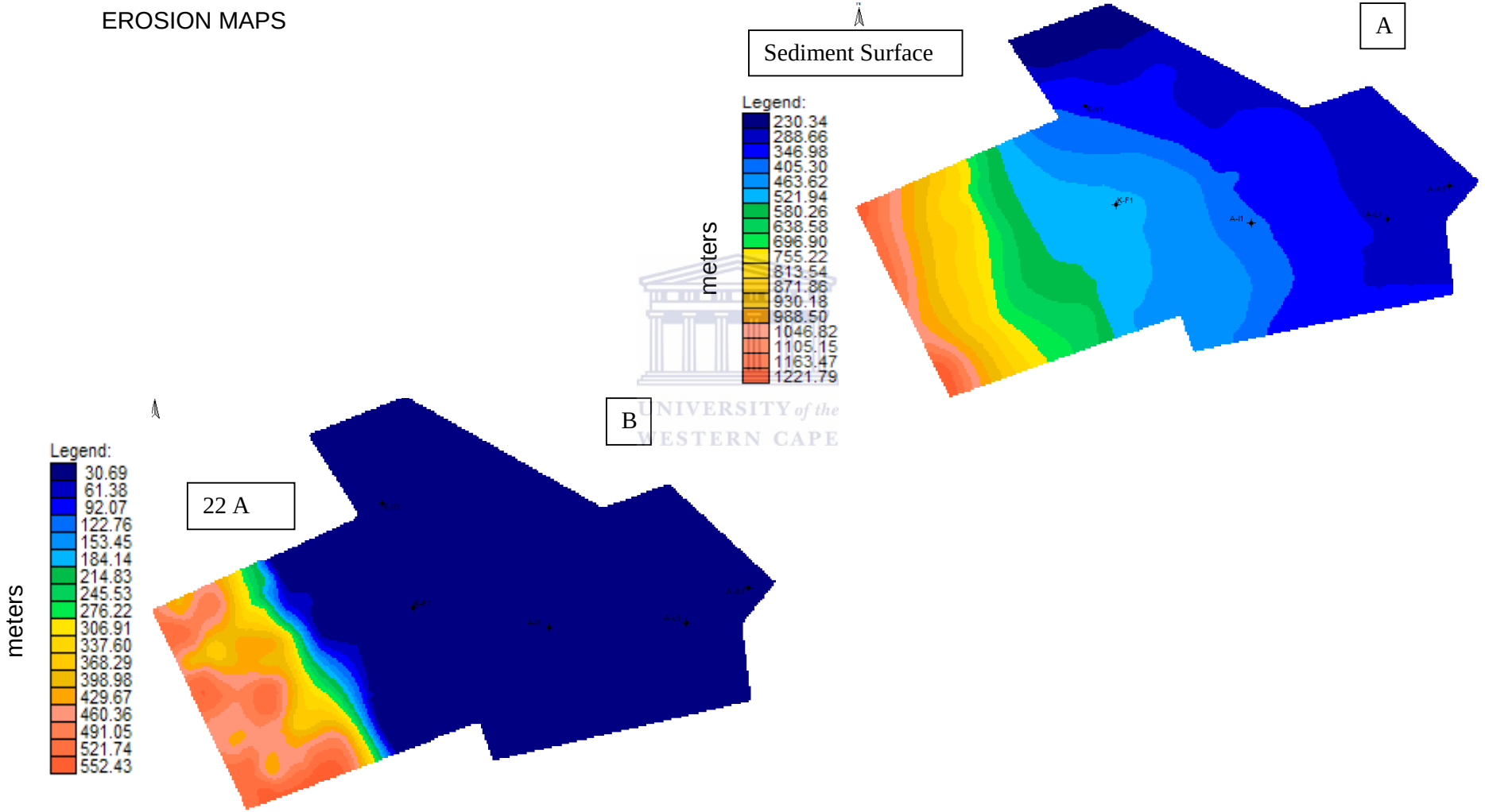

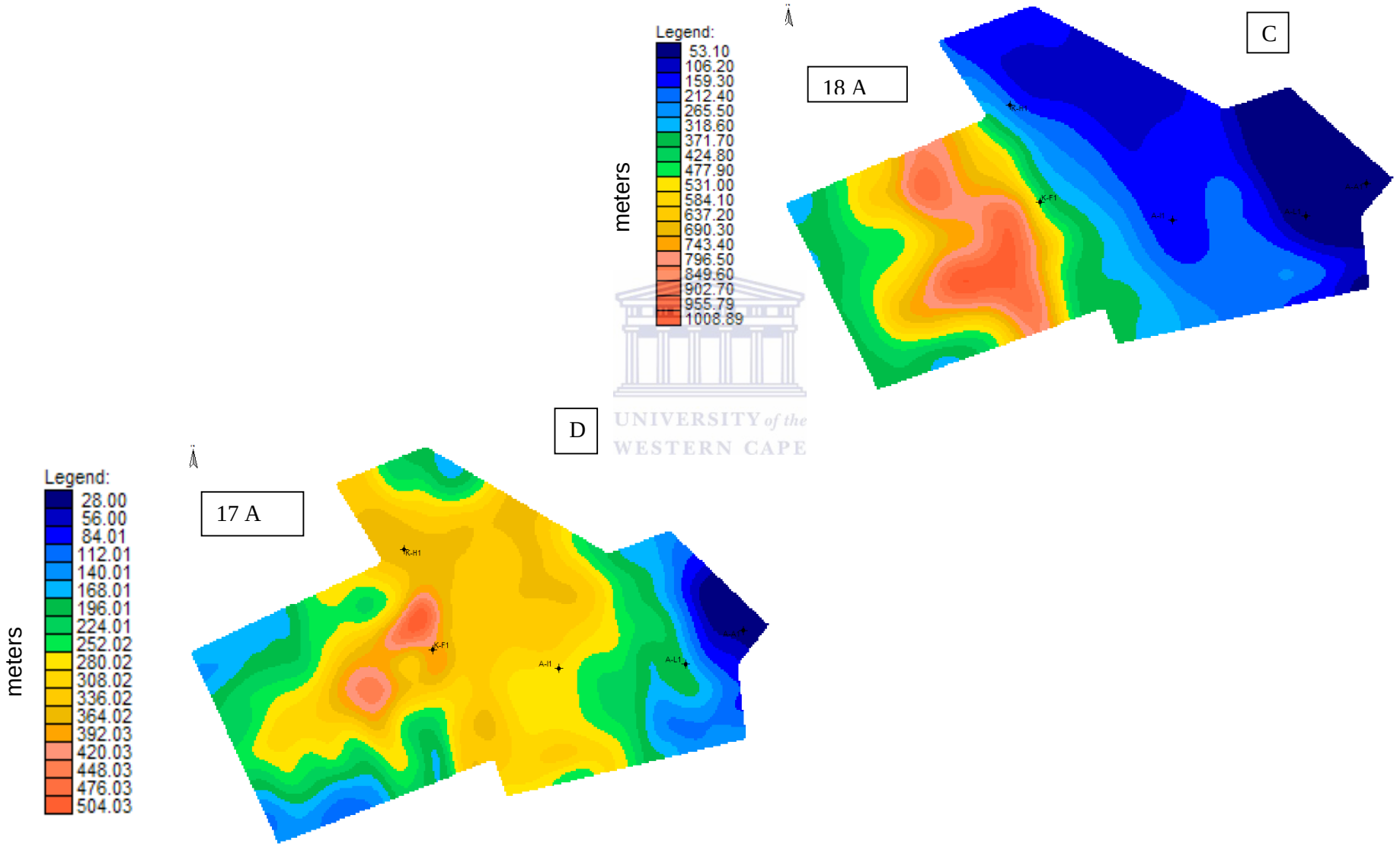

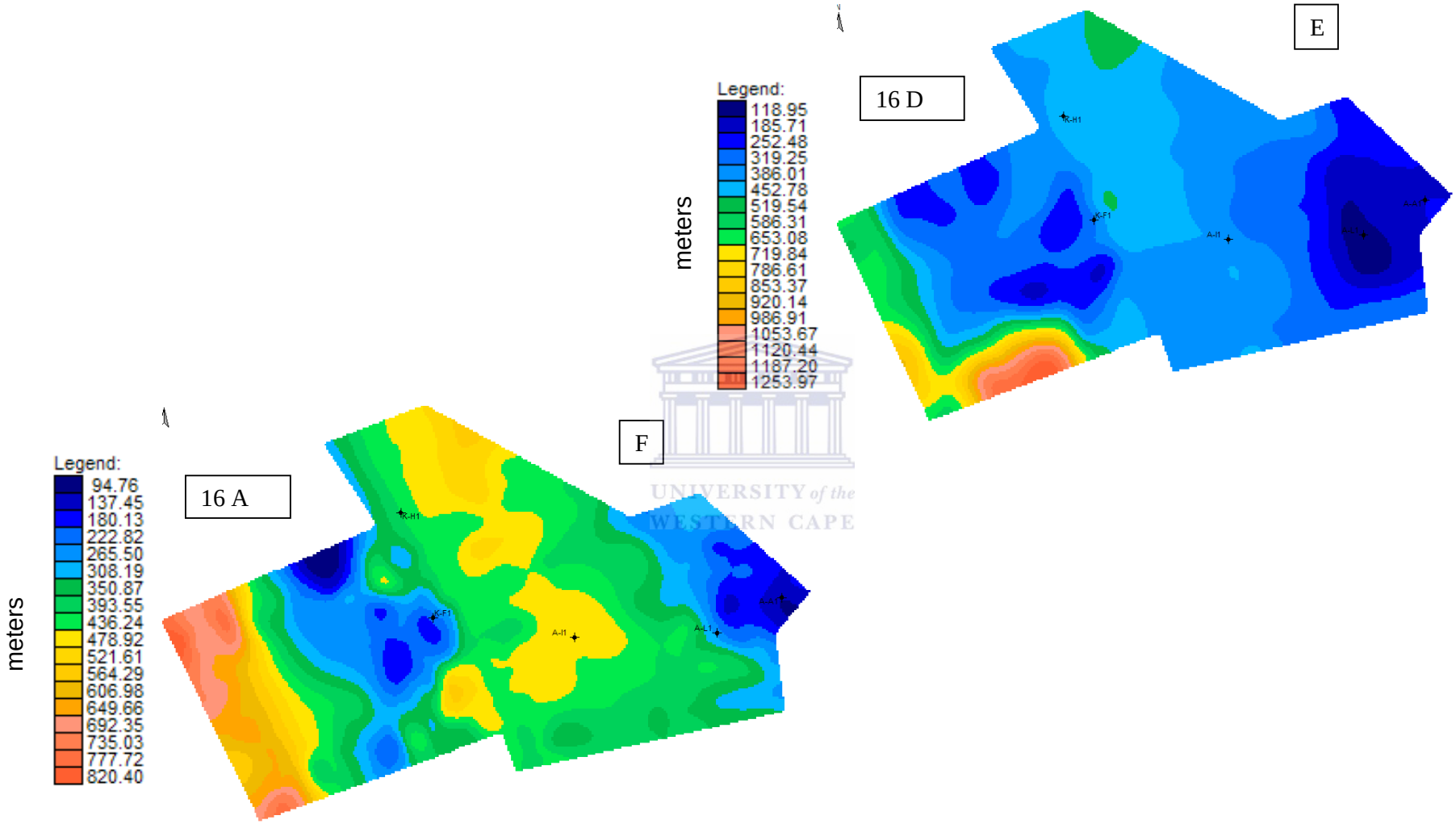

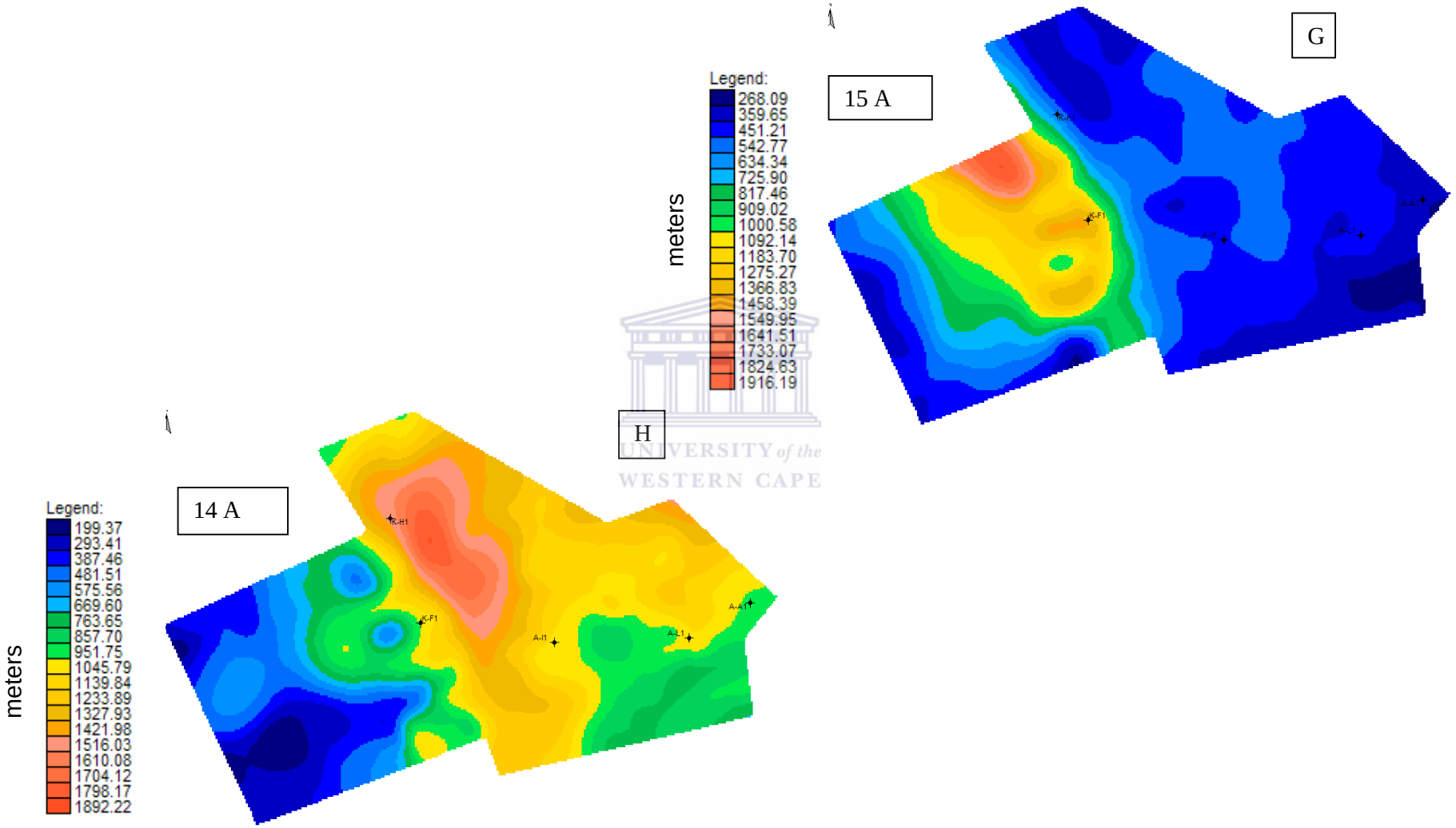

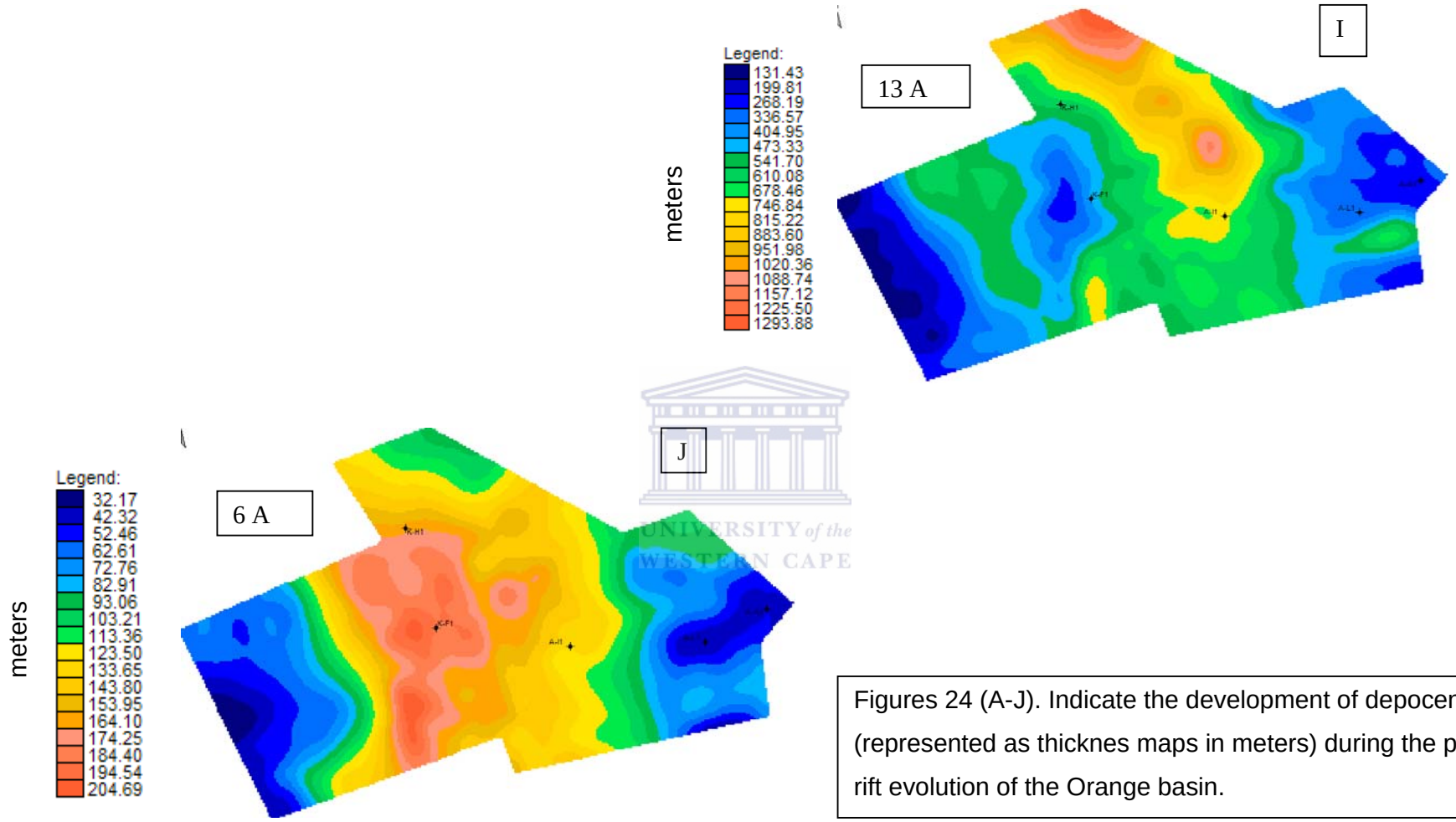

Figures 24 (A-J). Indicate the development of depocentres (represented as thicknes maps in meters) during the post rift evolution of the Orange basin.

POST – RIFT SEDIMENTOLOGICAL EVOLUTION

The post – rift sedimentological evolution of the Orange Basin, expressed above as thickness maps relevant to the study area indicates that the first of the post – rift sequences, sequence 6A (Figure 24 J) to have a depocentre developed in the mid section of the study area and thinning lardward and basinward. The subsequent sequences, sequences 13A and 14A (Figures 24 I and H) indicate a northward shift of the depocentres. The 15A (Figure 24 G) sequence indicates a depocentre in the midsection of the basin while sequences 16A and 16 D (Figures 24 F anf E) thickness maps show the thicker sediment further basinward. The 17A (Figure 24 D) thickness map indicates a thickening of the sequence in the midsectionf followed by the 18A (Figure 24 C) sequence indicates a thinner section on the shelf and a thick depocentre evolving off the shelf possibly as a result of Late Cretaceous erosion. The 22A (Figure 24 B) sequence in the study area indicates that most of the shelfal area has been eroded with sediments in excess of a hundred meters only further basinwars.

POST - RIFT EROSIONAL MAPS OF THE ORANGE BASIN INDICATING AMOUNT OF SEDIMENTS REMOVED IN METERS.

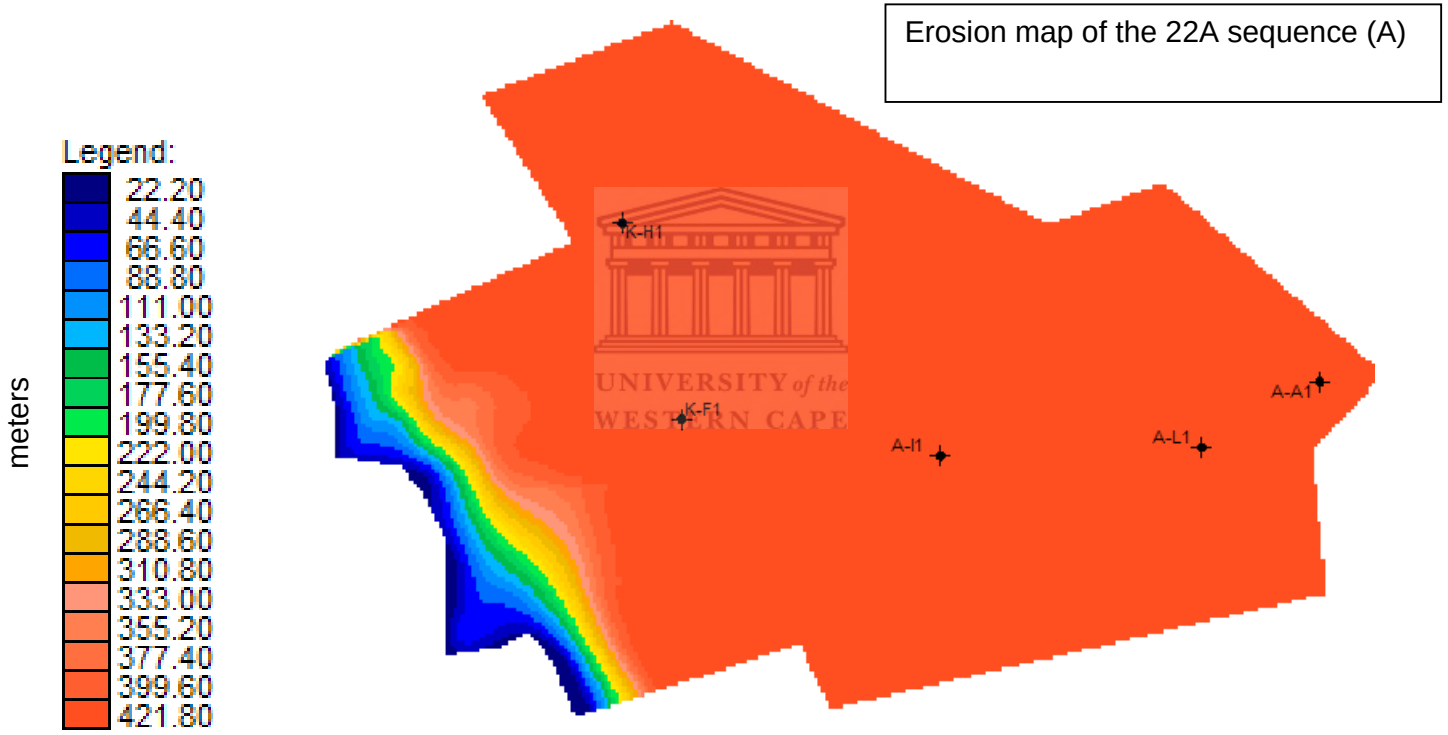

Erosion map of the18A sequence (B)

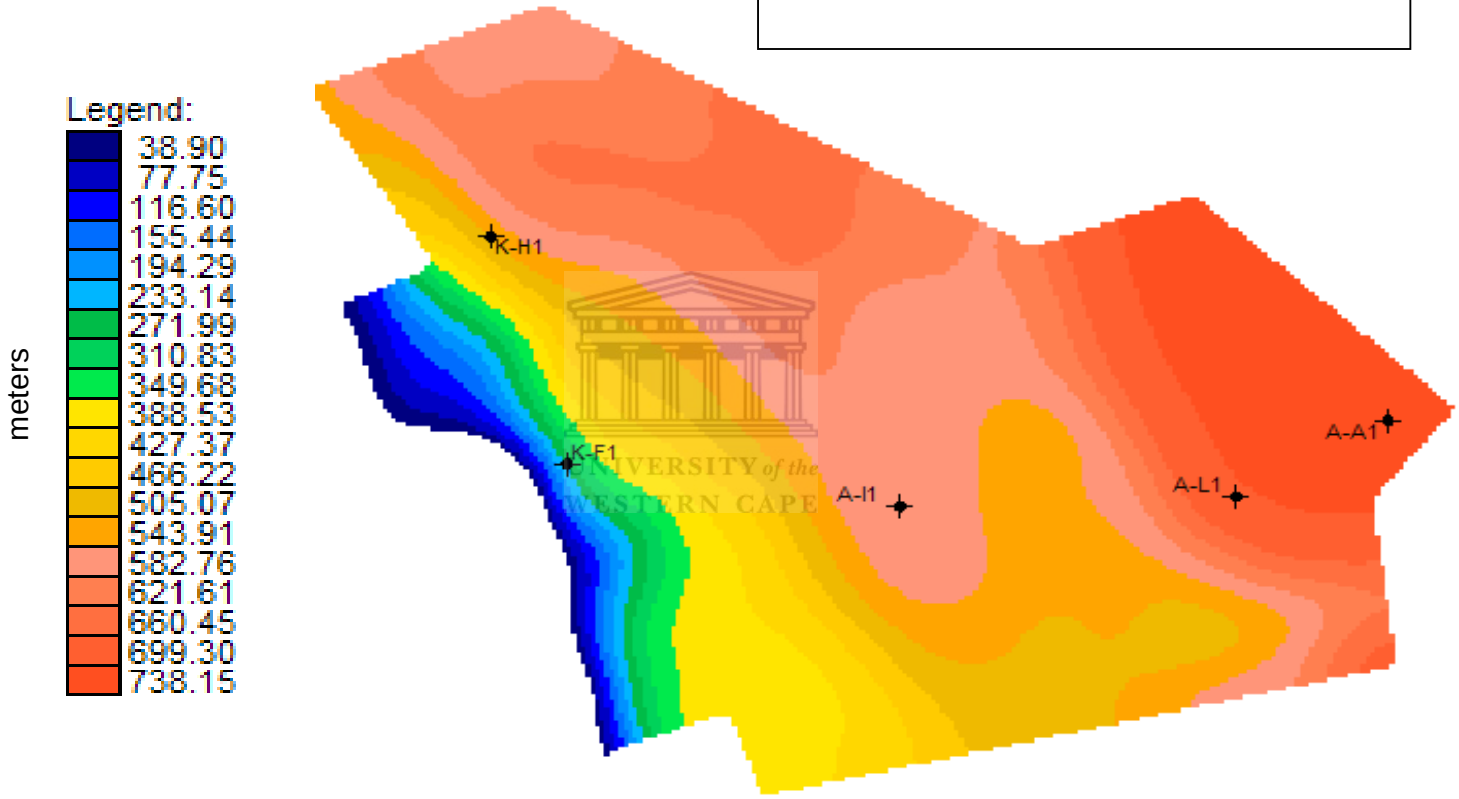

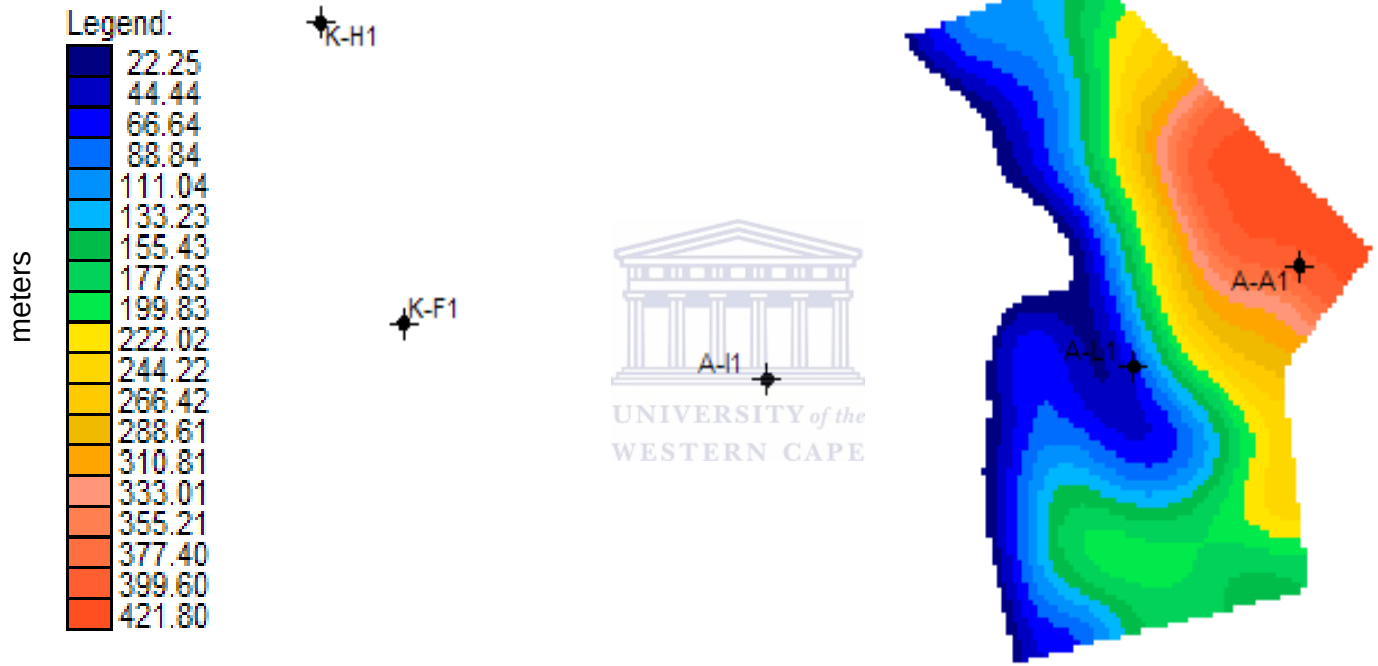

Figures 25. Erosional maps indicating the thickness (m) and extent of the two erosional events incorporated in the basin modeling study.

The youngest of the erosional events represented on the 22A erosion map (Figure 25 A) represent the a more extensive erosional compared to the presending erosional event. The older erosional event represented in the erosion maps 17A and 18A show that erosion was so intense that the entire 18A as well as the upper 17A sequence was removed from the inner shelf area relevant to the study area (Figures 25 B and C). The colour bar indicates the thickness of sediment removed with red being the highest and most sediment removed and blue the lowest with the least sediment removed.

4.1.3 LIMITATIONS OF THE CONCEPTUAL MODEL

A discrepancy was noted in the proximal section of the study after the surfaces were imported into PetroMod when the imported surfaces did not correlate to their well tops. This was probably due to the method used in the time-depth conversion, which was done by taking the average of the checkshots between intervals eg 22At1 to 18At1 at a specific well location. This was then done for the same interval in all the wells and the average of all these values was then used as the average velocity of the specific interval. However the discrepancy only affects the proximal area of the study. This error is illustrated by showing some of the surfaces and their respective misfits (Figure 26 (A) (B) and 27 (A) (B)). The inconsistency does not compromise the source rock modeling and was dealt with by remove the section affected in the source rock modeling.

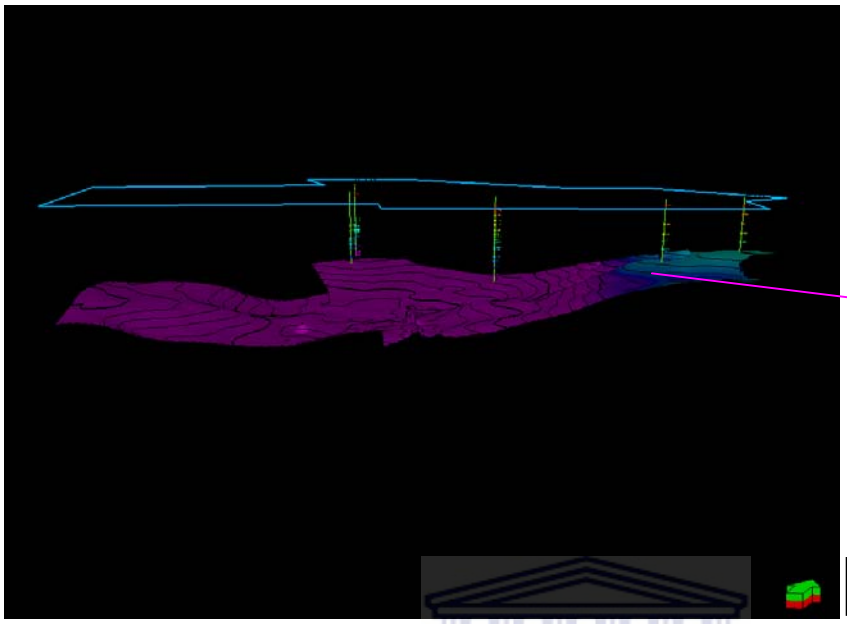

View of the mapped 6At1 surface after depth conversion

A

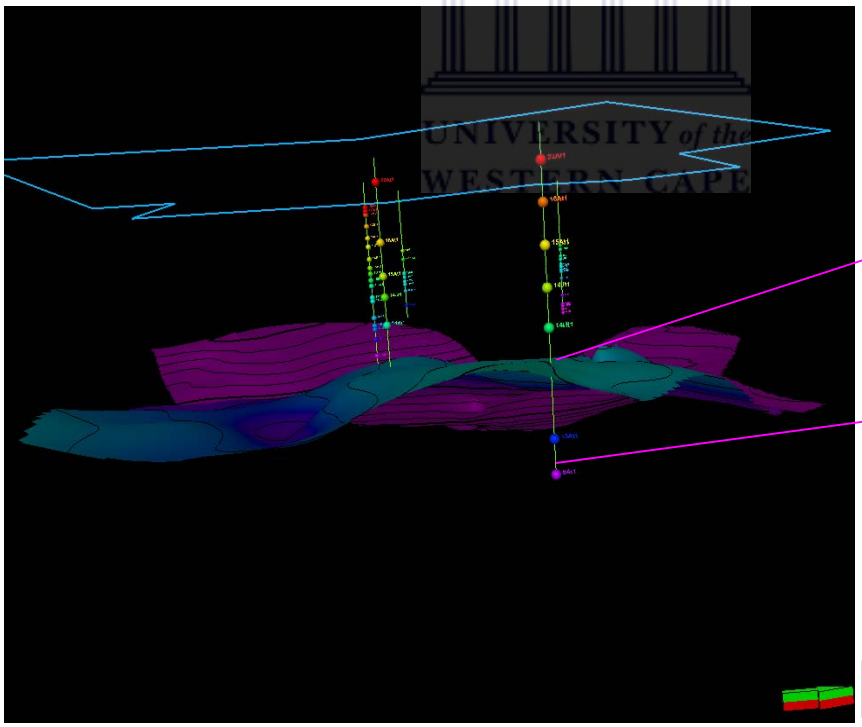

Surface location at well A-A1 after depth conversion.

6At1 well top at well A-A1.

B

Figures 26: (A) Side view of the 6At1 surface with the blue representing the shallower areas and the purple the deeper section of the surface. (B) Represents a close up view of the surface with the well top data of well A-A1 illustrated by the colored shells. It is then noted here that the surface plot is much higher then the actual well top of the 6At1 horizon.

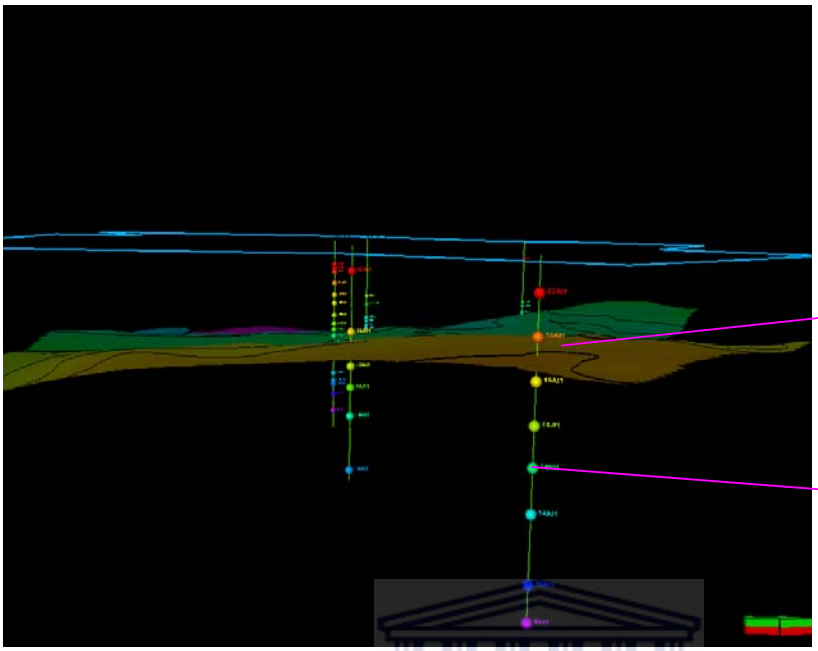

The mapped 15At1 surface at the well location A-A1.

The well top data of the 15At1 at the well location A-A1.

A

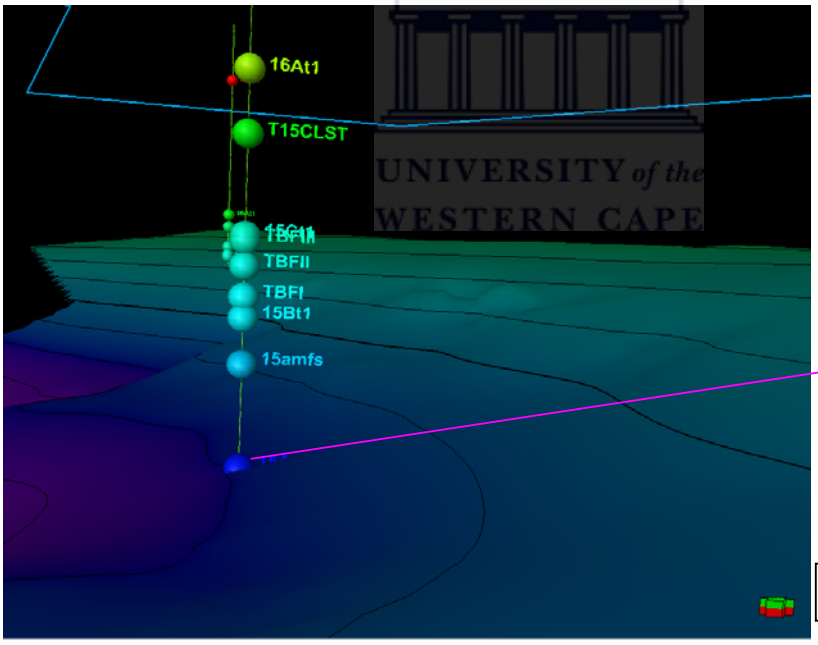

The correct tie of well top 15At1 and depth-converted surface at well location K-F1.

B

Figures 27: (A) Mistie of the 15At1 surface at well A-A1. (B) A close up view of the correct tie between the surface and the well top 15 At1 at the well location K-F1 deeper in the basin. It can therefore be deduced that there is a problem with the velocity model affecting the areas closer to shore more than the central areas.

4.2 WELL ANALYSES

4.2.1 WELL LOG INTERPRETATION

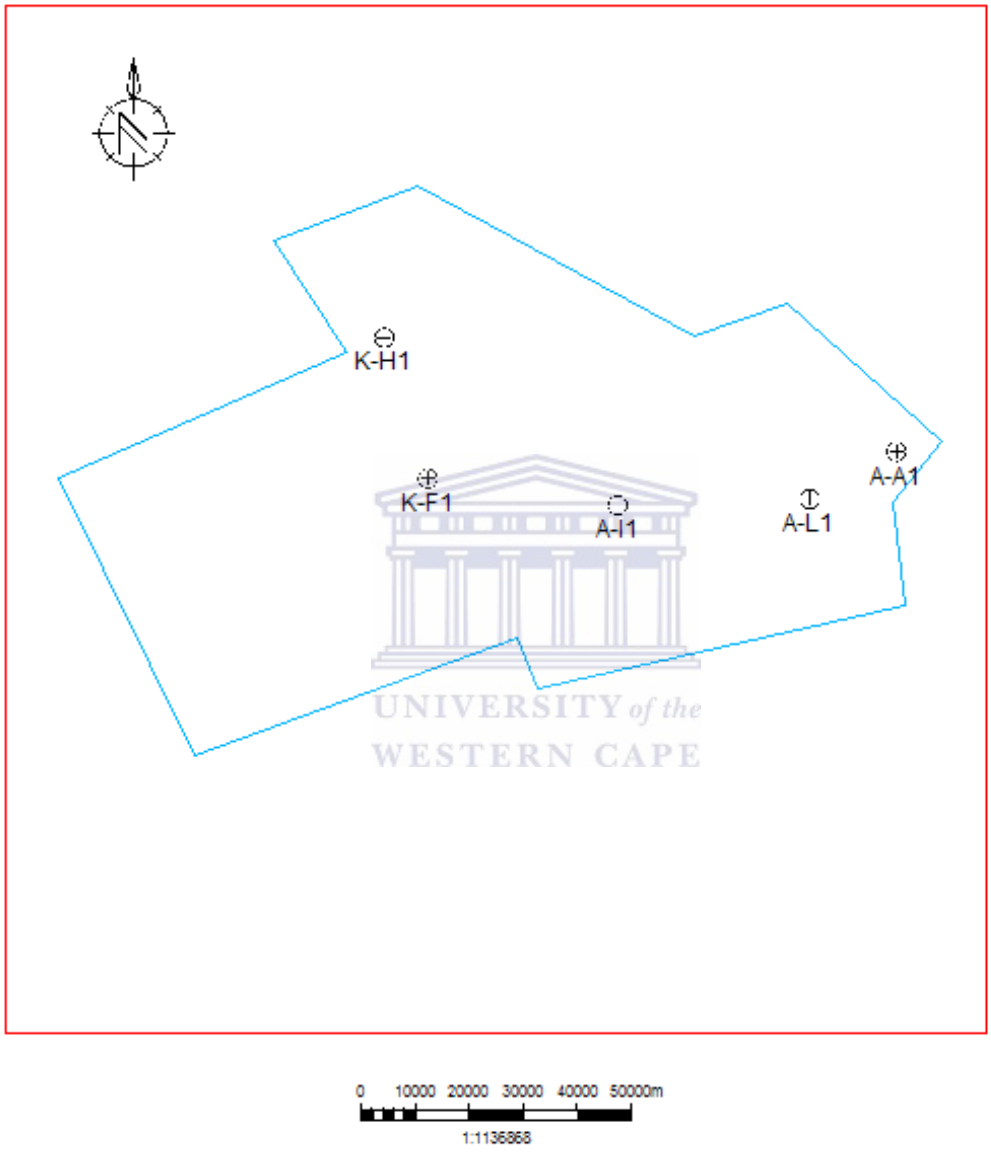

Figure 28. The geographical setting of the five wells utilized in the study.
(Study area outlined).

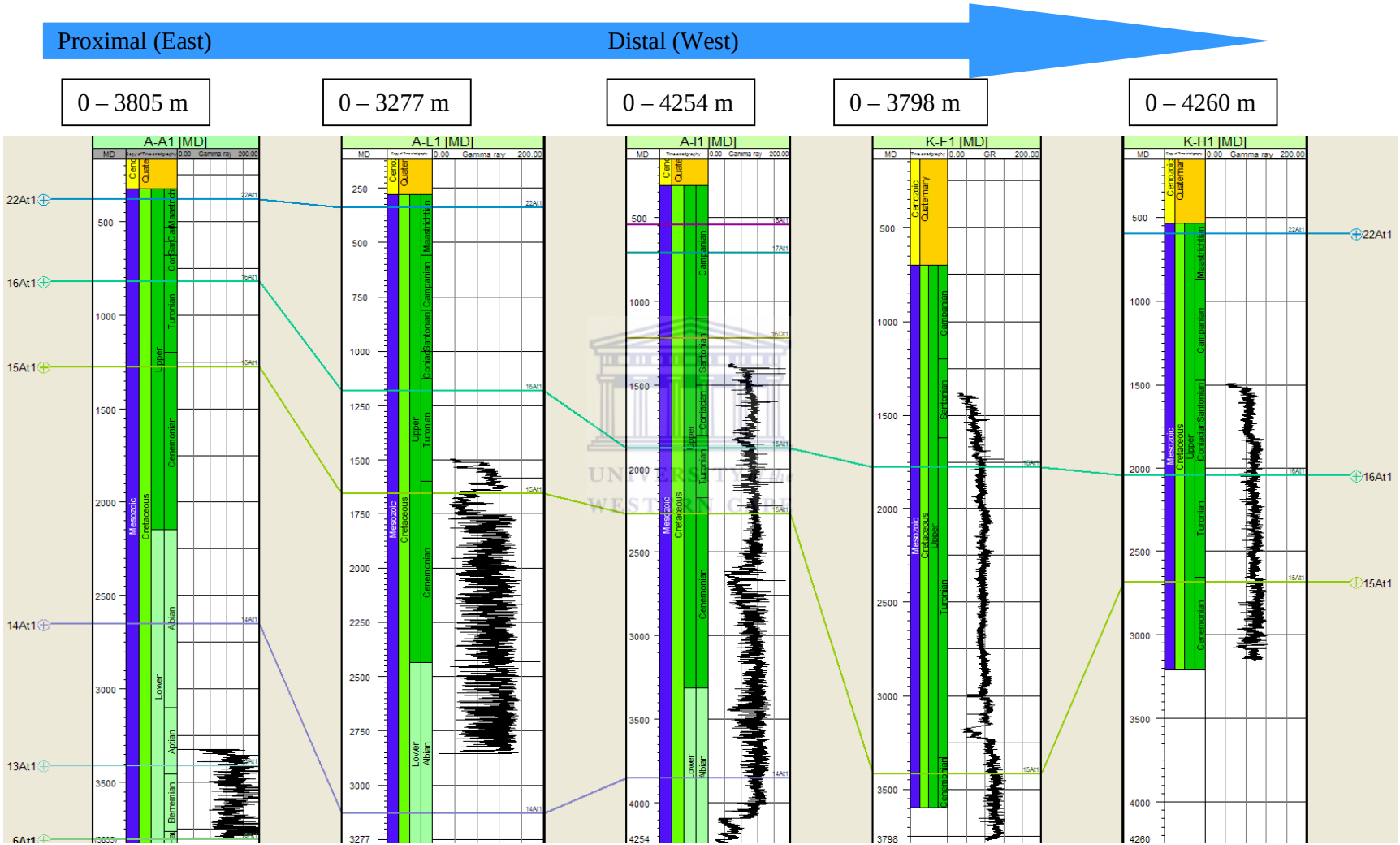

Figure 29: Wells with depth and gamma ray from proximal to distal correlating the well tops from east to west.

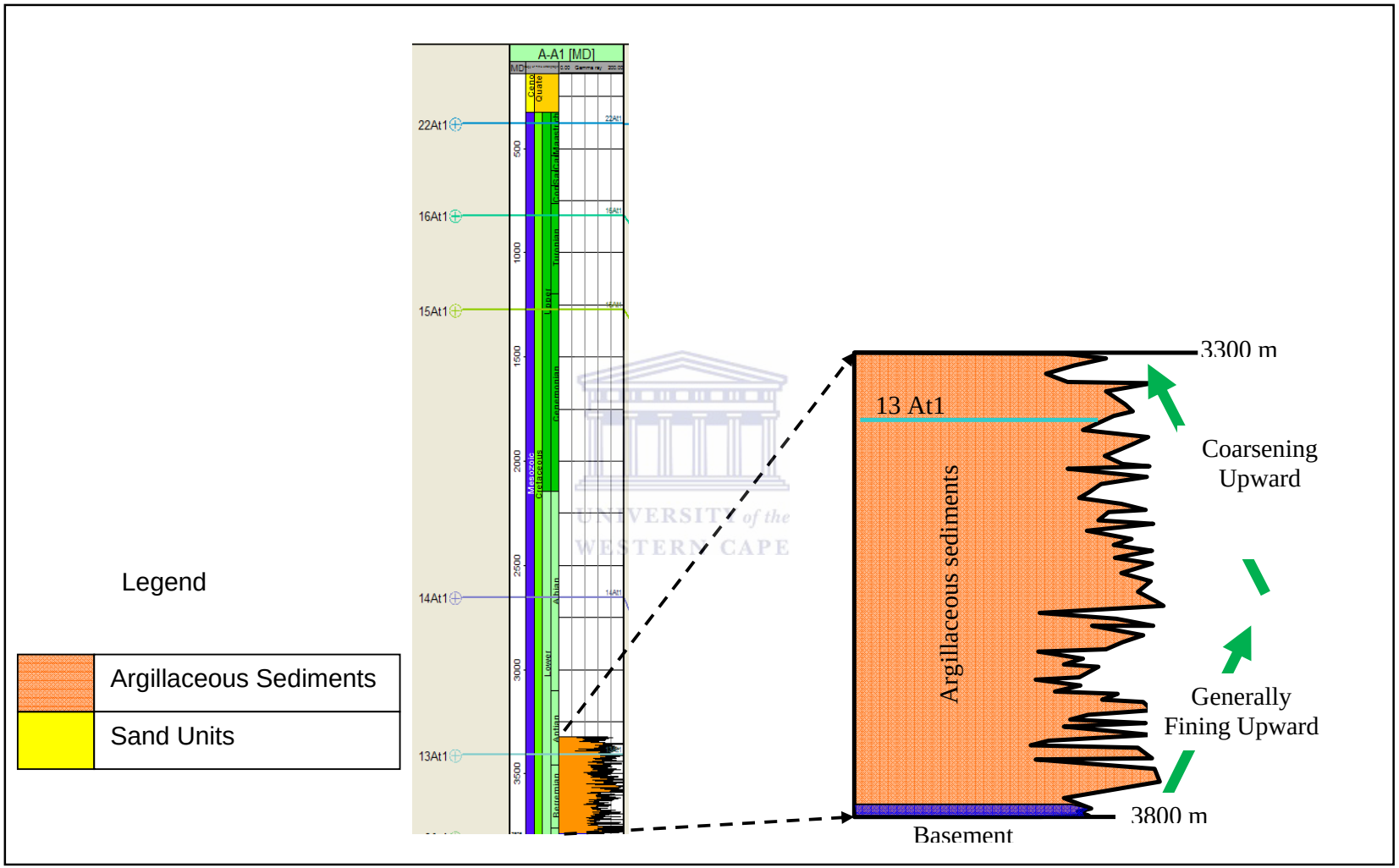

Figure 30: Sketch of gamma ray for well A-A1 indicating the inferred prograding and retrograding sequence from the gamma ray signature

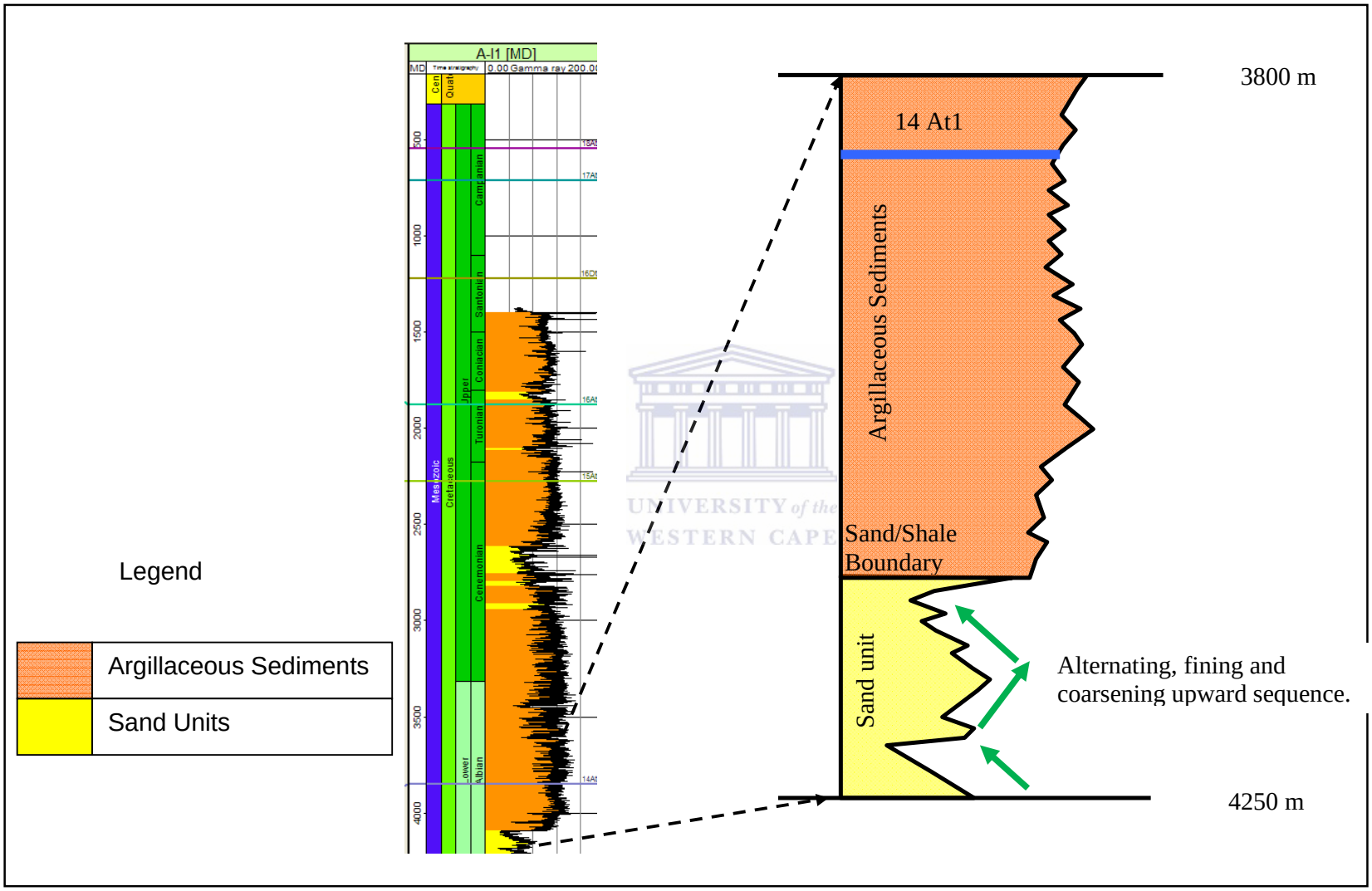

Figure 31: Sketch of gamma ray for well A-I1 indicating alternating fining and coarsening upward sand unit culminating in a sudden change to inferred argillaceous sediments.

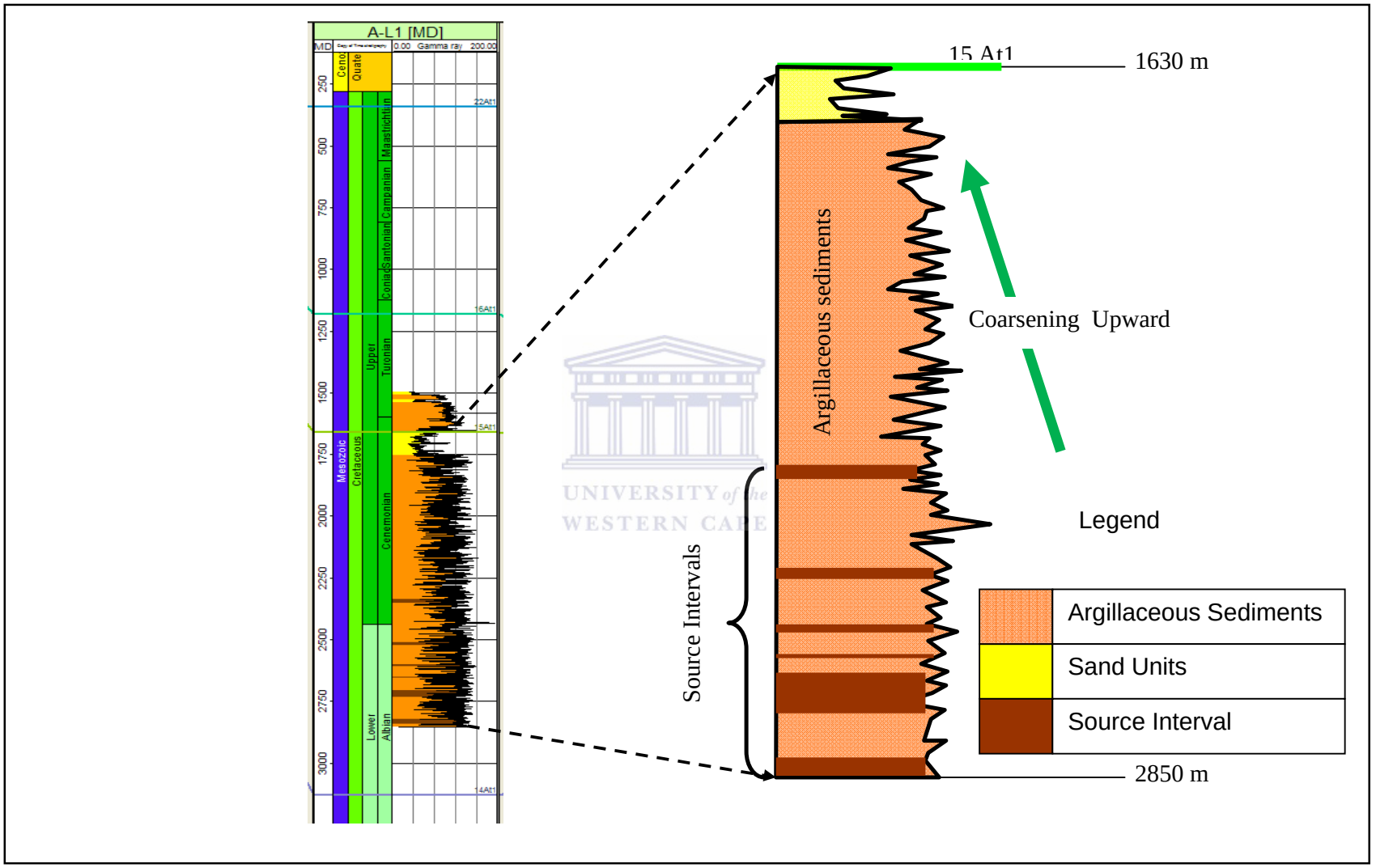

Figure 32: Sketch of gamma ray for well A-L1 indicating source intervals and the inferred fining upward sequence from the gamma ray signature.

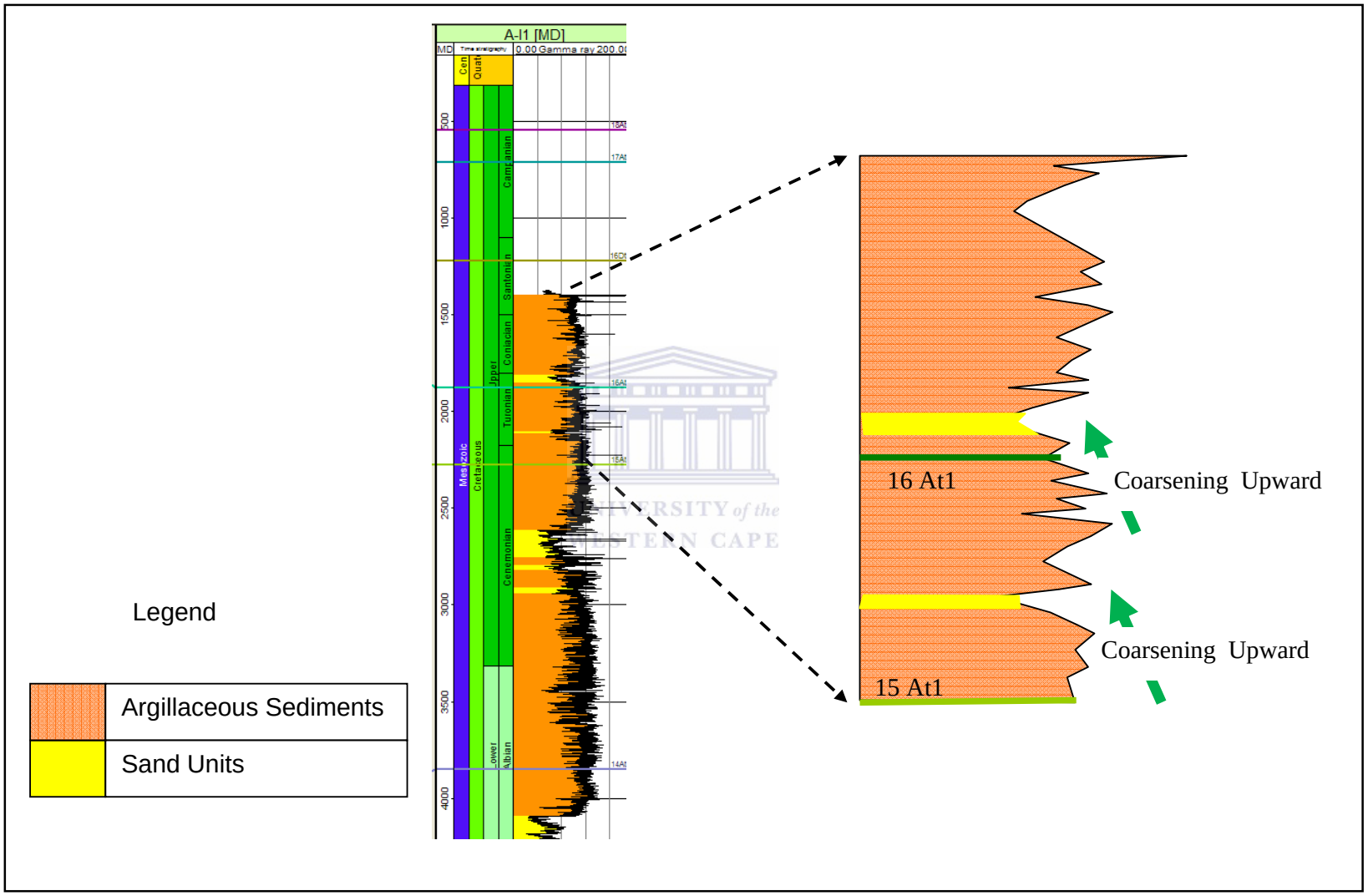

Figure 33: Sketch of gamma ray for well A-L1 indicating the coarsening upward sequence above the 15 and 16At1 unconformities.

All the wells (Figure 28) in the study area are concentrated on the shelf allowing for a more constrained well correlation whilst the more distal section of the study area are correlated through extrapolating lithological information from the shelfal wells.

Overlying the well tops onto the geophysical well logs the study could break up the Orange basin post rift successions and investigate the sedimentological nature of each of the post rift sequences (Figure 29). Well A-A1 is the only well that reaches basement (Figure 30) where the succession based on the gamma ray log can generally be described as fining upward sequence as a general increase in gamma ray occurs from a depth of 2800 to 2500 meters followed by a coarsening upward trend as the gamma ray decreases between 2500 to 3300 meters depths as indicated by the arrows in (Figure 30).

The optimum data available to study Supersequence 13 is in wells A-I1 (Figure 31). The sequence is characterised by a period of regression followed by transgression (Brown et al., 1995). This is evident in the GR log as a fairly low gamma ray interval (evident for sandstone) was possibly deposited as sea level fell and river systems moved basinward (Figure 31) followed by an abrupt succession of a high gamma ray interval (evident of a muddy interval) possibly associated with a flooding event as the deposition of finer grained sediment succeeds coarser sediments.

Supersequence 14 is characterised by a general coarsening upward sequence possibly (Figure 32) due to a drop in sea level. The following Supersequences 15 the only sequence that could be correlated throughout the study area (Figure 34) to 16 and 17 to 20 are expected to share the same log character as sea level are assumed to continue falling (Figure 34).

The interpretation of the cross plots for the gamma ray (red line) and the neutron porosity (black line) of the wells A-L1 and K-H1 (Figure 35) indicate a general decrease in gamma ray from older to younger sediments whilst the neutron porosity on the other hand shows an increase from the older to younger sediment. Based on this observation the entire post rift succession of the Orange Basin could therefore be said to be a major coarsening upward sequence in the study area (Figure 35).

The relative depths of the two post rift source rock units are indentified on the gamma ray log of wells A-A1, A-L1 and K-H1 and K-F1 (Figure 36) and is expressed with reference to the average total organic (TOC) content to both have approximatly the same average total organic content (Figure 37). The two source rocks intervals are characterised in (Table 7) indicating the average total organic content, hydrogen indices, oxygen indices and Tmax values over the source units. A cross plot of the Tmax and hydrogen indices across the intercepted source intervals are overlain with the kerogen types to indicate the organic matter type represented by the source rock units in the study area (Figures 38 and 39)

Correlating the log profiles of gamma ray, total organic content values and the cross plot of hydrogen and oxygen indices the levels of potential source rock as well as the quality are indentified and correlated to the sequence stratigraphic framework relating to the depositional environment at the time of source rock deposition (Figure 40 - 43). It is apparent from the cross plots of hydrogen and oxygen indices for the wells A-A1, A-L1, K-F1 and K-H1 that all the source rocks have higher oxygen indices than hydrogen indices and therefore could be said to be of terrestrial Type III or IV kerogen nature (Figure 40 (A) – 43(A)).

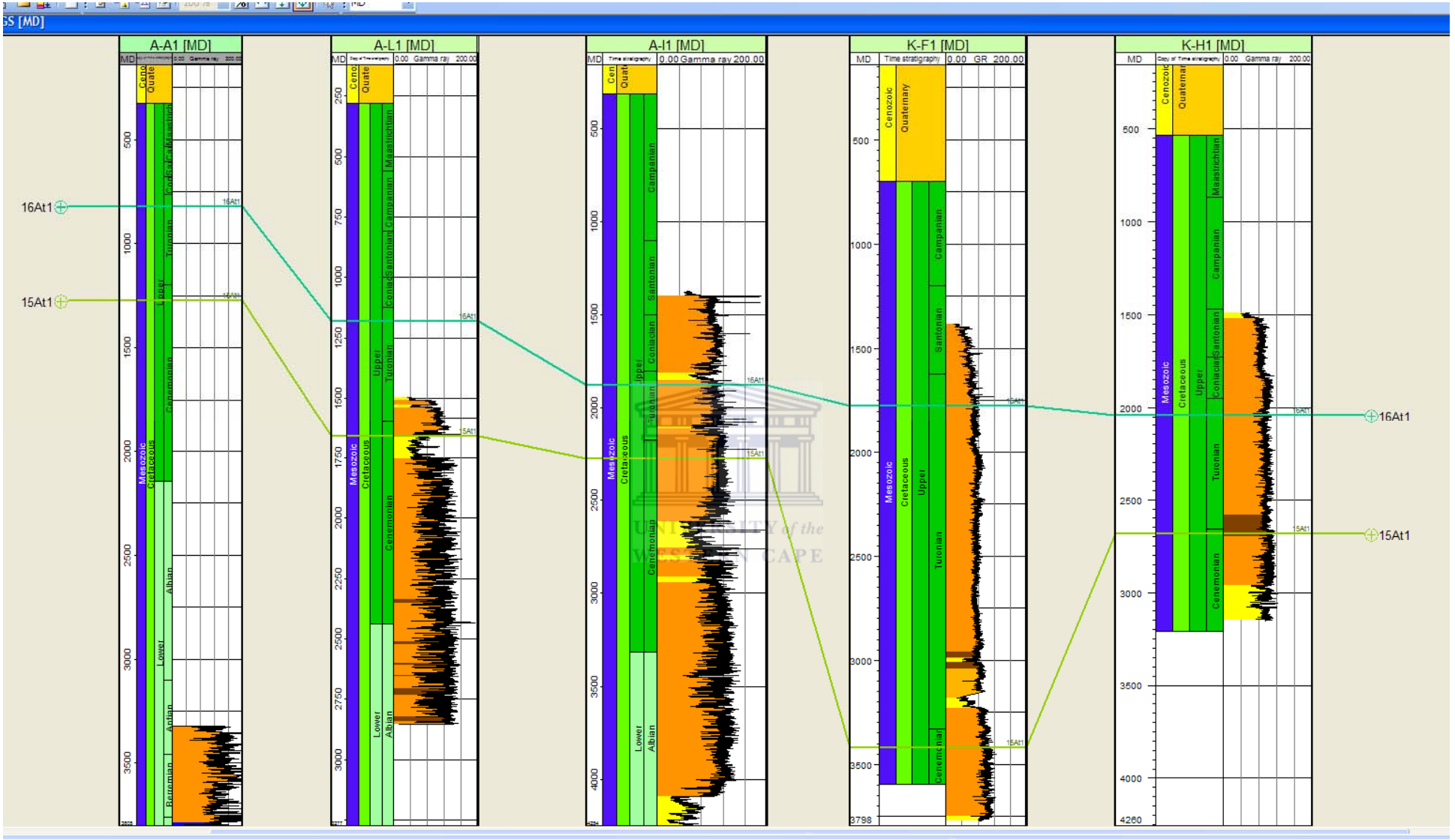

Figure 34. Correlation of wells from proximal to distal with the gamma ray filled in with the corresponding lithologies. Sequence 15 A is the only sequence that could be correlated throughout the five wells.

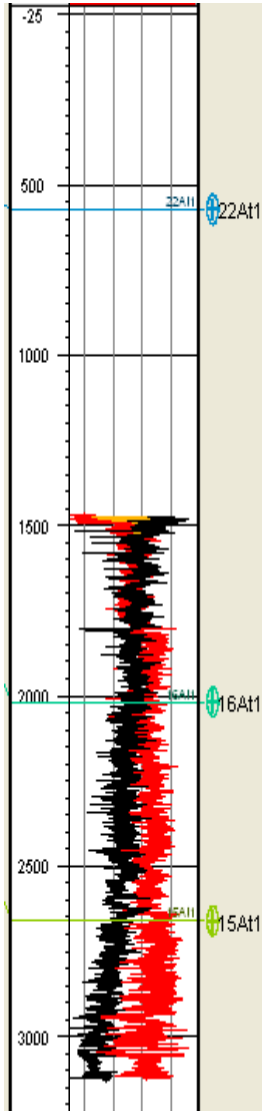

Figure 35. Cross plots of gamma ray and neutron porosity for well A-L1 and K-H1 indicating coarsening upward sequences in the Orange Basin.

Legend

Gamma Ray

Neutron Porosity

Inferred Sandstone

K-H1

A-L1

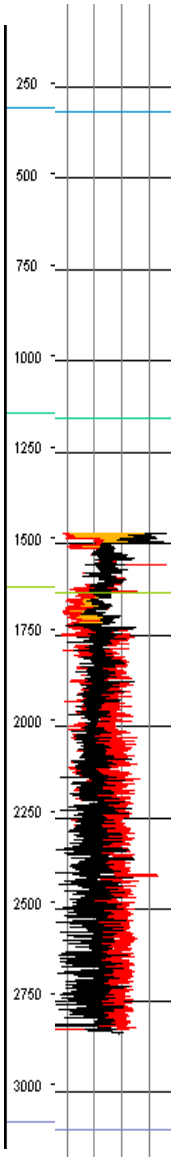

4.2.2 SOURCE ROCK CHARACTERISTICS

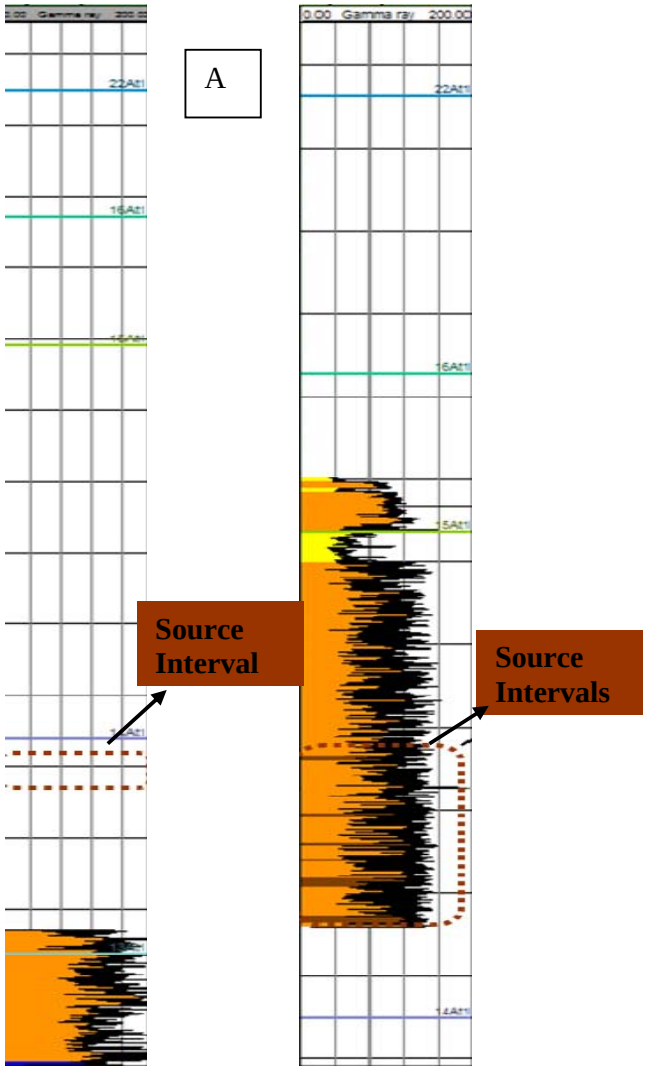

Cenomanian to Turonian source rock

K-F1

2961 m – 2987 m (DG)
3010 m – 3040 m (DG)
3040 m – 3051 m (DG-WG)

K-H1

2580 m – 2657 m (DG)
2657 m – 2697 m (DG)

Barremian – Early aptian source rock

A-A1

2730 m – 2830 m (DG-WG)

A-L1

1616 m – 1634 m (DG)
2335 m – 2830 m (scattered)
DG-WG

DG = Dry Gas
WG = Wet Gas

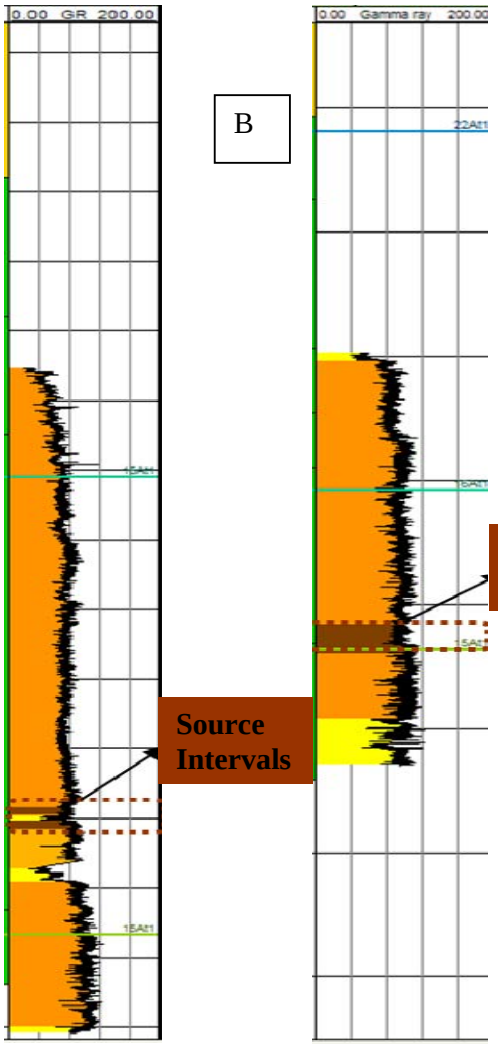

Figure 36. Shows source rock intervals in well A-A1, A-L1, K-H1 and K-F1.

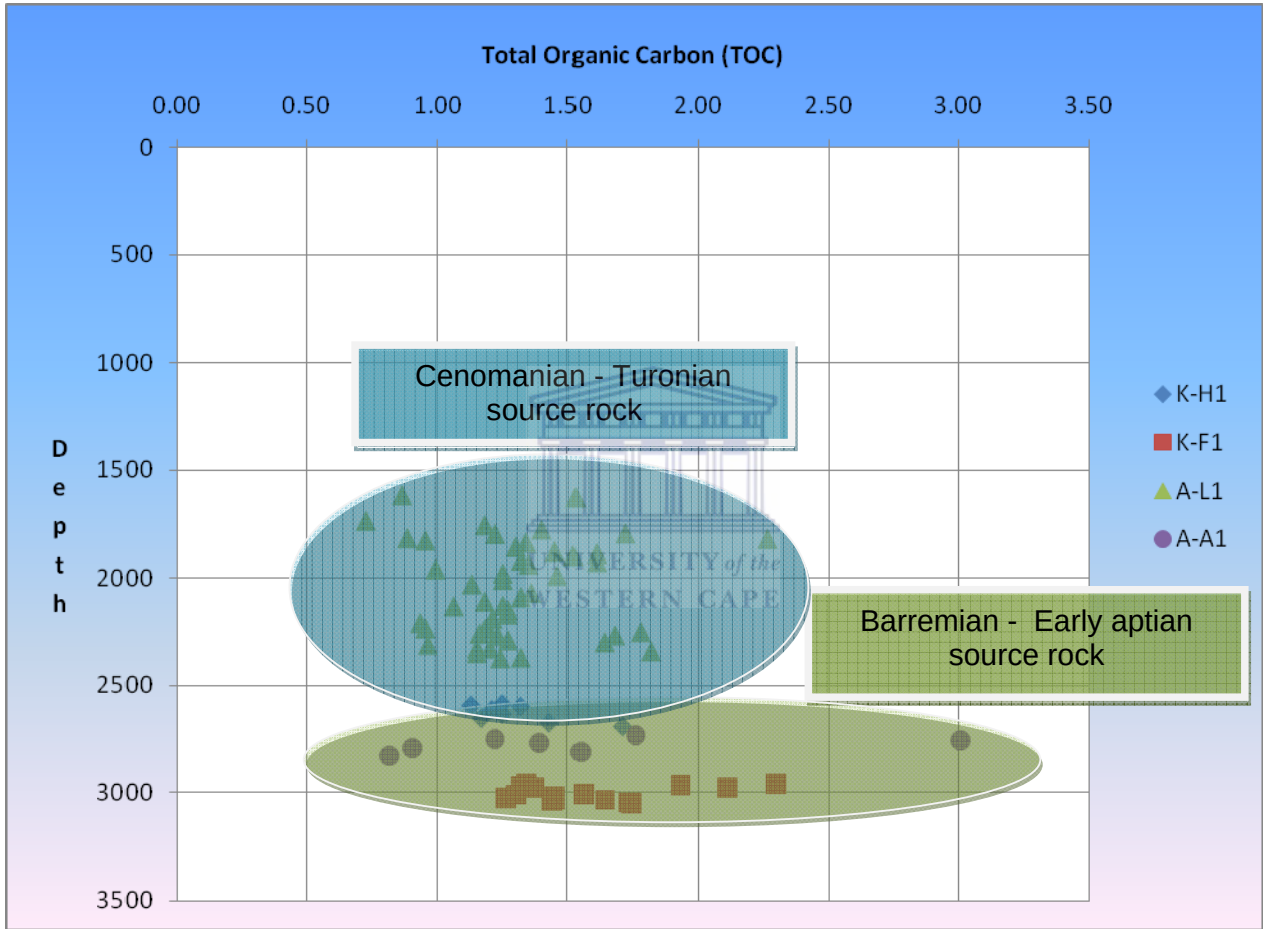

Figure 37. Total organic carbon (TOC) plots for the Cenomanian - Turonian source rock and Barremain – Early Aptian source rock.

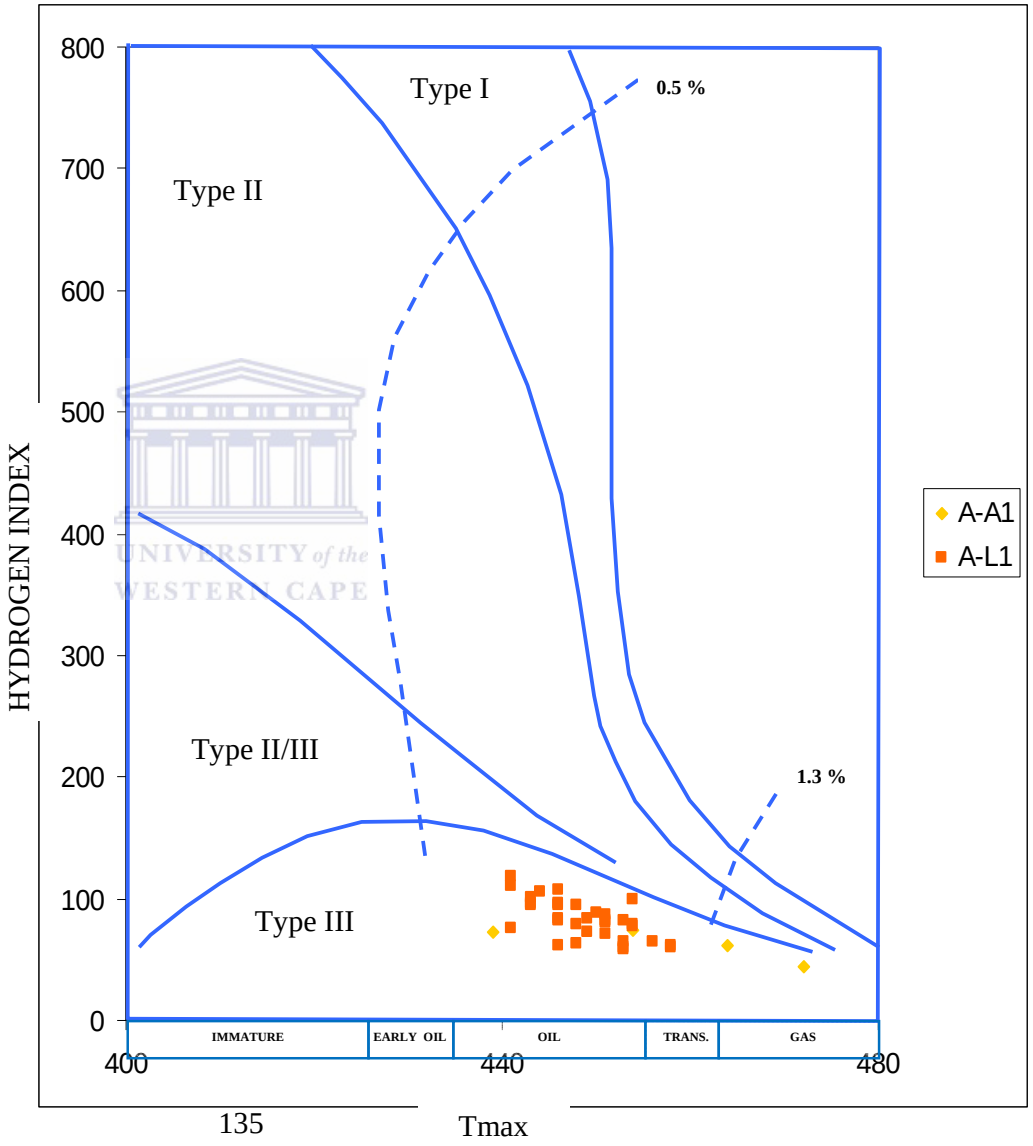

Figure 38: Hydrogen Index plotted against Tmax with the kerogen types overlain for the the Barremain – Ealy Aptian source rock intercepted in well A-A1 and A-L1.

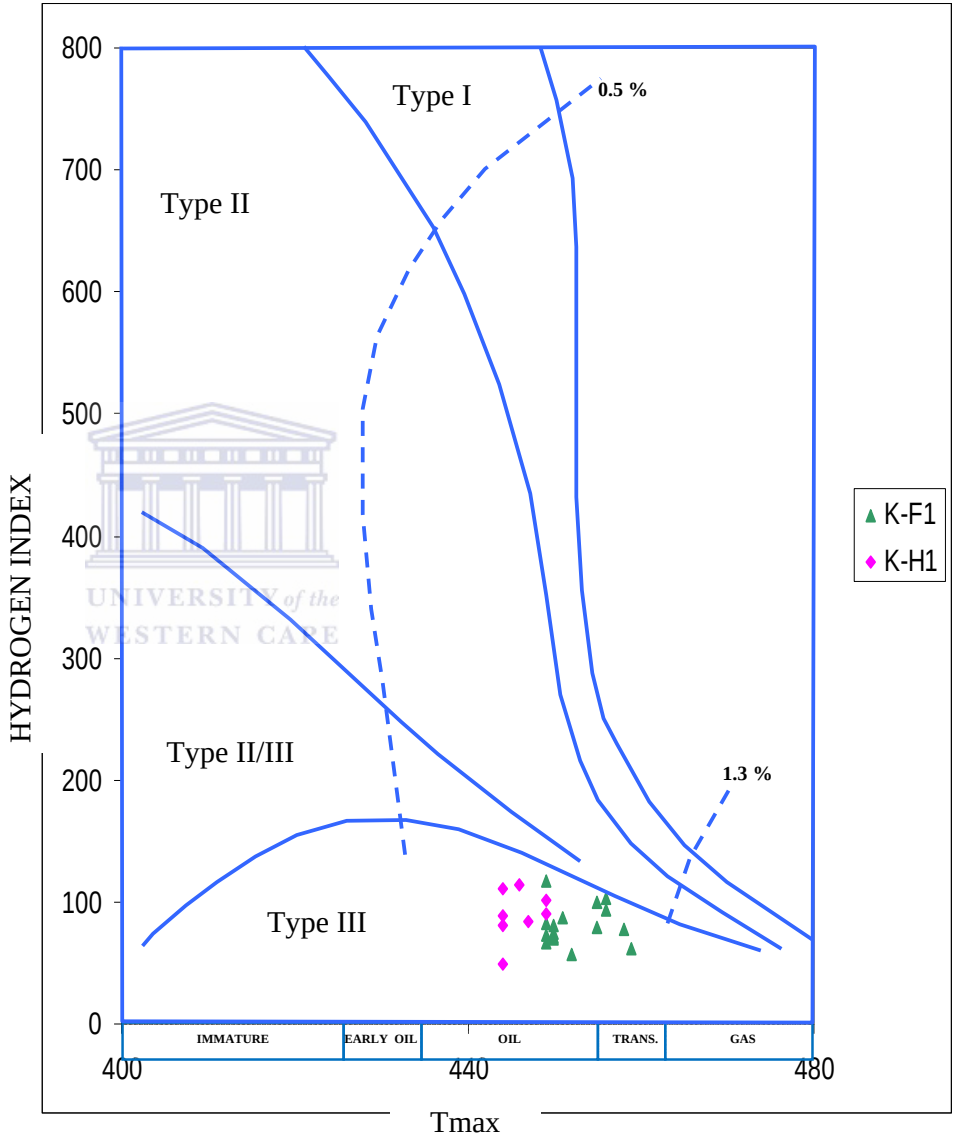

Figure 39: Hydrogen Index plotted against Tmax with the kerogen types overlain for the the Cenomanian - Turonian source rock intercepted in well K-F1 and K-H1.

BARREMIAN – EARLY APTIAN					
	DEPTH	TOC	HI	OI	T-MAX
A-A1	2730-2830	1.52	89.37	78.47	402.28
A-L1	1616-1634	1.2	113.38	130.96	437
	2335-2830	1.3	83.95	112.52	448.9
Average		**1.3**	**95.6**	**107.3**	**429.4**
CENOMANIAN - TURONIAN					
	DEPTH	TOC	HI	OI	T-MAX
K-F1	2961-2987	1.73	83.31	92.09	452.33
	3010-3051	1.5	81.95	76.23	452.4
K-H1	2580-2697	1.31	96.84	123.68	445.87
Average		**1.5**	**87.3**	**97.3**	**450.2**

Table 7: Source intervals and their geochemical characteristics.

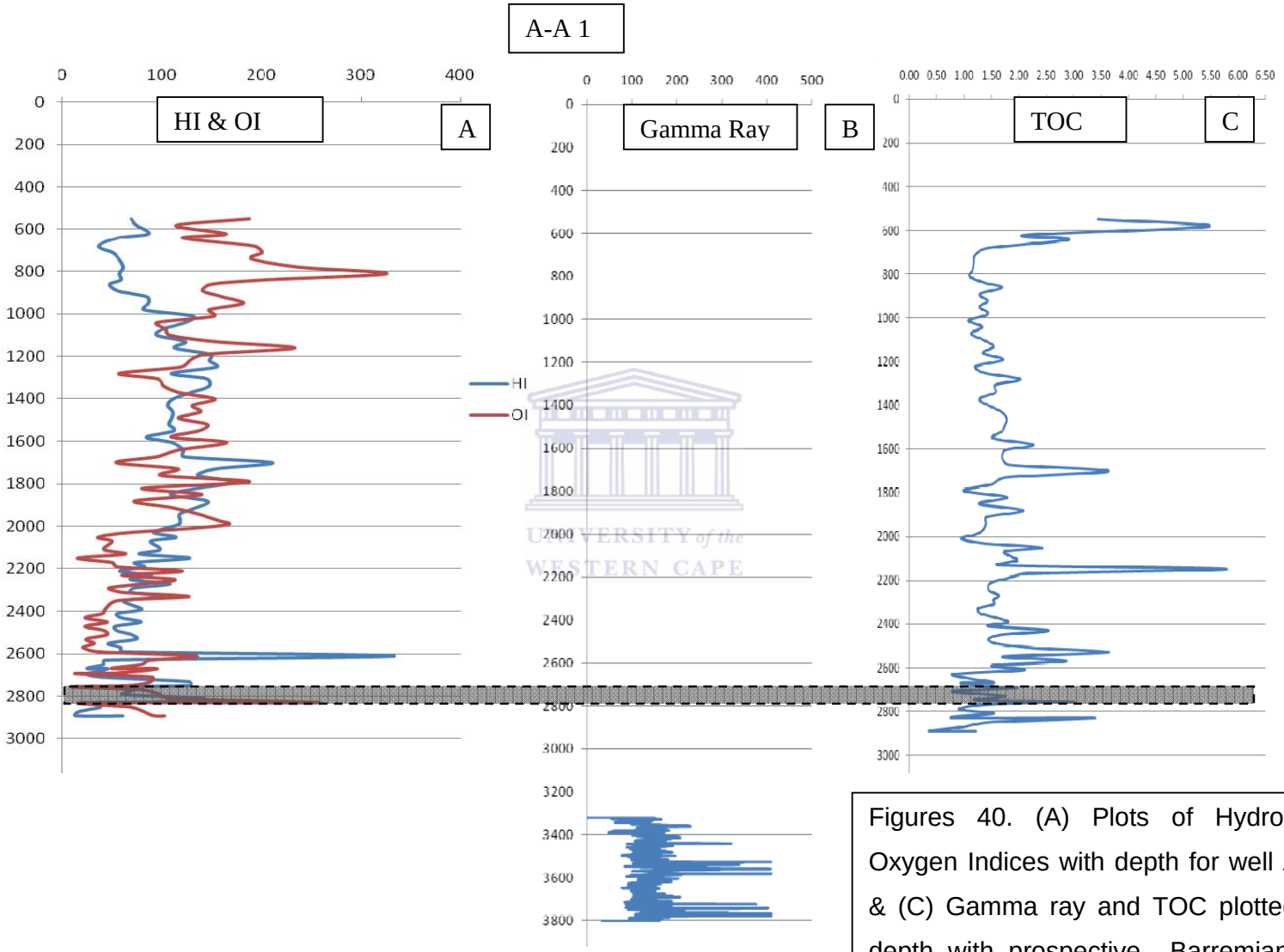

Figures 40. (A) Plots of Hydrogen and Oxygen Indices with depth for well A-A1. (B) & (C) Gamma ray and TOC plotted against depth with prospective Barremian – Early Aptian source interval overlain in grey for well A-A1.

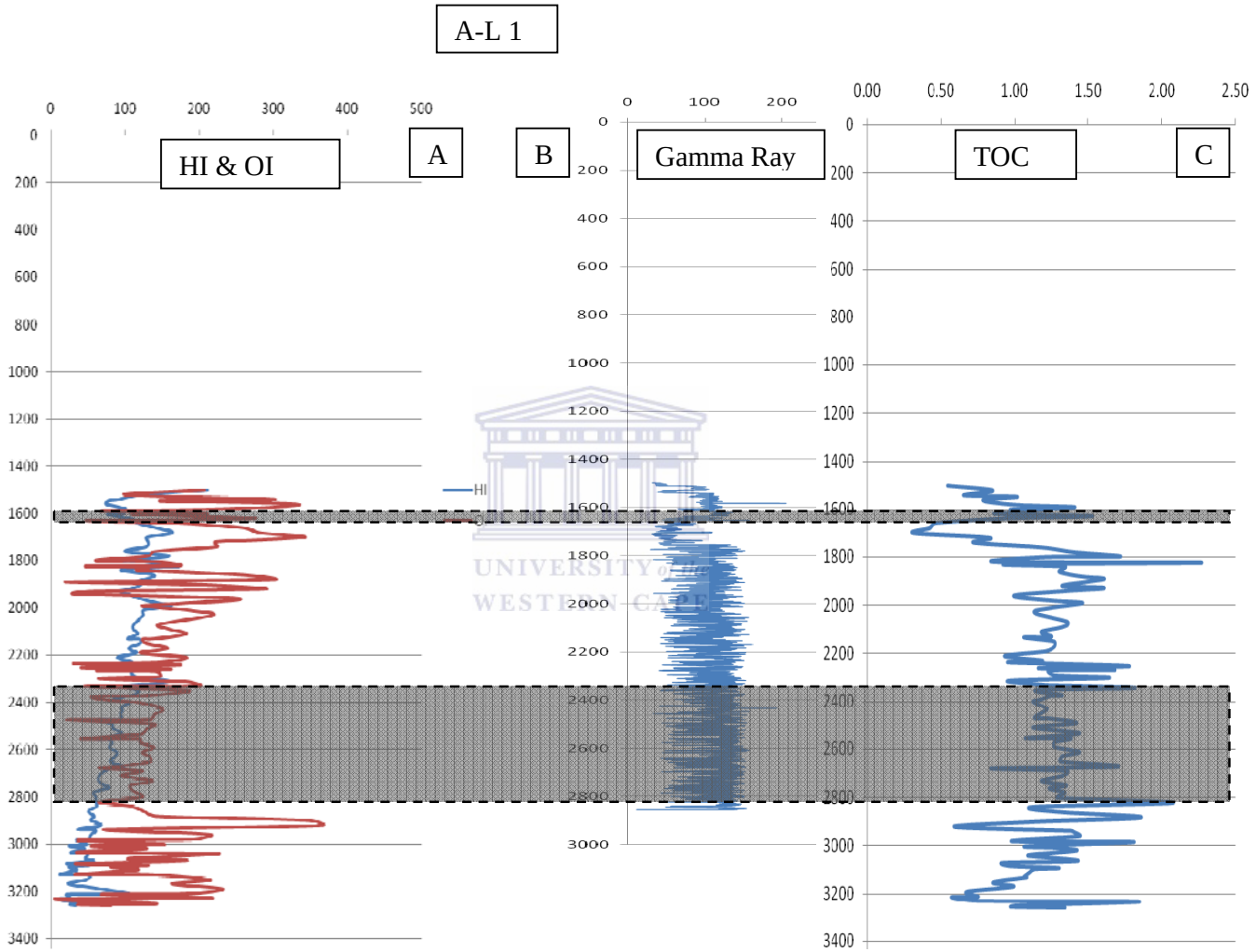

Figures 41. (A) Plots of Hydrogen and Oxygen Indices with depth for well A-L1. (B) & (C) Gamma ray and TOC plotted against depth with prospective Barremian – Ealy Aptian source interval overlain in grey for well A-L1.

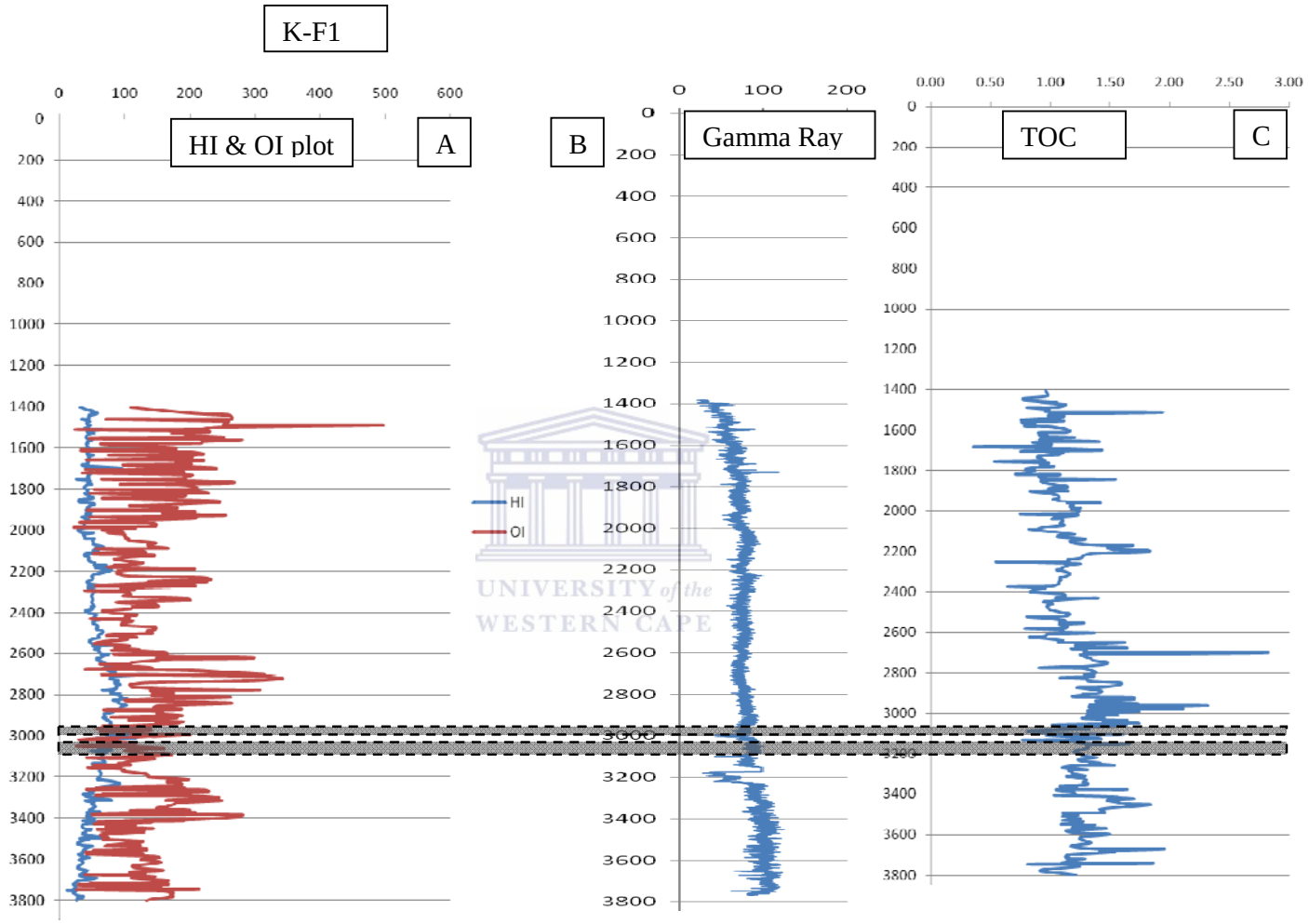

Figures 42. (A) Plots of Hydrogen and Oxygen Indices with depth for well K-F1. (B) & (C) Gamma ray and TOC plotted against depth with prospective Cenomanian - Turonian source interval overlain in grey for well K-F1.

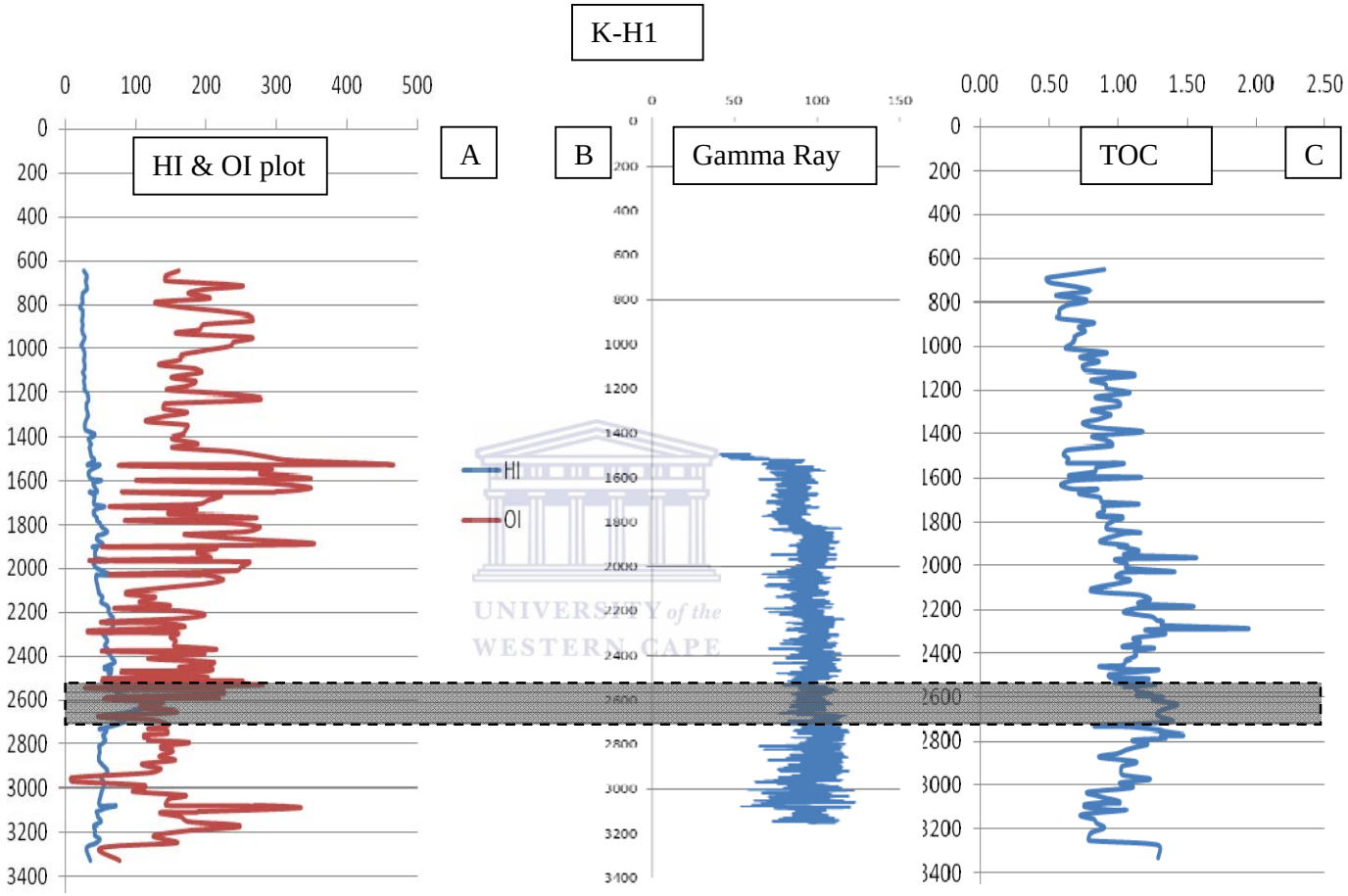

Figures 43: (A) Plots of the Hydrogen and Oxygen Indices for well K-H1. (B) & (C) Gamma ray and TOC plotted against depth with prospective Cenomanian - Turonian source interval in grey for well K-H1.

PETROLEUM SYSTEM MODELING

The following section discusses the results of the petroleum system modeling. In this study two source rocks intervals which include the Barremian - Early Aptian and the Cenomanian - Turonian source rock are included in the modeling in order to characterise the post rift evolution of source rock maturation as well as their present day maturity. These source rocks are of different age and were deposited under different environmental conditions. During the modeling stages it was noted that the basin heat flow played a major role with respect to the timing of source rock maturation resulting in the utilization of two different heat flow models including a rift – drift heat flow with a decaying heat flow peaking during rifting and decaying to present day (Figure 44 (A) (B) (C)) and a constant heat flow subsequent to rifting (from drift to present) (Figure 45 (A) (B) (C)). The results of these two heat flow models on the thermal history will be presented and discussed in the following section.

RIFT - DRIFT HEAT FLOW MODEL

Parameter Results

Heat flow curves

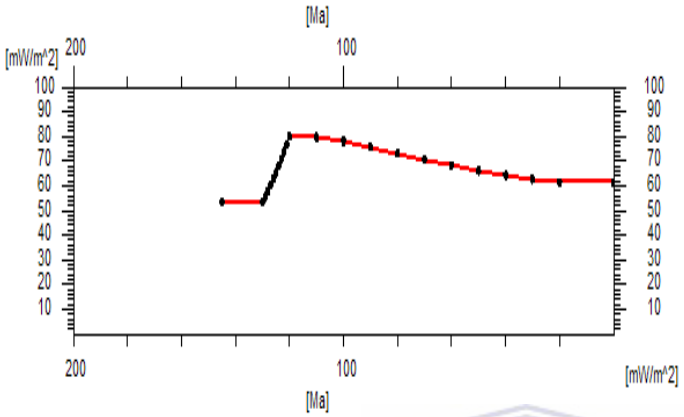

(A)

(B)

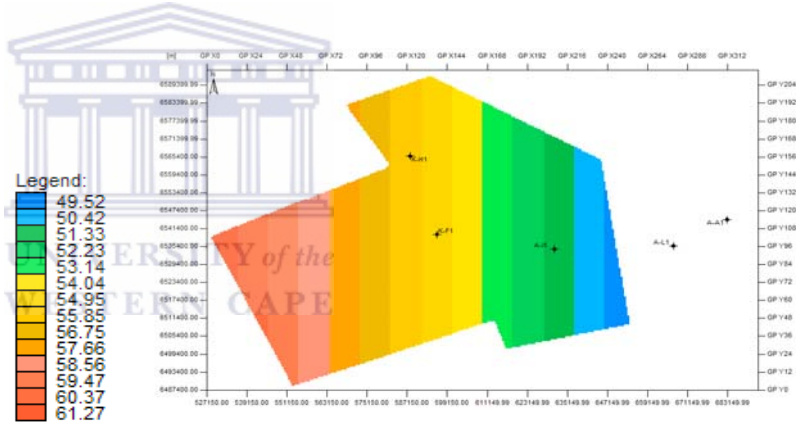

(C)

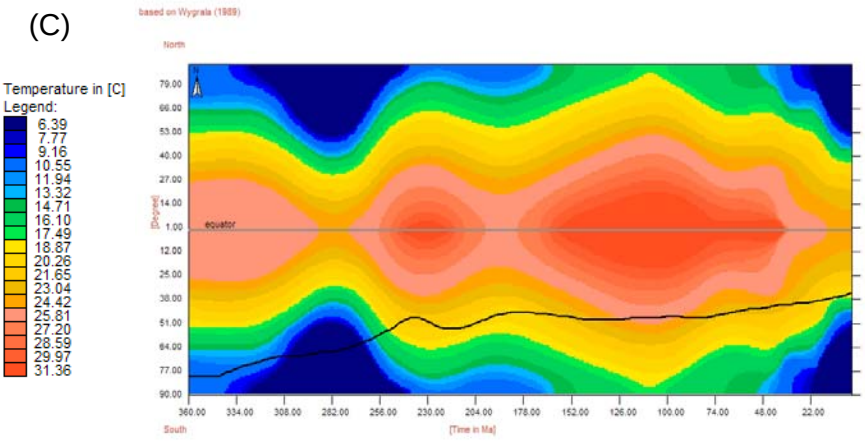

Figures 44: (A) Heat flow trend with a heat flow spike at the point of rifting decreasing to a present day. (B) Map view of the heat flow trend over the study area. (C) Global mean surface temperature or the sediment water interface temperature for the southern hemisphere at latitude 33.

CONSTANT HEAT FLOW MODEL

(A)

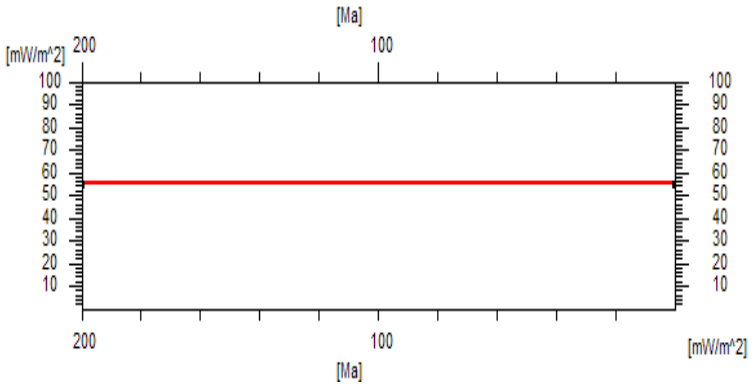

(B)

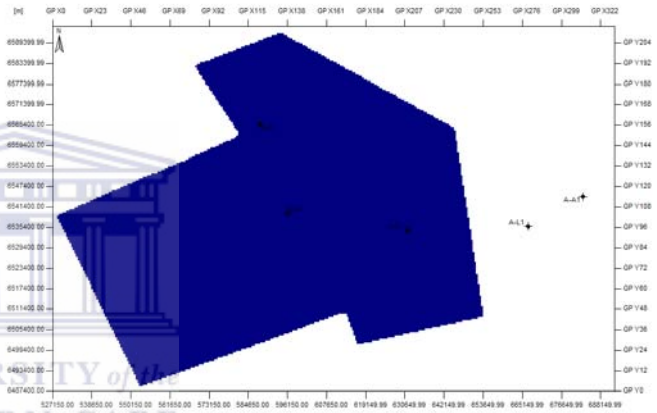

(C)

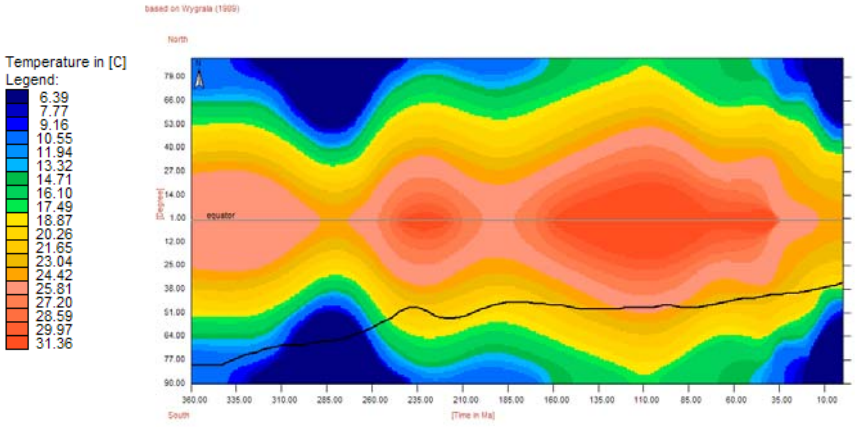

Figures 45: (A) Constant heat flow trend (B) Map view of the heat flow trend over the study area. (C) Global mean surface temperature or the sediment water interface temperature for the southern hemisphere at latitude 33.

RIFT - DRIFT MODEL

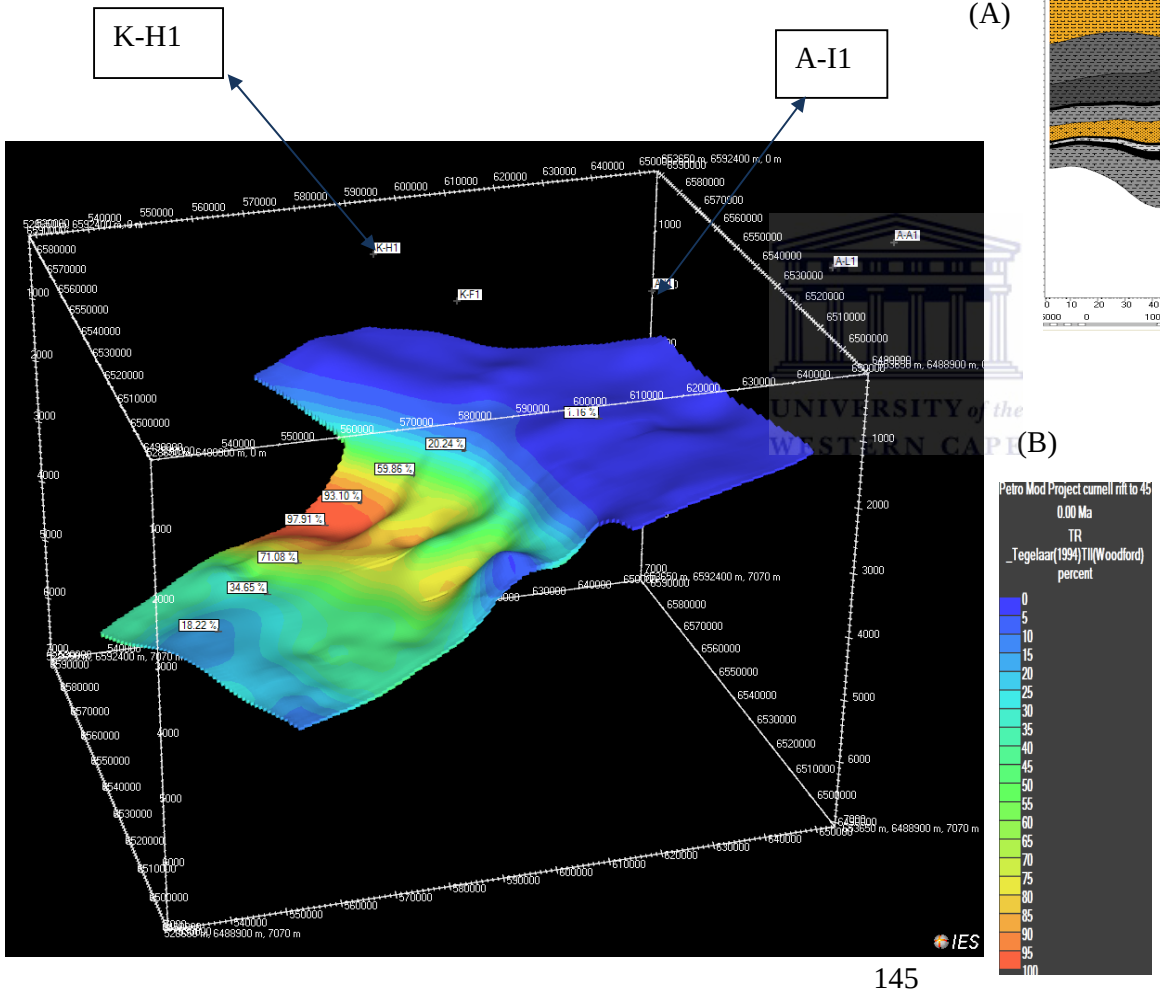

Figures 46: (A) Simulated Image of a cross-section of a section of the Orange Basin indicating the source rock intervals.

(B) Cenomanian - Turonian source rock with the maturity maps overlain under the rift – drift heat flow model.

(A)

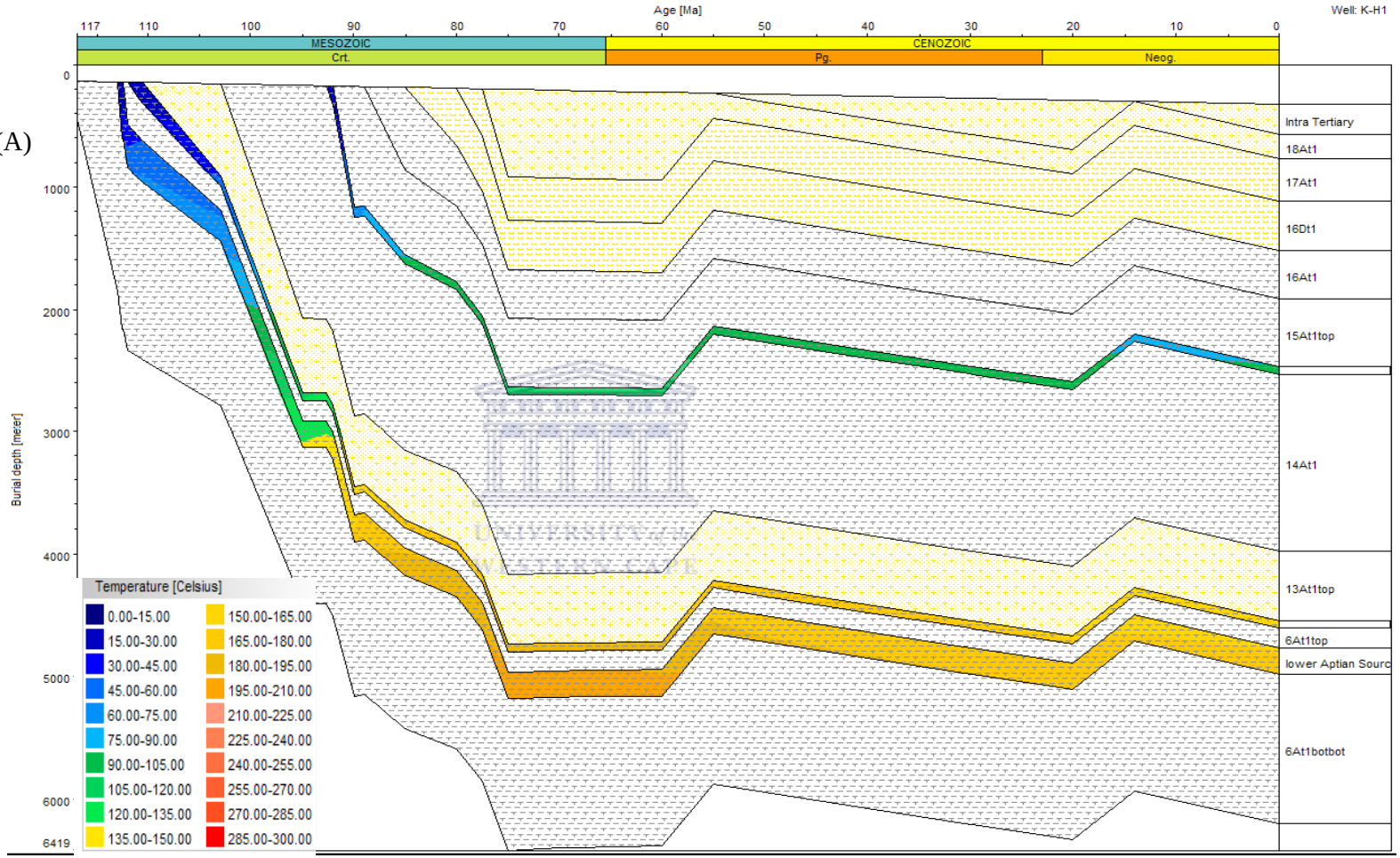

Assumption of an oil window between 60 and 120 degrees celsius, indicated by the color legend to be between light blue and dark green

Assumption of an oil window between 60 and 120 degrees celsius, indicated by the color legend to be between light blue and dark green

(B)

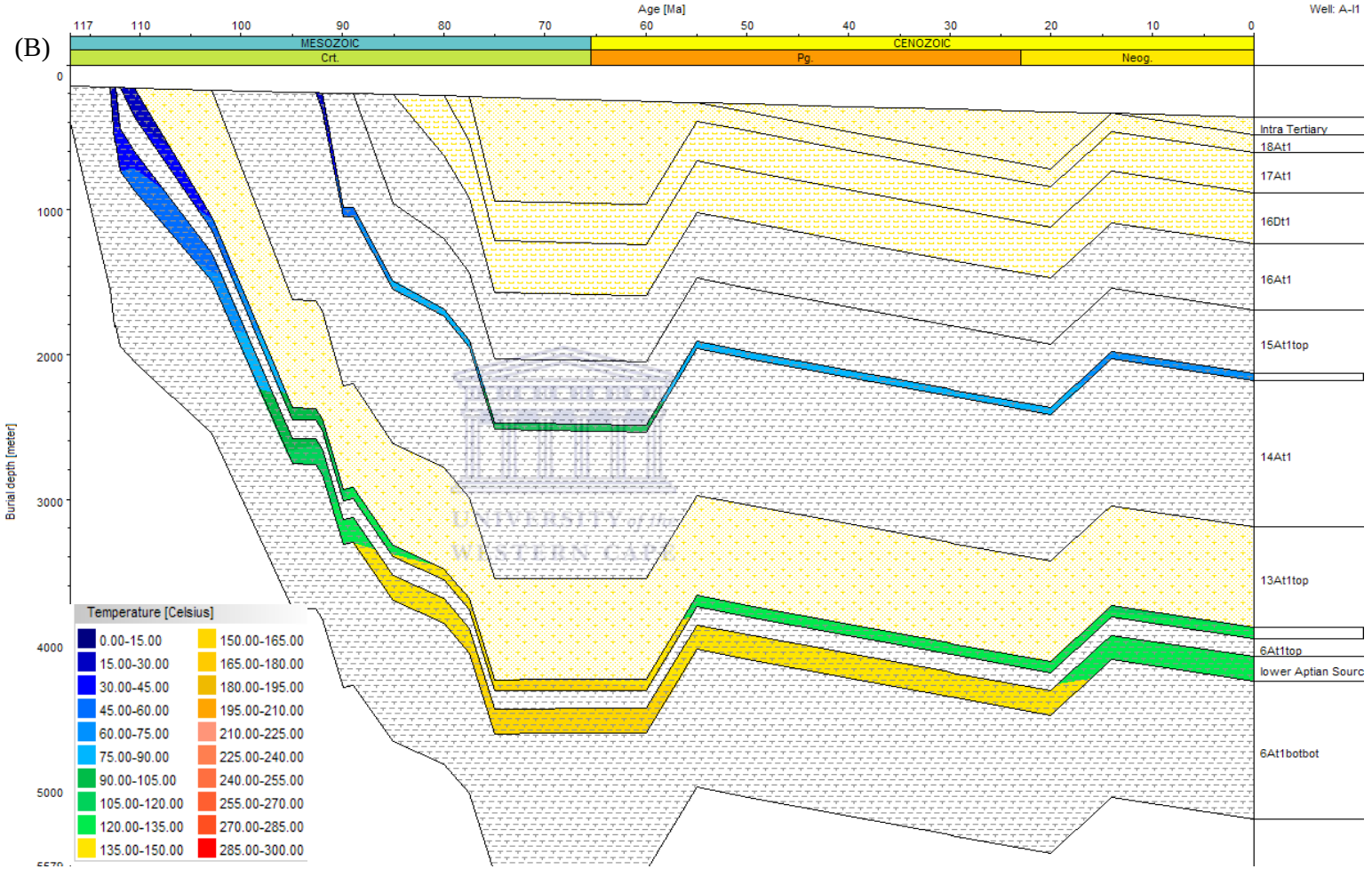

Figures 47: (A) (B) Burial history curves from the Cretaceous to the Tertiary based on strata penetrated in well K-H1 and A-I1 in the Orange Bains.

(A)

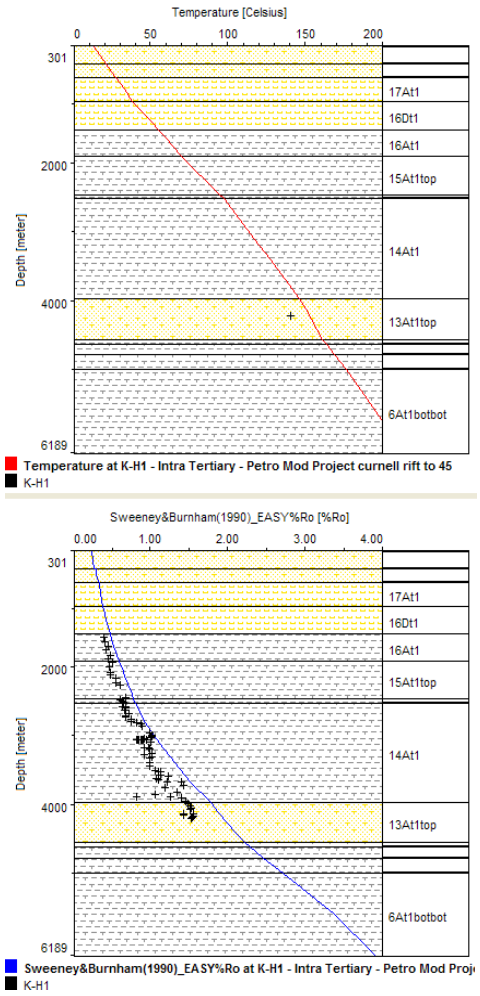

(B)

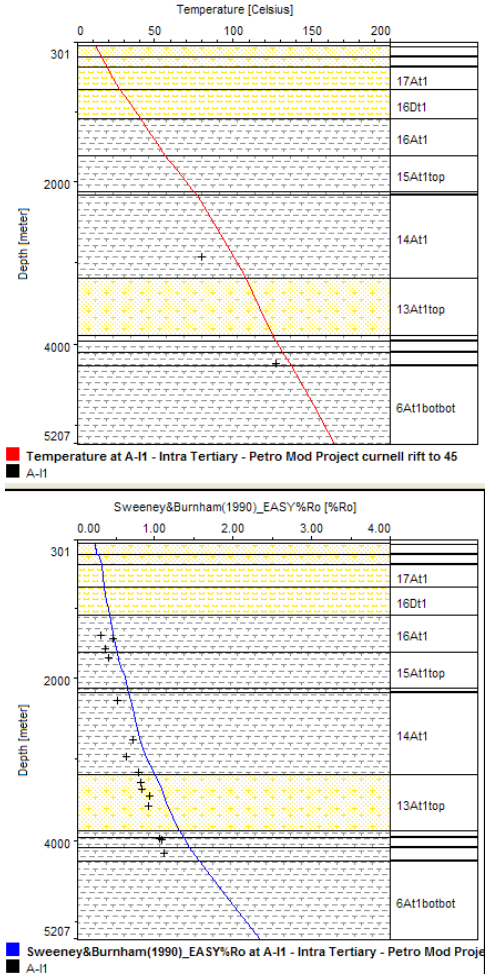

Figures 48: (A) (B) Modeled calibration indicate the modeled temperature and vitrinite reflectance parameters against the actual values of well K-H1 and A-I1 respectively.

(A)

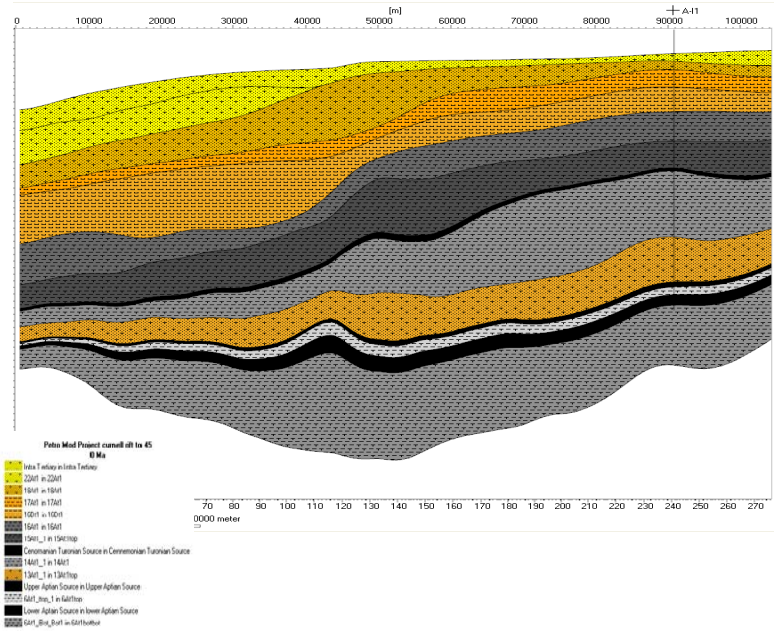

(B)

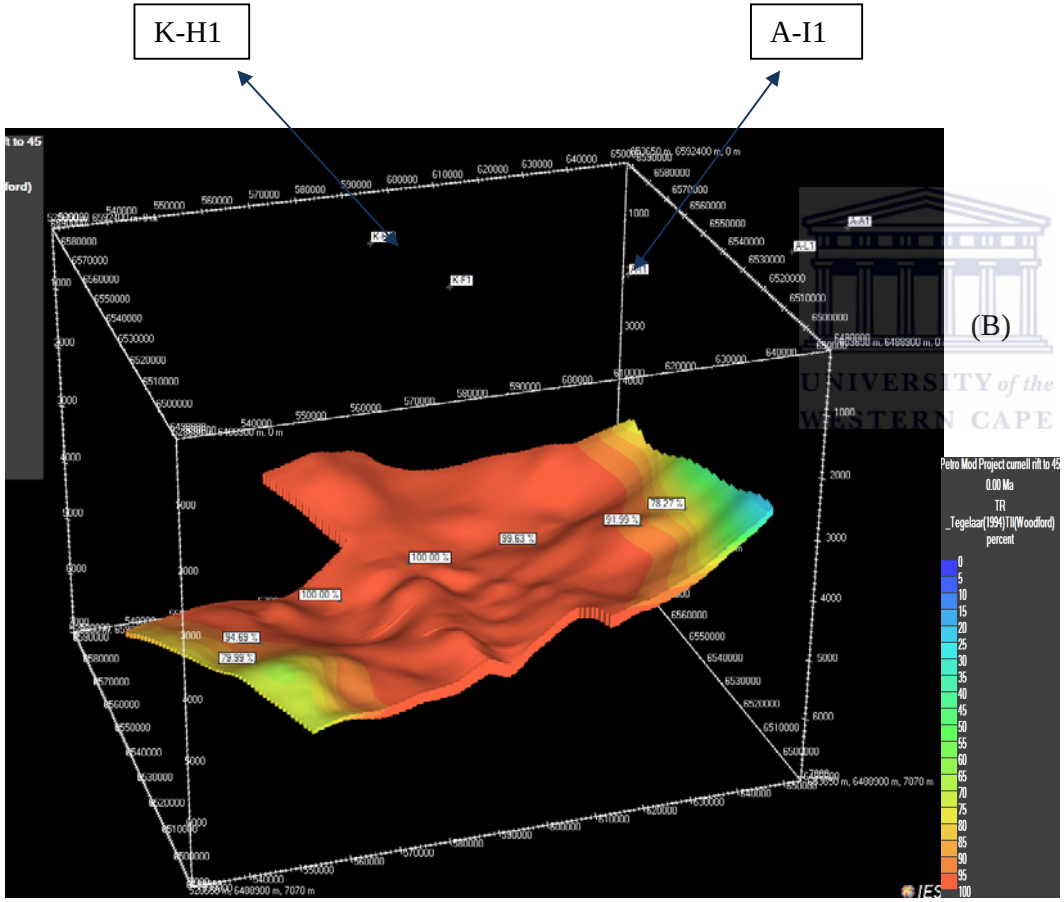

Figures 49: (A) Simulated Image of a cross-section of a section of the Orange Basin indicating the source rock intervals.
(B) Barremian - Early Aptian source rock with the maturity maps overlain under the rift – drift heat flow model.

(A

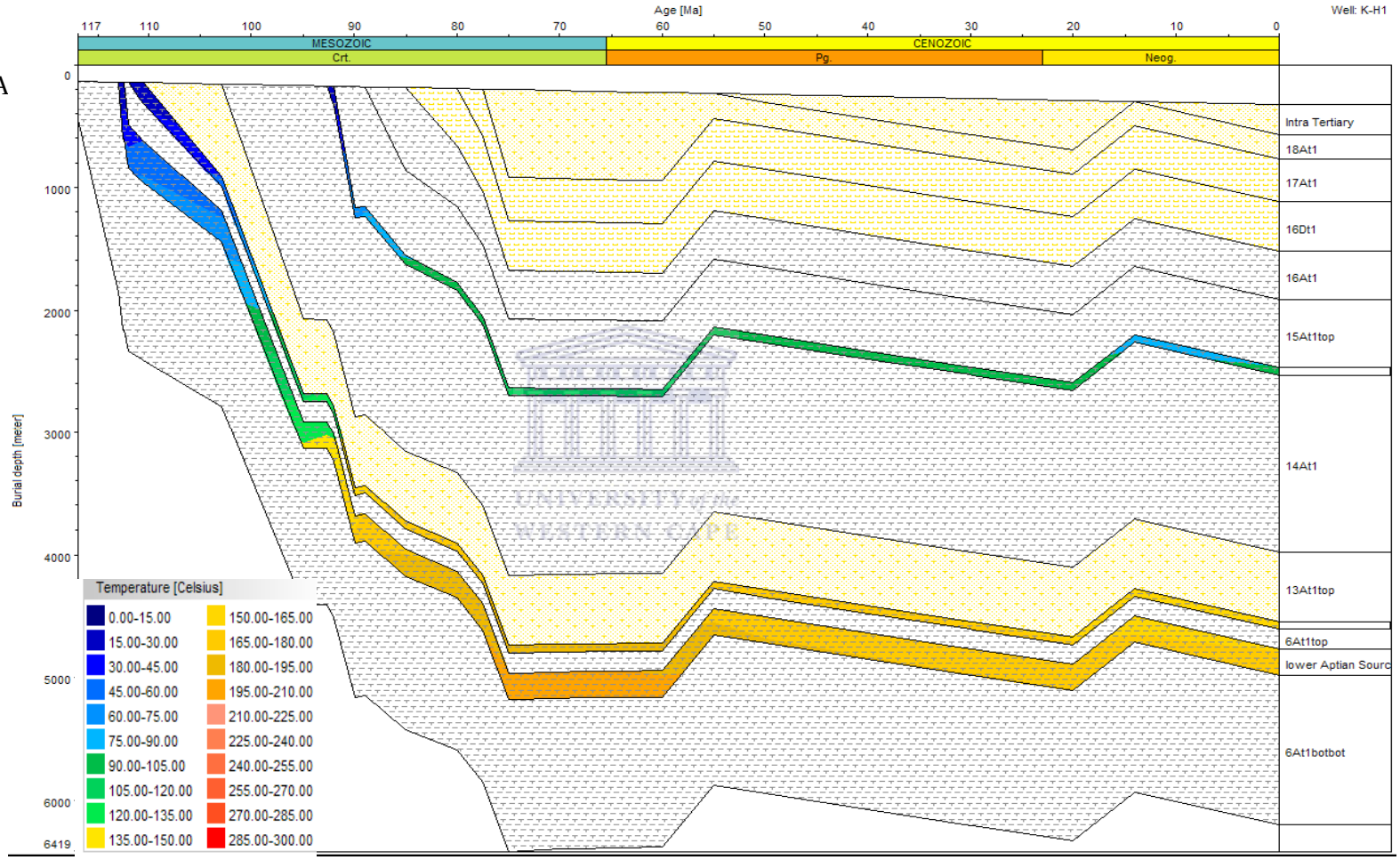

Assumption of an oil window between 60 and 120 degrees celsius, indicated by the color legend to be between light blue and dark green

Assumption of an oil window between 60 and 120 degrees celsius, indicated by the color legend to be between light blue and dark green

(B)

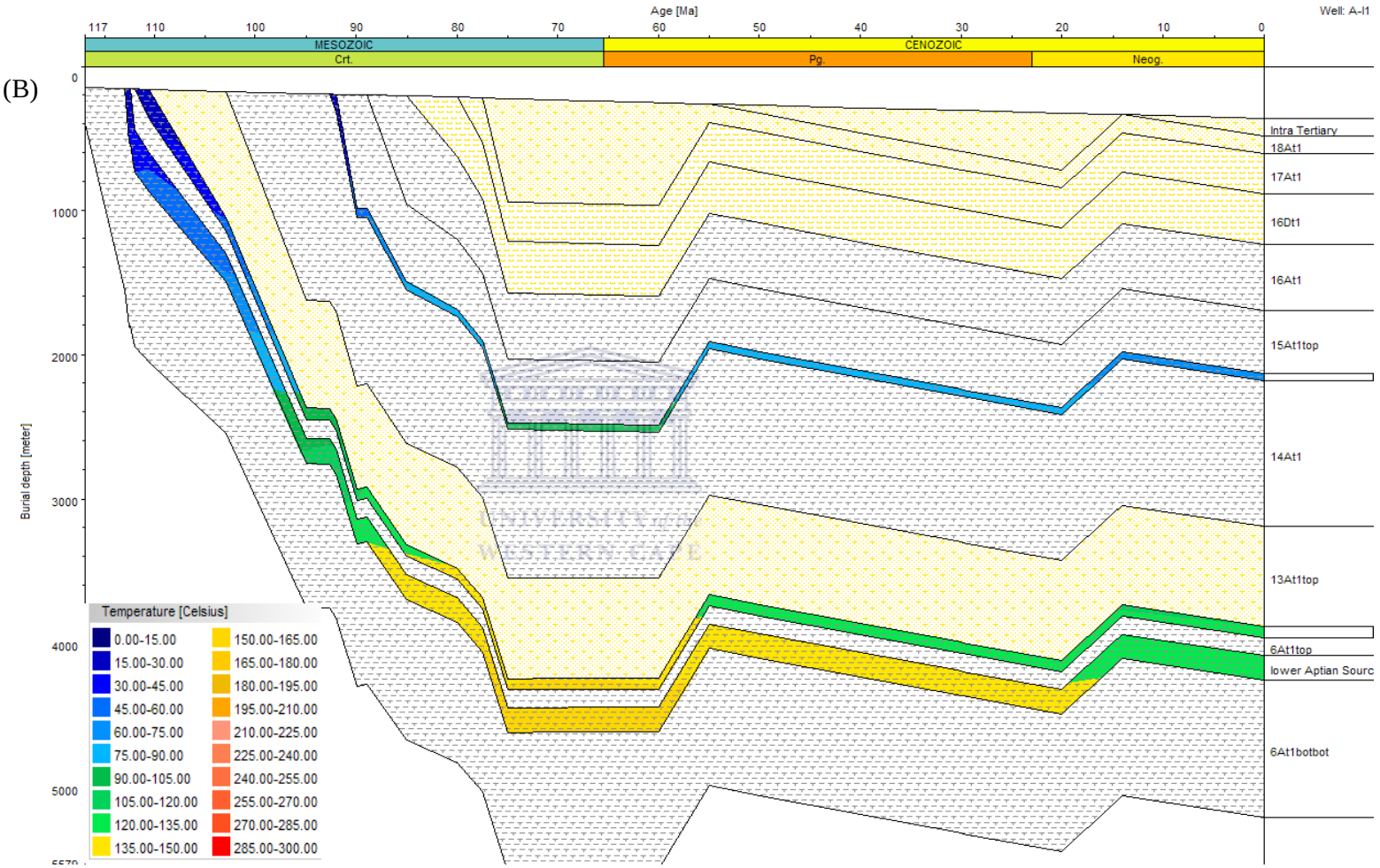

Figures 50: (A) (B) Burial history curves from the Cretaceous to the Tertiary based on strata penetrated in wells K-H1 and A-I1 in the Orange Basin.

(A)

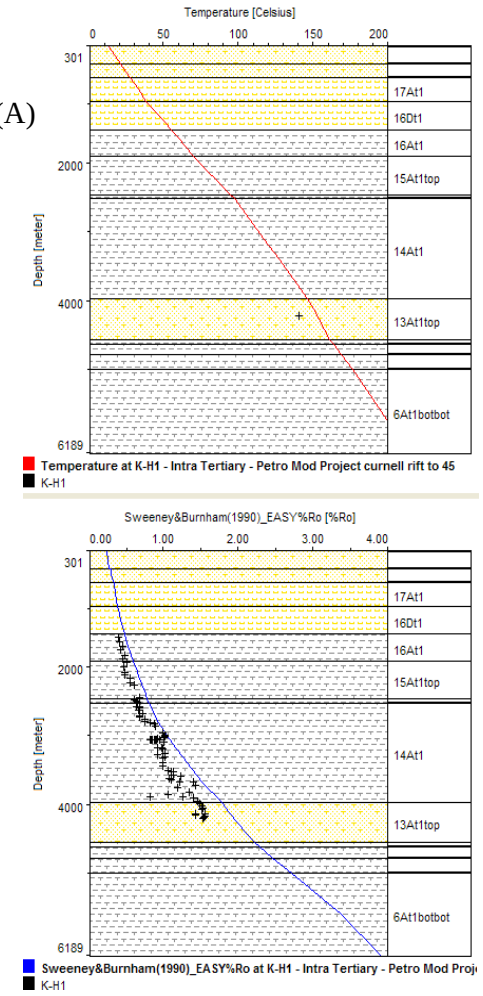

(B)

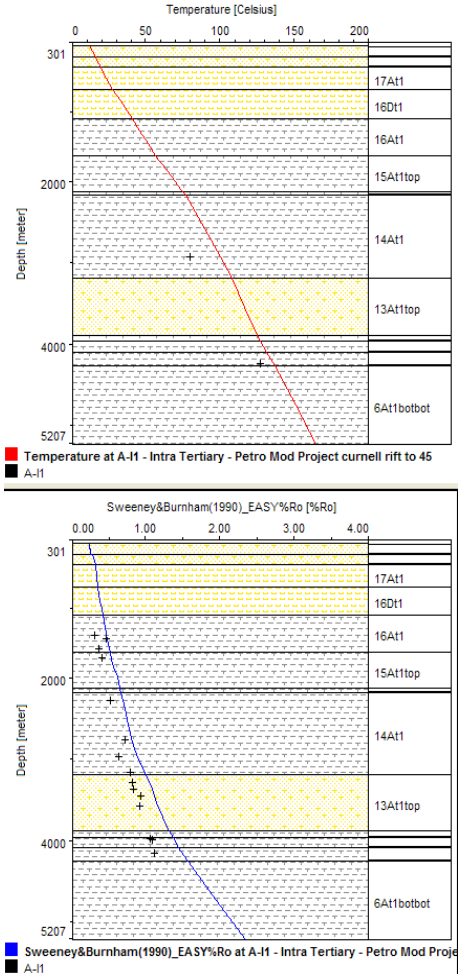

Figures 51: (A) (B) Modeled calibration indicate the modeled temperature and vitrinite reflectance parameters against the actual values of well K-H1 and A-I1 respectively.

In the rift-drift model the transformation ratio (percentage of source rock that has reached thermal maturation) overlay over the younger postulated Cenomanian - Turonian source rock (Figure 46 (B)) show that the source rock is in the oil window and contain a centrally mature region similar to the older Barremian - Early Aptian source rock. The transformation ratio overlay over the older Barremian - Early Aptian source rock indicates that the source rock has been almost completely transformed (matured) with complete maturation in the mid section decreasing basinward and landward (Figure 49 (B)).

The burial history diagram for wells A-I1 and K-H1 indicate that on deposition of the intermediate sequence continued subsidence for the post rift sediments of the Orange Basin continued for approximately 42 Million years to a maximum depth of approximately 5600 meters at well A-I1 and 6500 meters at well K-H1 (Figures 47 (A) (B), 50 (A) (B)) . The subsidence is followed by two periods of uplift with subsequent erosion indicated on the burial history charts (Figures 47 (A) (B), 50 (A) (B)) with the first period active for 5 Million years removes an estimated 960 meters of sediments from the shelf.

The second period of uplift is less forceful and occurs over a longer time span of 6 Million years removing only 420 meters of sediment. Isotherms superimposed onto the burial history diagrams give an indication of temperature change with depth with closely spaced isotherms indicating a greater increase in temperature with depth compared to more spread out isotherms indicating a moderate increase in temperature with depth (Figures 47 (A) (B), 50 (A) (B)). These isotherms are more closely spaced in well K-H1 indication a more accelerated increase in temperature with depth at well K-H1 compared to well A-I1.

Utilizing the burial history charts to investigating the affect of these factors mentioned above on the evolution of the source rocks it reveals that the Barremian - Early Aptian source rock have entered the oil window earlier at well location K-H1 compared to the same source rock in the vicinity of well A-I1 (Figures 47 (A) (B), 50 (A) (B)).

This is based on the assumption of an oil window between 60 and 120 degrees celsius, indicated by the color legend to be between light blue and dark green in the burial history chart of well K-H1 and A-I1 (Figures 47 (A) (B), 50 (A) (B)). The burial history chart also indicate that the source rock reach a maximum depth of approximately 5000 meters at well K-H1 and 4500 meters at well A-I1 and maximum temperatures of approximately 200 degrees Celsius at well K-H1 and 180 degrees Celsius at location A-I1 (Figures 47 (A) (B), 50 (A) (B)). This source rock can therefore be classified as overmature as indicated in the transformation ratio overlay and based on the maximum temperature the source rock has been subjected to. The source rock is uplifted but remains in the mature stage at well location K-H1 however the source rock at well location A-I1 is presently found in the temperature range designated to be the oil window. The source rock at this location has thus passed through the oil window into the thermal maturation phase and is being uplifted back into the oil window after two periods of uplift (Figures 47 (A) (B), 50 (A) (B)).

The Cenomanian - Turonian source rock appear to also follows the same trend as the older Barremian - Early Aptian source rock where the source rock also enter the oil window first around well K-H1 with a maximum depth of 2800 and 2300 meters and temperatures of approximately 120 and 90 degrees celsius at well location K-H1and A-I1 respectively (Figures 47 (A) (B), 50 (A) (B)). This source rock can therefore be classified as slightly matured as indicated in the transformation ratio overlay over the source rock and based on the maximum temperature the source rock has been subjected to. The Cenomanian-Turonian source rock is at present found within the thermal window of between 60 and 75 degrees Celsius at well location A-I1. The source rock entered the thermal window of 75 to 90 degrees Celsius after the first period of upliftment and was later cooled further after the second period of upliftment resulting in the present location of the source rock in the 60 to 75 degrees Celsius thermal window (Figures 47 (A) (B), 50 (A) (B)).

At well location K-H1 the source rock at present also finds itself in the thermal window between 75 and 90 degrees Celsius but has only entered this stage after the second period of upliftment (Figures 47 (A) (B), 50 (A) (B)). Studying the calibration of the model with temperature and vitrinite reflectance the model parameters can be closely correlated to the actual evolution of the Orange Basin sediments. (Figures 48 (A) (B), 51 (A) (B)).

CONSTANT HEAT FLOW MODEL

(A)

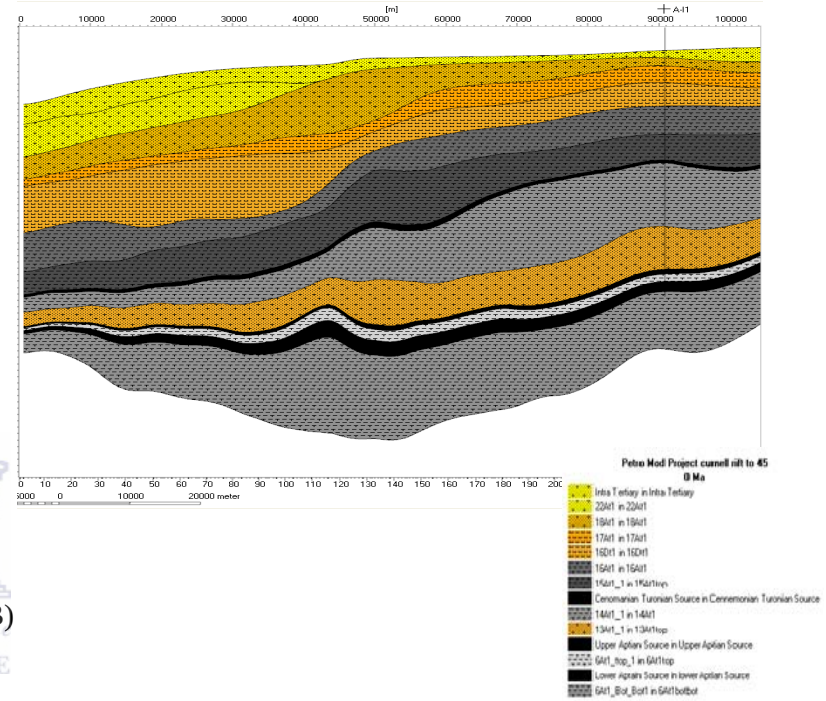

(B)

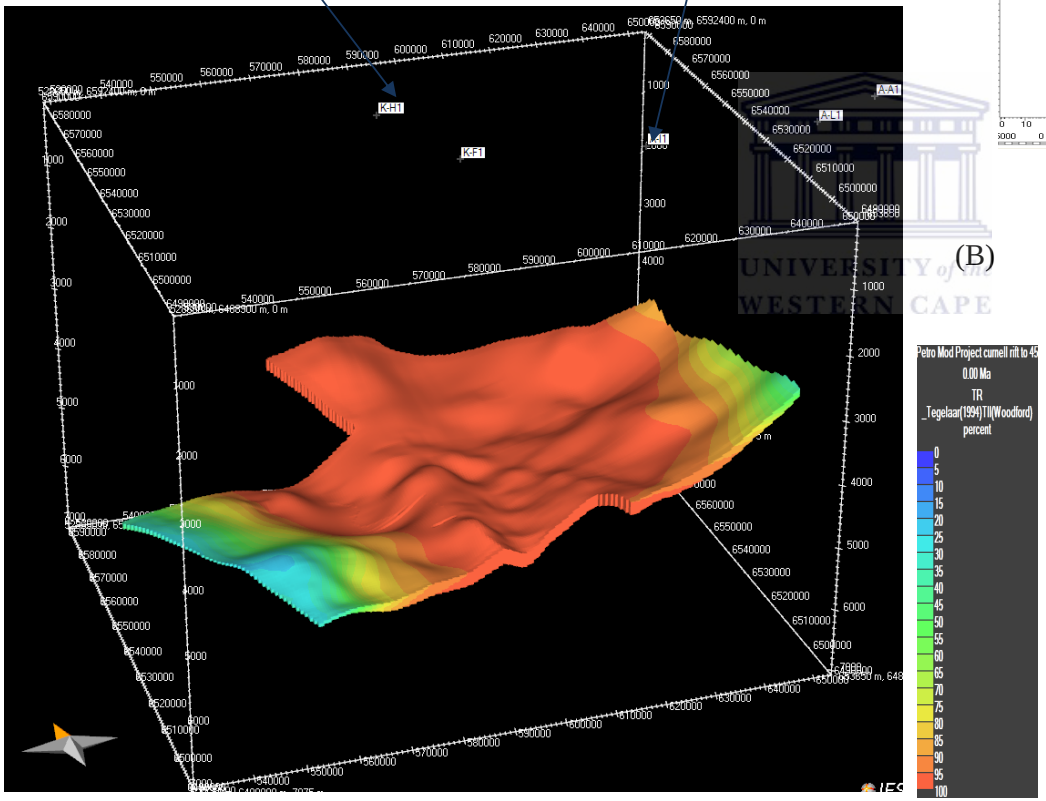

Figures 52: (A) Simulated Image of a cross-section of a section of the Orange Basin indicating the source rock intervals.
(B) Barremian - Early Aptian source rock with the maturity maps overlain under the constant heat flow model.

(A)

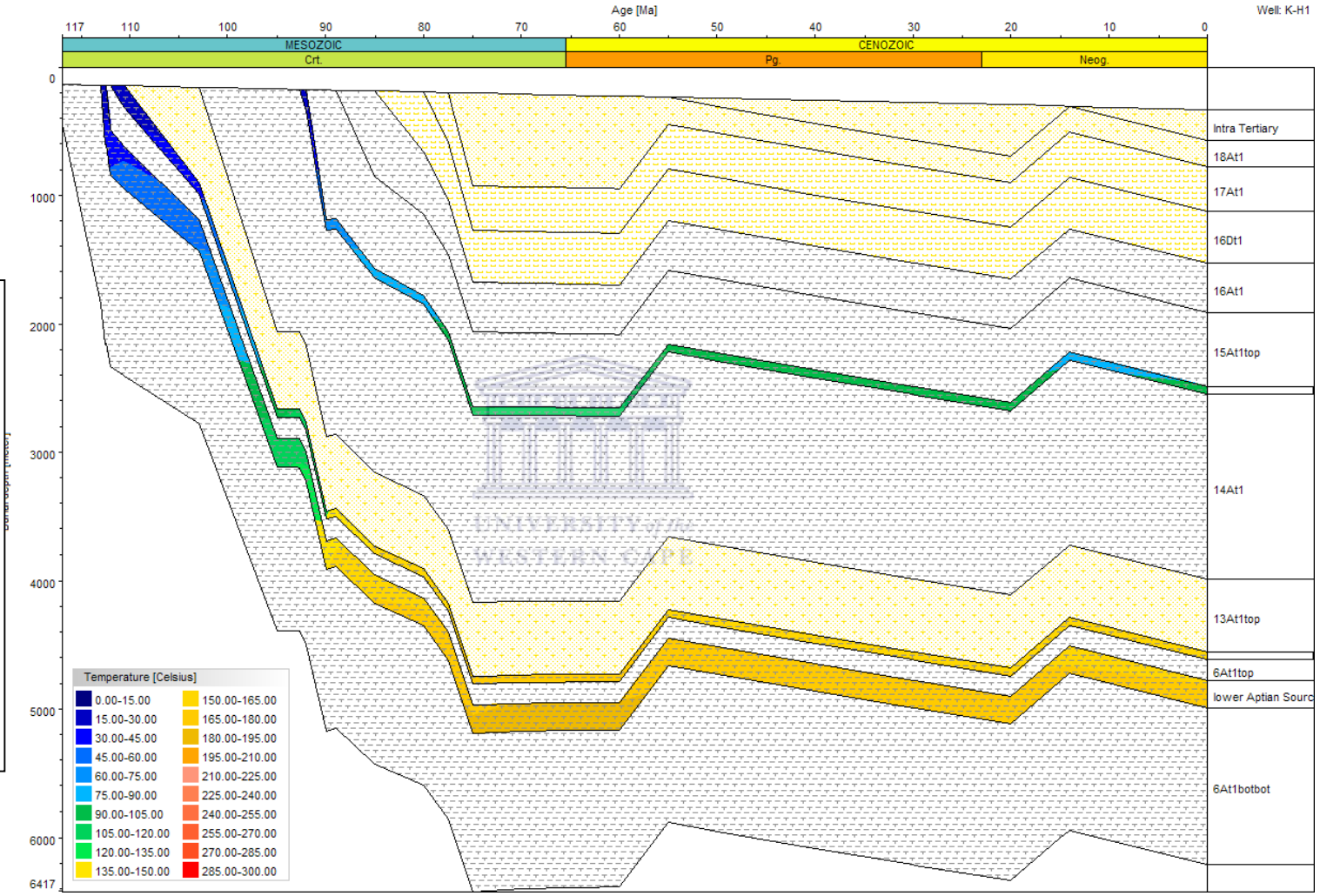

Assumption of an oil window between 60 and 120 degrees celsius, indicated by the color legend to be between light blue and dark green

(B)

Assumption of an oil window between 60 and 120 degrees celsius, indicated by the color legend to be between light blue and dark green

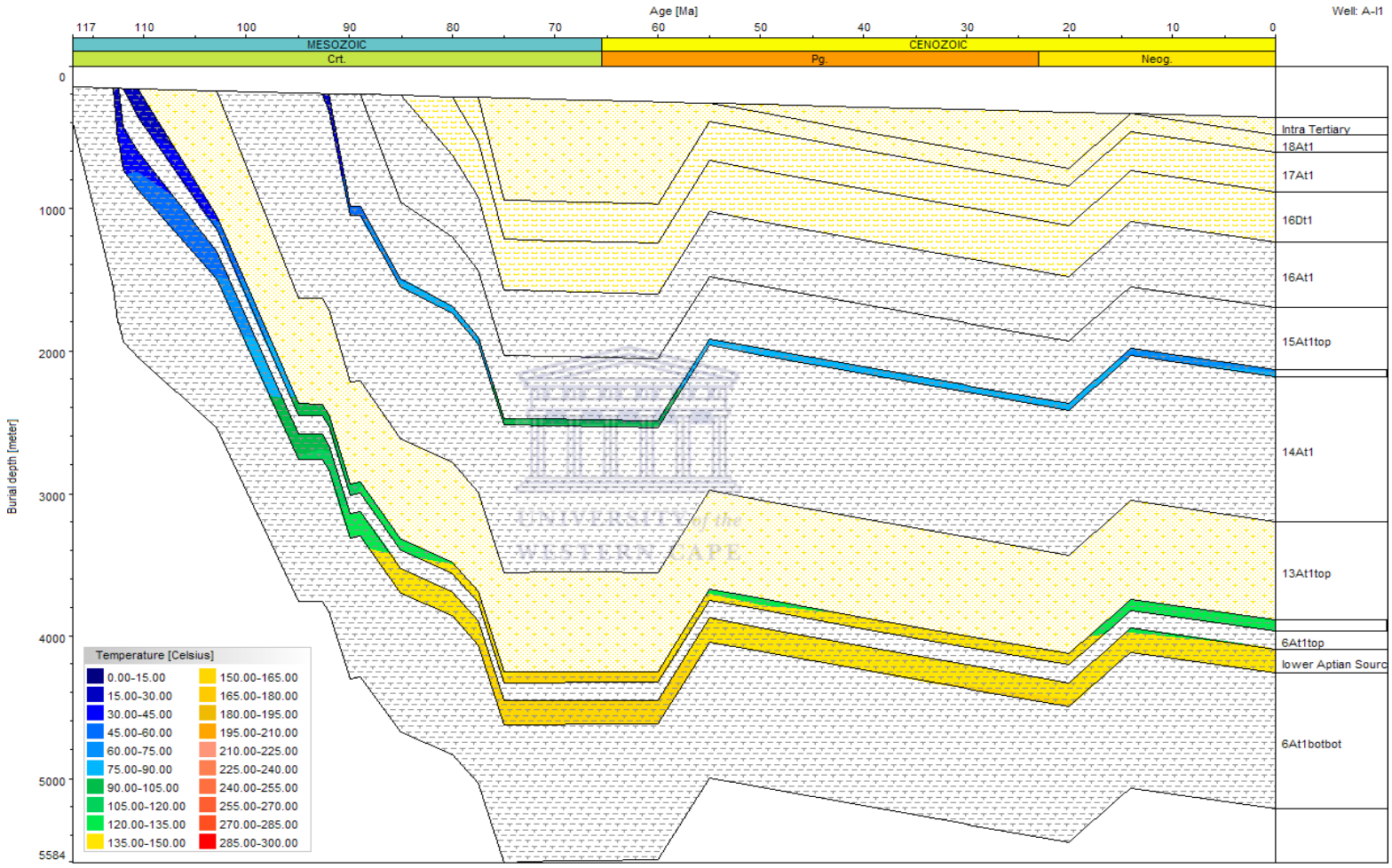

Figures 53: (A) (B) Burial history curves from the Cretaceous to the Tertiary based on strata penetrated in wells K-H1 and A-I1 in the Orange Basin.

(A)

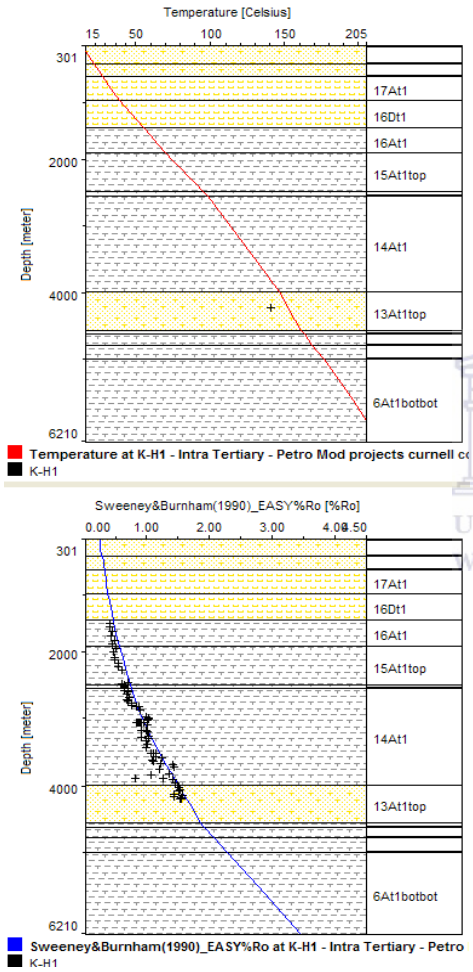

(B)

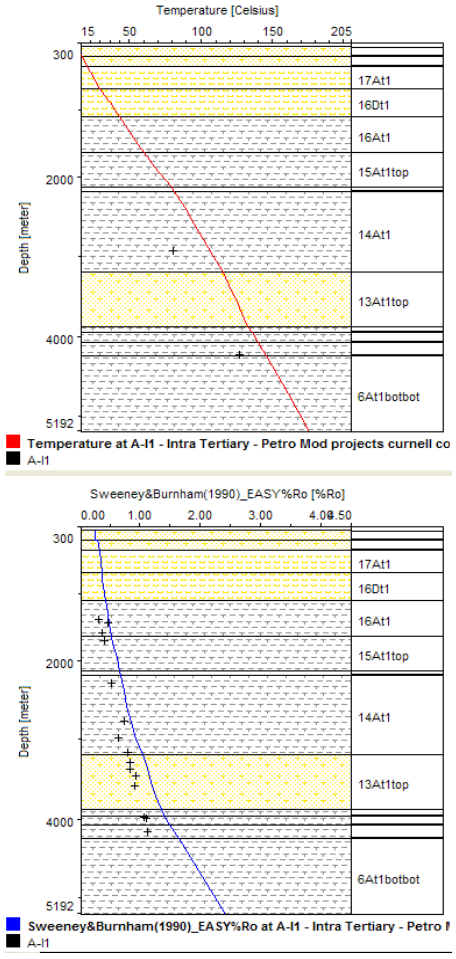

Figures 54: (A) (B) Modeled calibration indicate the modeled temperature and vitrinite reflectance parameters against the actual values of well K-H1 and A-I1 respectively.

(A)

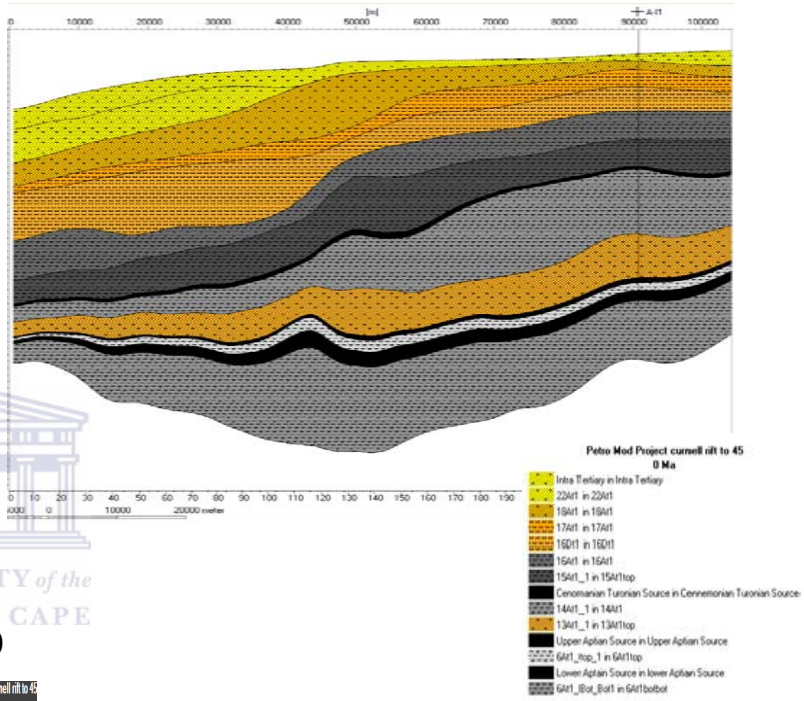

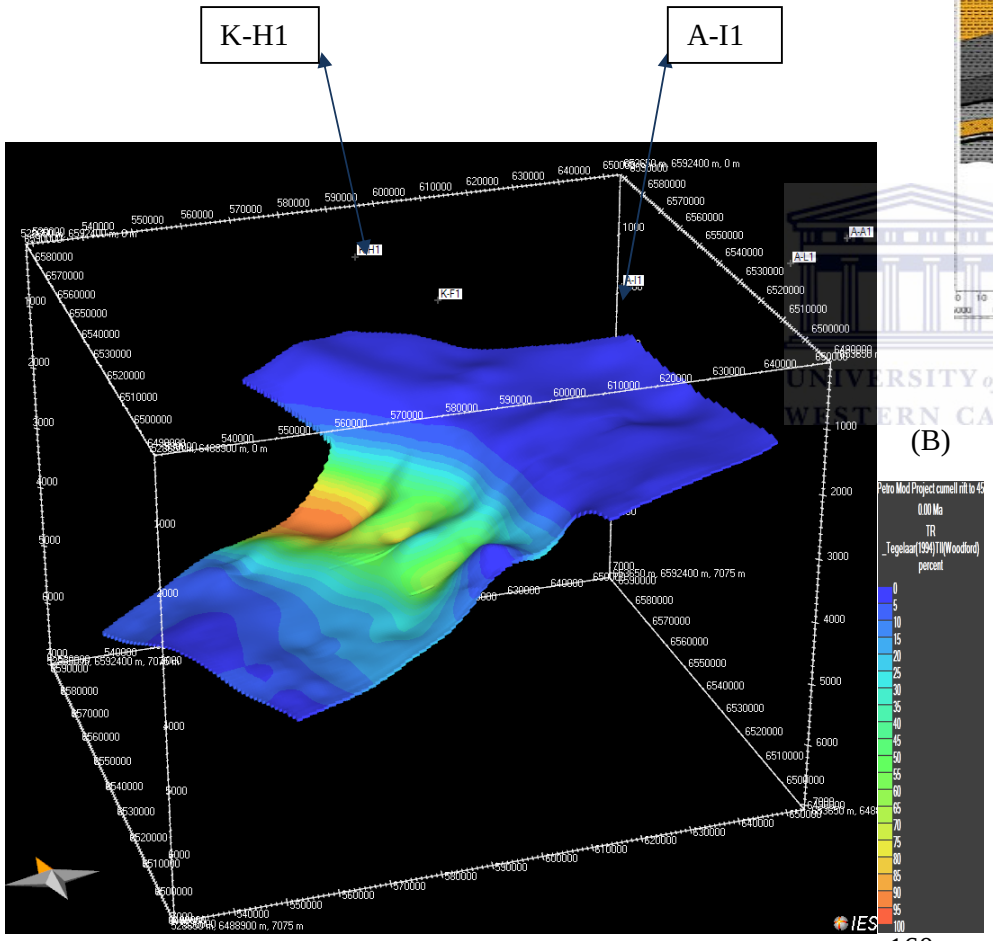

(B)

Figures 55: (A) Simulated Image of a cross-section of a section of the Orange Basin indicating the source rock intervals.

(B) Cenomanian - Turonian source rock with the maturity maps overlain under the constant heat flow model.

(A)

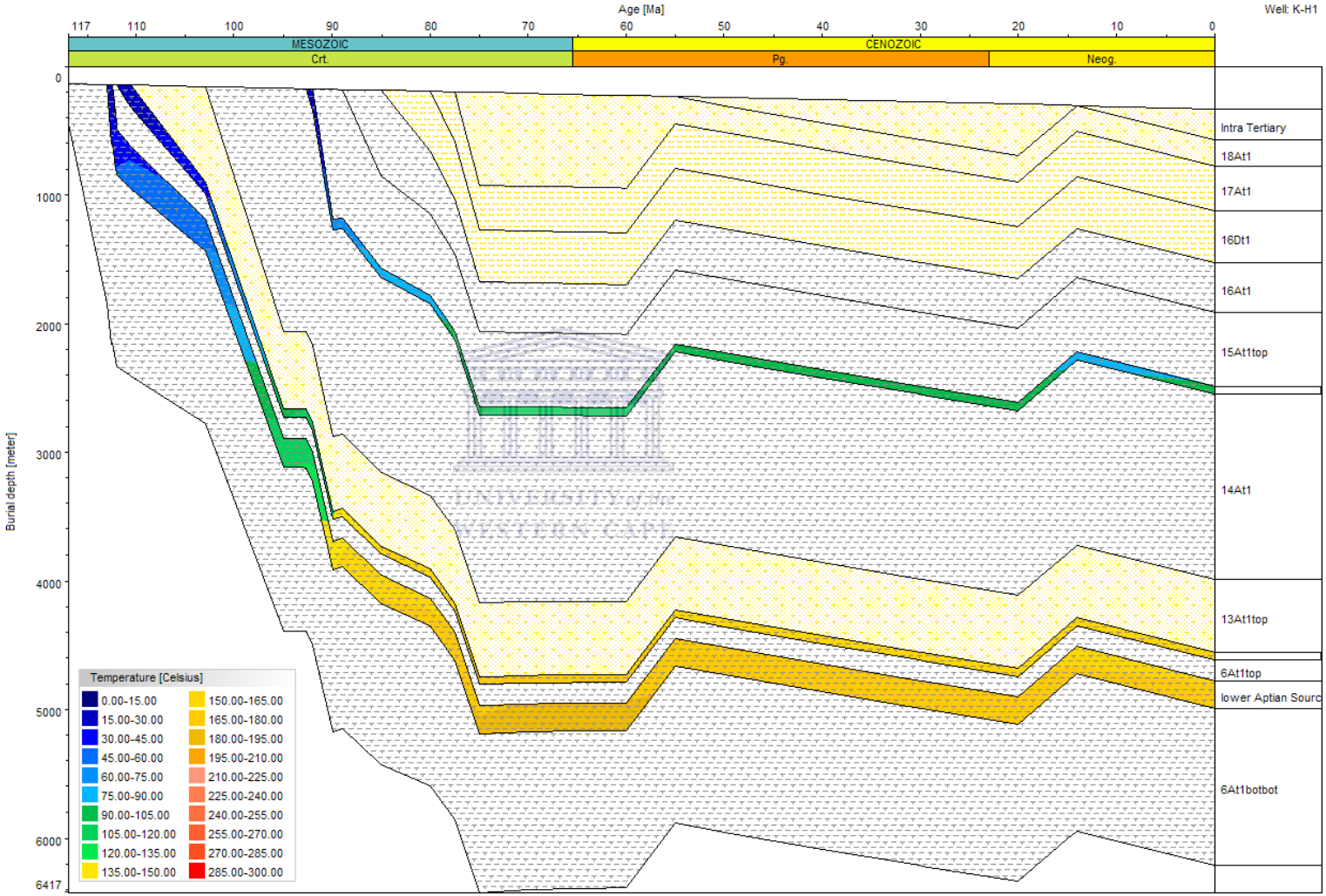

Assumption of an oil window between 60 and 120 degrees celsius, indicated by the color legend to be between light blue and dark green

(B)

Assumption of an oil window between 60 and 120 degrees celsius, indicated by the color legend to be between light blue and dark green

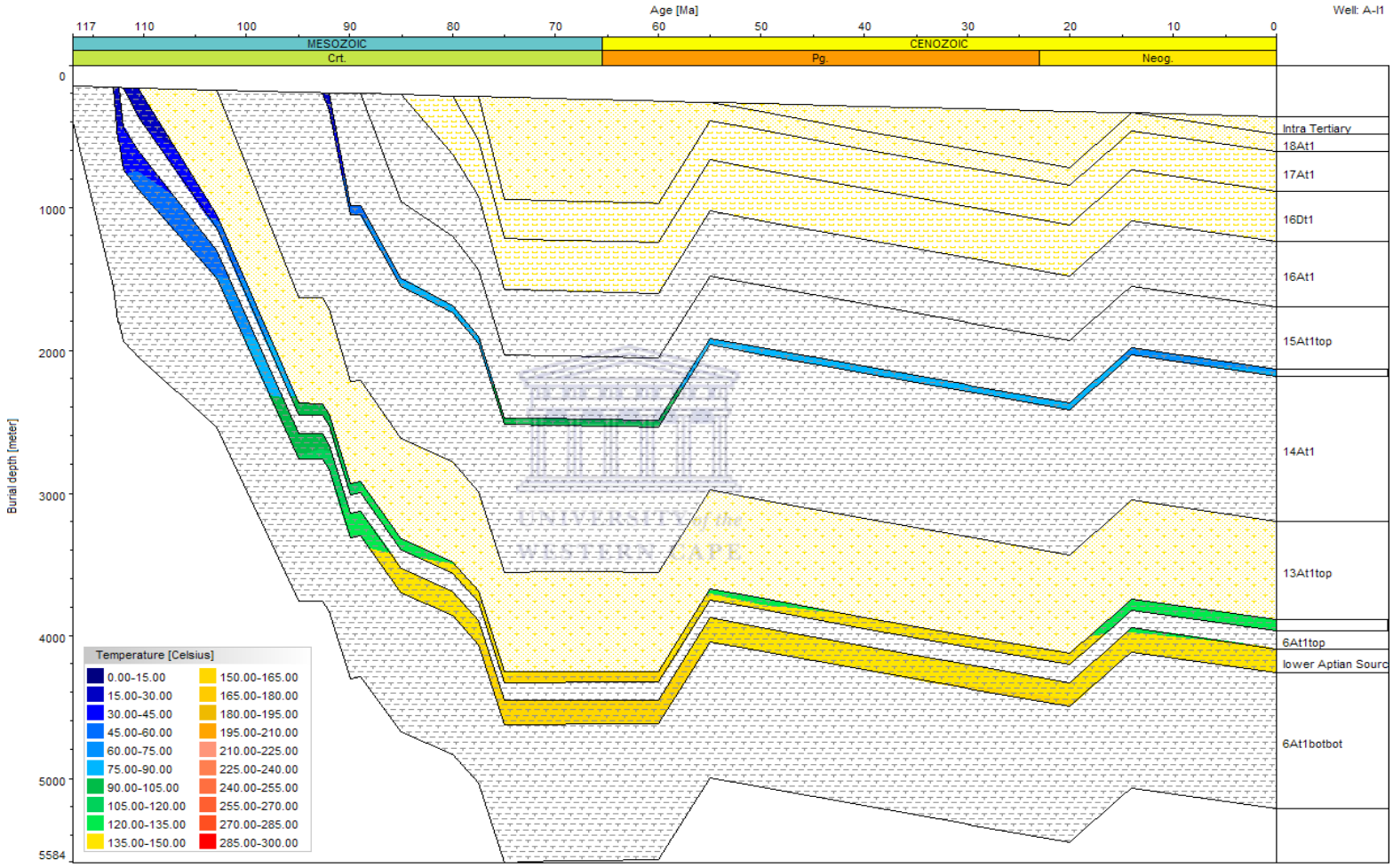

Figures 56: (A) (B) Burial history curves from the Cretaceous to the Tertiary based on strata penetrated in wells K-H1 and A-I1 in the Orange Basin.

(A)

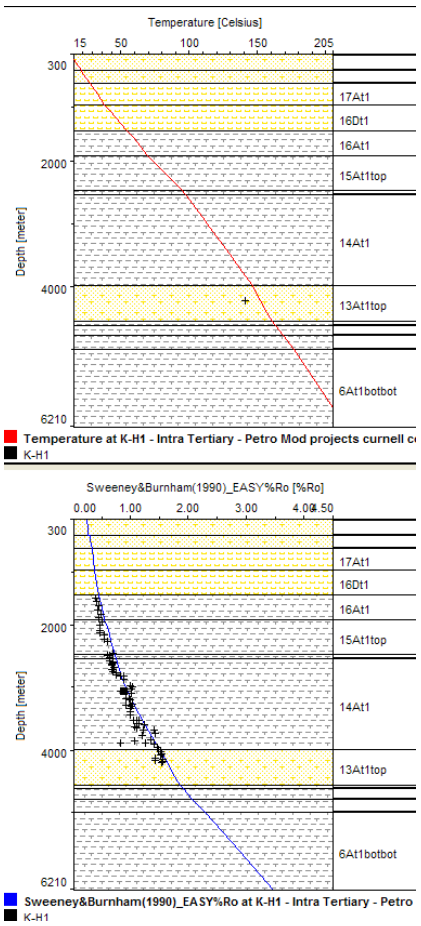

(B)

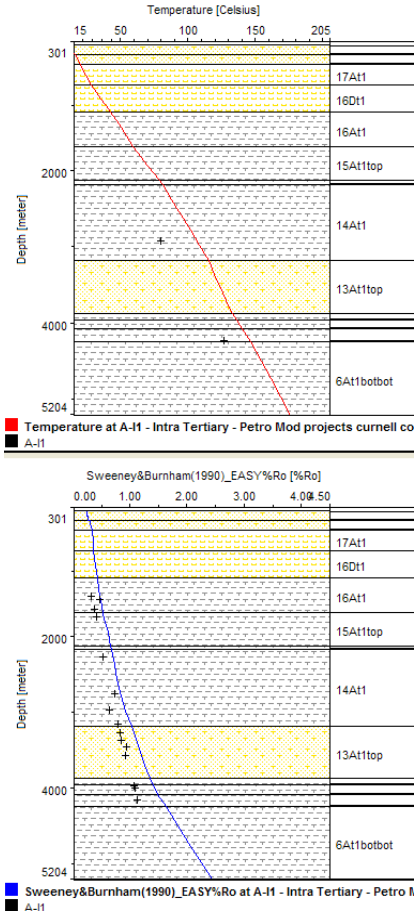

Figure 57: (A)(B) Modeled calibration indicate the modeled temperature and vitrinite reflectance parameters against the actual values of well K-H1 and A-I1 respectively.

In the constant heat flow model the transformation ratio (percentage of source rock that has reached thermal maturity) overlay over the older Barremian - Early Aptian source rock show that the source rock is matured with complete maturation in the mid section, decreasing basinward and lanward (Figure 52 (B). The transformation ratio overlay over the younger Cenomanian - Turonian source rock indicate that most of the source rock has not reached the thermal maturation threshold with the exception of the midsection which displays almost complete maturation (Figure 55 (B)).

The burial history diagram for wells A-I1 and K-H1 remains the same as the rift-drift model with a maximum depth reached at approximately 5600 meters at well location A-I1 and 6500 meters at well location K-H1 and two periods of uplift and subsequent erosion (Figures 53 (A) (B), 56 (A) (B)). Investigating the evolution of the source rock under the constant heat flow model conditions the burial history diagram reveal that the Barremian Early Aptian source rock follows the same maturation trend at well A-I1 and K-H1 but with continues burial and increasing temperature at well location K-H1 the source rock becomes more mature at this location (Figures 53 (A) (B), 56 (A) (B)). The source rock at present is above the 120 degrees Celsius isotherm at well location K-H1 while the top of the source rock at well location A-I1 has moved through the 120 degrees Celsius and back into the 120 to 135 degrees Celsius thermal window consecutively after each period of uplift (Figures 53 (A) (B), 56 (A) (B)).

Burial history of the Cenomanian-Turonian source rock indicates that the source maturation is slightly accelerated at well location K-H1 indicated by the rapid increased temperature at well location K-H1 (Figures 53 (A) (B), 56 (A) (B)). At present the Cenomanian-Turonian source rock is in the 60 to 75 degrees Celsius thermal window at well location A-I1 (Figures 53 (A) (B), 56 (A) (B)). The source rock has entered this stage only after the second period of uplift before which it was subjected to a thermal regime of between 75 and 90 degrees Celsius subsequent to the first period of uplift (Figures 53 (A) (B), 56 (A) (B)).

At well location K-H1 the Cenomanian-Turonian source rock just entered the 90 to 105 degrees Celsius thermal window. This source rock has been in the 90 to 120 degrees Celsius thermal window after the first period of uplift and entered the 75 to 90 degrees Celsius thermal window after the second period of uplift but with continues burial temperatures increased above the 90 degrees Celsius for the Cenomanian-Turonian source rock (Figures 53 (A) (B), 56 (A) (B)).

Studying the calibration of the model with temperature and vitrinite reflectance the model parameters can be closely correlated to the actual evolution of the Orange Basin sediments. The constant heat flow model show a better fit in vitrinite reflectance at well K-H1 and A-I1 compared to the rift – drift model (Figures 53 (A) (B), 56 (A) (B)).

TIME EXTRACTIONS FOR RIFT-DRIFT HEAT FLOW MODEL

Cenomanian - Turonian Source Rock

Temperature evolution

(A)

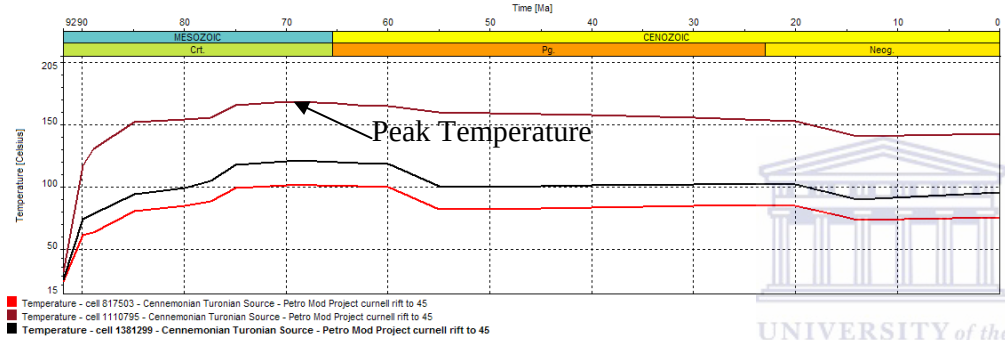

- Red line is at location A-I1 (shelfal area of basin)
- Brown line is at the depocentre area of the basin
- Black line at location K-H1 (middle of basin)

Maturation evolution

(B)

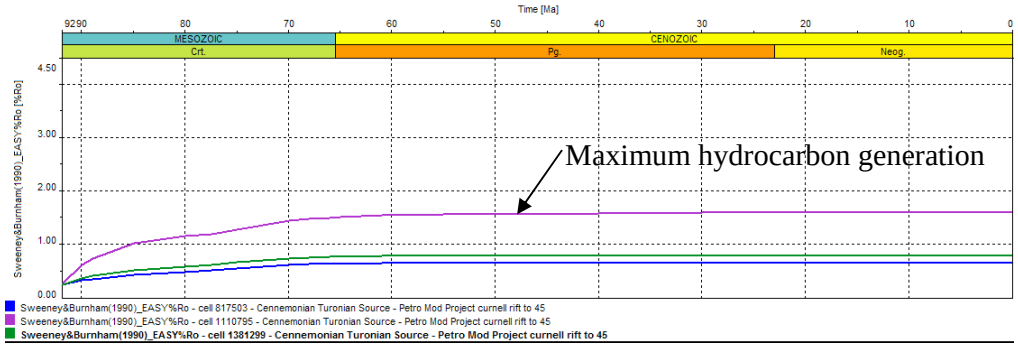

- Blue line is at location A-I1 (shelfal area of basin)
- Purple line is at the depocentre area of the basin
- Green line at location K-H1 (middle of basin)

Figures 58: (A) (B) Time extractions at various well locations in the basin indicating peak temperature and maturation for the Cenomanian - Turonian Source Rock for the rift-drift heat flow model.

Barremian - Early Aptian Source Rock

Temperature evolution

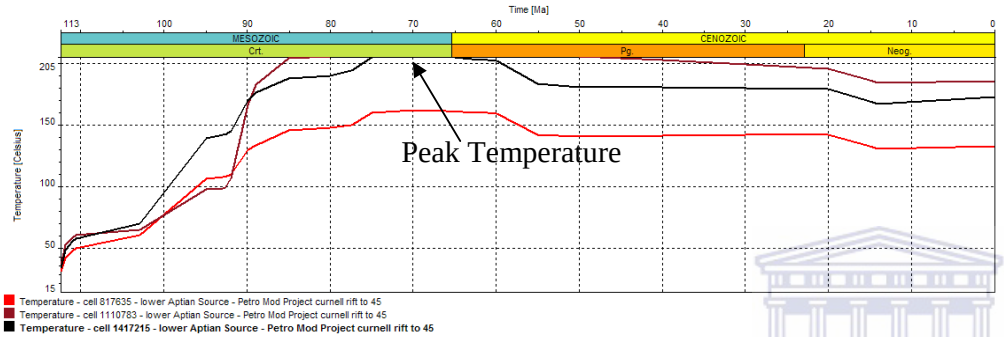

(A)

- Red line is at location A-I1 (shelfal area of basin)
- Brown line taken from the depocentre area of the basin
- Black line at location K-H1 (middle of basin)

Maturation evolution

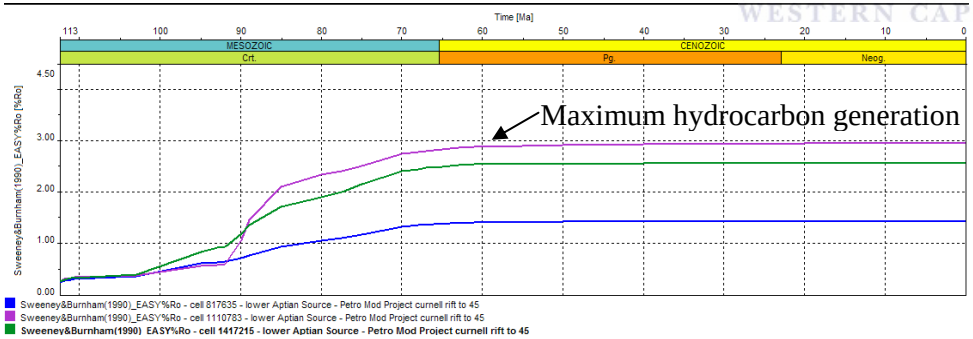

(B)

- Blue line is at location A-I1 (shelfal area of basin)
- Purple line taken from the depocentre area of the basin
- Green line at location K-H1 (middle of basin)

Figures 59: (A) (B) Time extractions at various well locations in the basin indicating peak temperature and maturation for the Barremian - Early Aptian Source Rock for the rift-dift heat flow model

TIME EXTRACTIONS FOR CONSTANT HEAT FLOW MODEL

Cenomanian - Turonian Source Rock

Temperature evolution

(A)

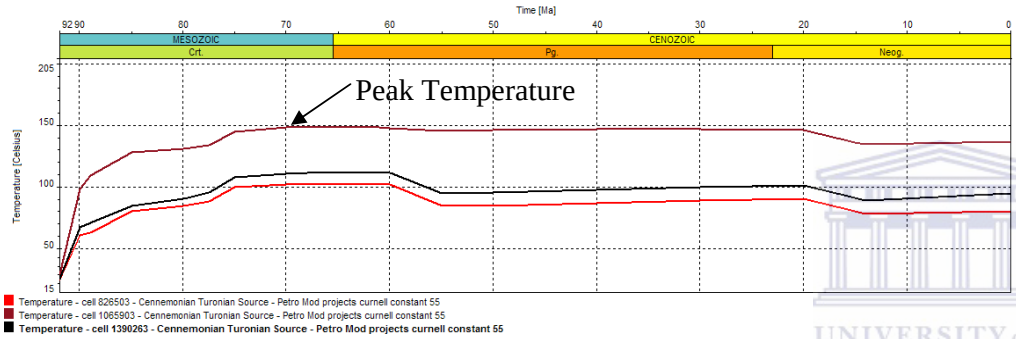

- Red line is at location A-I1 (shelfal area of basin)
- Brown line taken from the depocentre area of the basin
- Black line at location K-H1 (middle of basin)

Maturation evolution

(B)

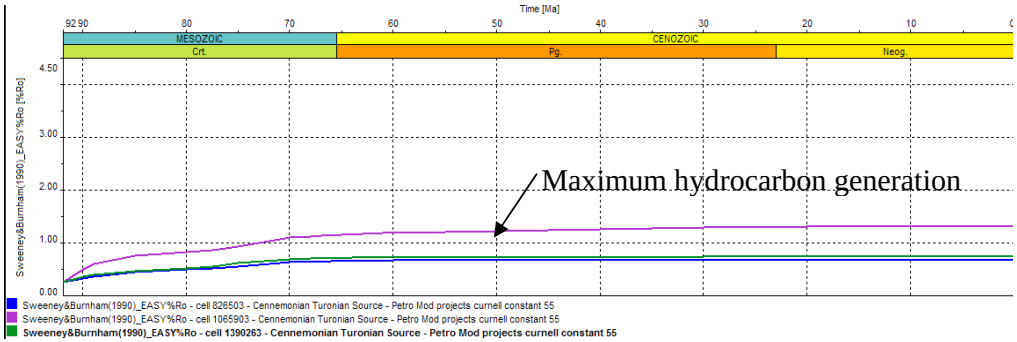

- Blue line is at location A-I1 (shelfal area of basin)
- Purple line taken from the depocentre area of the basin
- Green line at location K-H1 (middle of basin)

Figures 60: (A) (B) Time extractions at various well locations in the basin indicating peak temperature and maturation for the Cenomanian Turonian Source Rock for the constant heat flow model.

Barremian - Early Aptian Source Rock

Temperature evolution

(A)

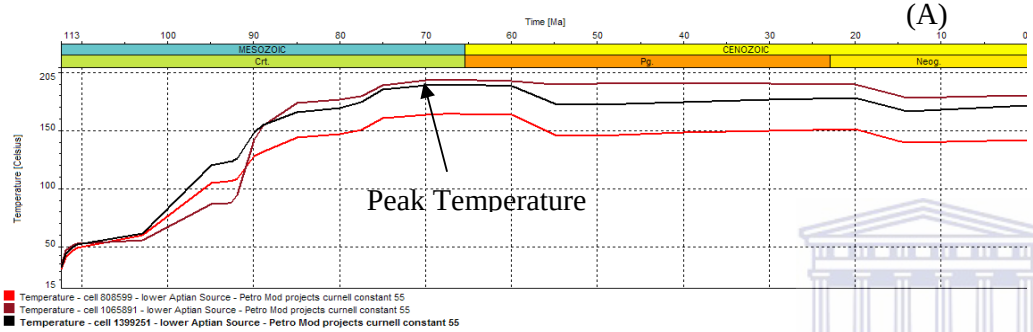

- Red line is at location A-I1 (shelfal area of basin)
- Brown line taken from the depocentre area of the basin
- Black line at location K-H1 (middle of basin)

Maturation evolution

(B)

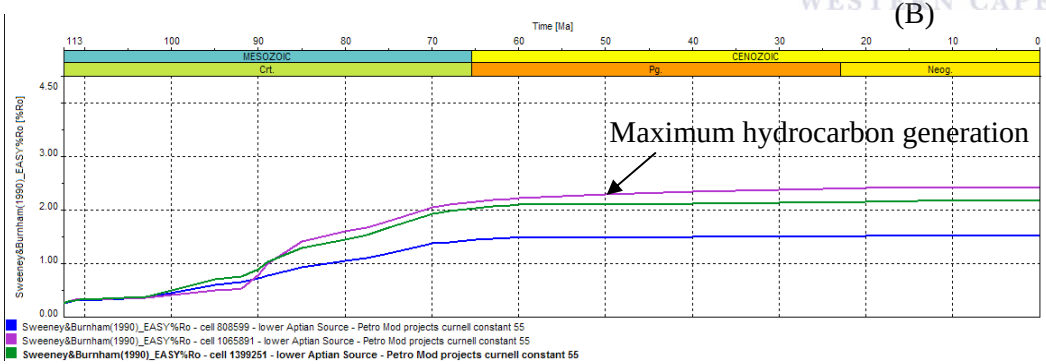

- Blue line is at location A-I1 (shelfal area of basin)
- Purple line taken from the depocentre area of the basin
- Green line at location K-H1 (middle of basin)

Figures 61: (A) (B) Time extractions at various well locations in the basin indicating peak temperature and maturation for the Barremian - Early Aptian Source Rock for the constant heat flow model.

COMPARING TIME EXTRACTIONS FOR CONSTANT HEAT FLOW MODEL WITH THE RIFT – DRIFT HEAT FLOW MODEL

RIFT – DRIFT HEAT FLOW MODEL

(A)

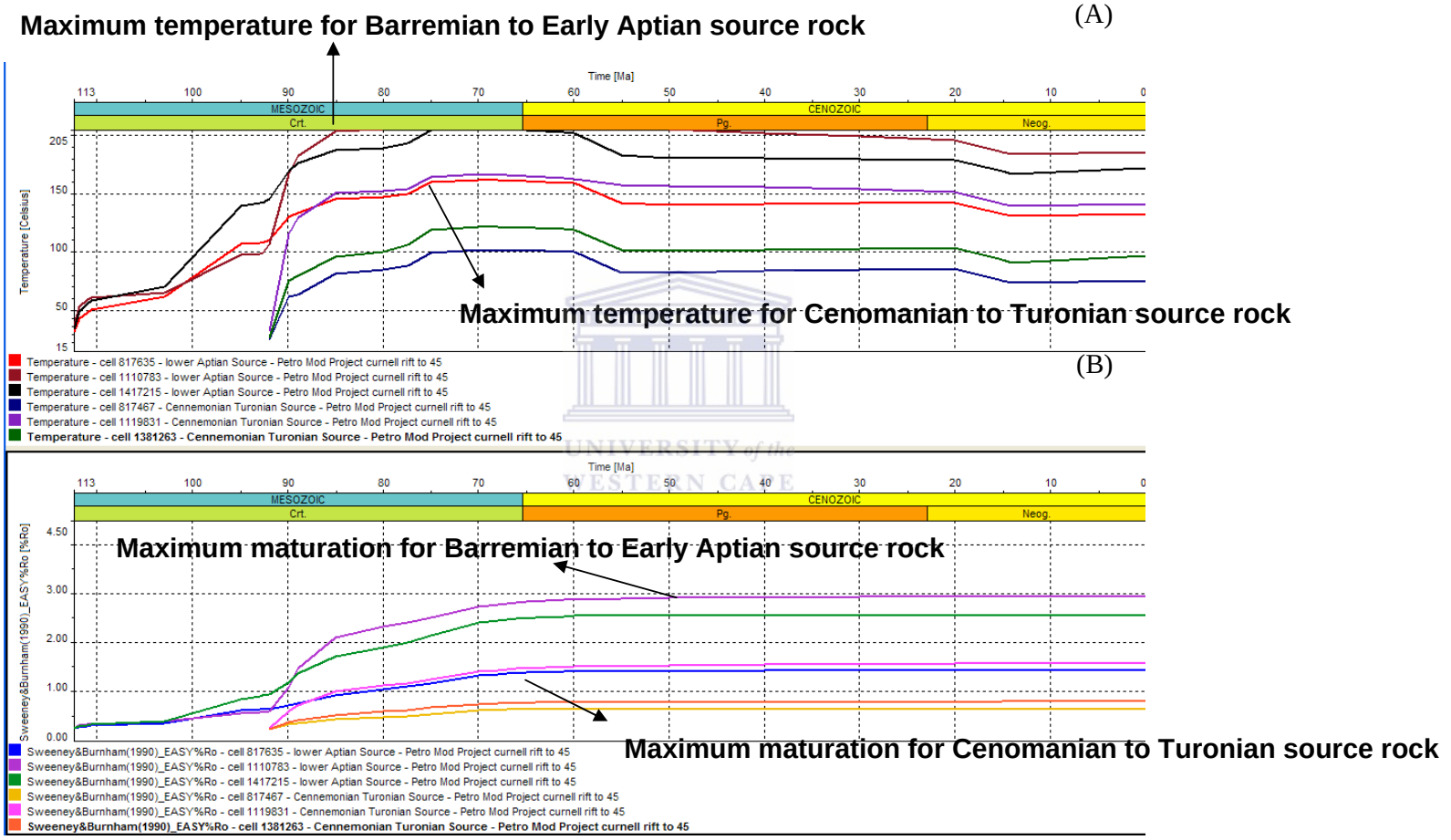

Figures 62: (A) (B) Time extractions at various well locations in the basin for both source rocks concurrently for the Constant heat flow model.

CONSTANT HEAT FLOW MODEL

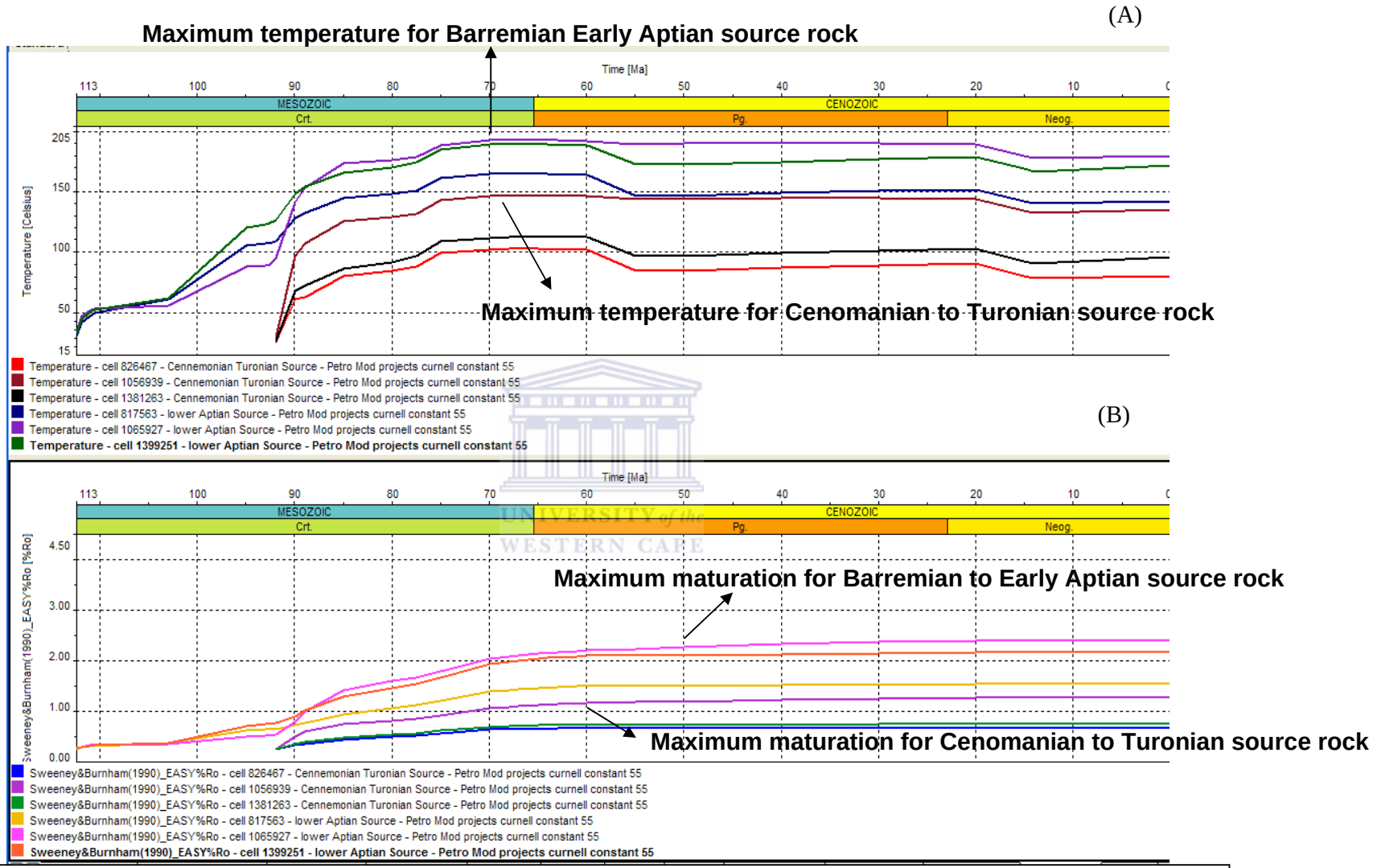

Figures 63: (A) (B) Time extractions at various well locations in the basin for both source rocks concurrently for the Constant heat flow model.

Time extractions

The time extraction of the older Barremian - Early Aptian and the Cenomanian - Turonian source rock at various well locations aims to depict the timing of maturation of the source rock at various location within the basin (Figures 58 (A) (B) – 63 (A) (B)). Studying the two diagrams temperature and maturation it is determined at what time maximum temperature and maturation was reached. Time extractions for the Cenomanian - Turonian source rock under the rift to drift heat flow model indicate that peak temperature was reached during the late Cretaceous with maximum maturity achieved during the Early Tertiary (Figure 58 (A) (B)). Time extractions of the older Barremian - Early Aptian source rock under the rift to drift heat flow model also indicate that temperature peaked during the Late Cretaceous and the maturation was at its maximum during the Early Tertiary (Figure 59 (A) (B)). Based on the timing of maximum temperature and subsequent maturation reached for both source rocks, both reach their peak temperature and maturation during the same time frame. The older Barremain - Early Aptian source rock is however over matured compared to the Cenomanian - Turonian source when maximum temperature and maturation is reached (Figure 58 (A) (B), 59 (A) (B)).

Temperature and maturation results from the constant heat flow model show that maximum temperature and maturation for this heat flow model are almost similar to that of the rift – drift heat flow model. When comparing the temperature and maturation for both source rocks under a constant heat flow and under a rift related heat flow we observe a similar trend but both the Cenomanian - Turonian and the Barremain - Early Aptian source rock in the constant heat flow model (Figure 60 (A) (B), 61 (A) (B)) reach a higher temperture and subsequent maturation in the depocentre area compared in the rift – drift heat flow model (Figure 60 (A) (B) – 63 (A) (B)).

Comparative study

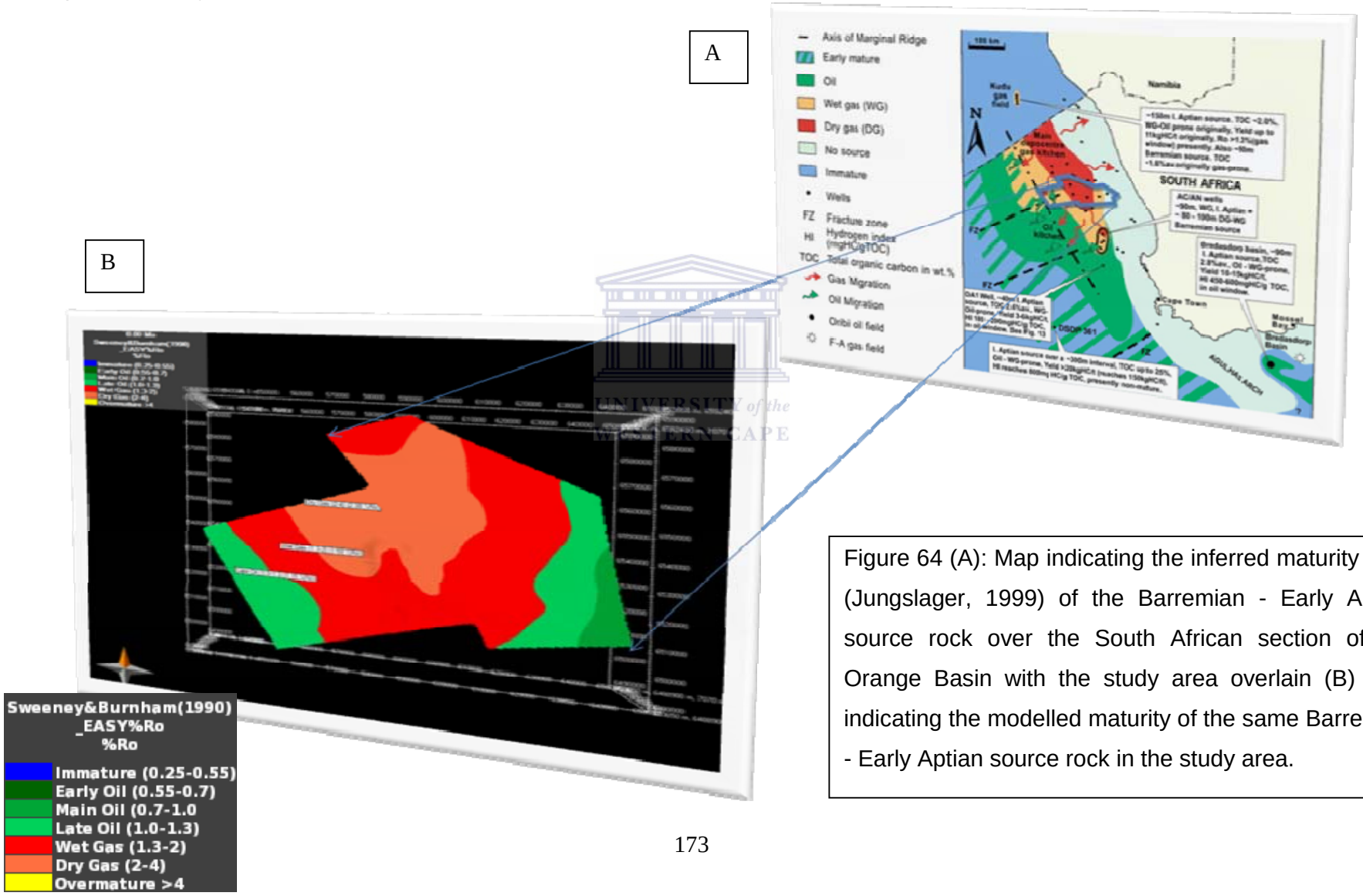

Figure 64 (A): Map indicating the inferred maturity after (Jungslager, 1999) of the Barremian - Early Aptian source rock over the South African section of the Orange Basin with the study area overlain (B) Map indicating the modelled maturity of the same Barremian - Early Aptian source rock in the study area.

Basin modeling conducted by Jungslager (1999) depict that Barremian - Early Aptian source rock to have a central dry gas zone surrounded both basinward and landward with a wet gas zone and reaches the oil stage deeper in the basin (Figure 64 (A)). The basin model conducted by this study reaches similar results depicting the Barremian - Early Aptian source rock to have a central dry gas zone surrounded by a wet gas zone and late oil stage being reached for source rock deeper in the basin (Figure 64 (B)).

CHAPTER FIVE

DISCUSSION

Late Cretaceous rifting resulted in the separation of the South American and African plates and generated accommodation space in the form of grabens and half grabens. These grabens provide the setting for the deposition of the Lower Cretaceous synrift sediments, mainly composed of siliciclastic lacustrine rocks (Muntingh and Brown, 1993) and accommodated the first known source rock in the Orange Basin. This active rifting sedimentation was terminated at the onset of thermal subsidence, which brought about deposition of the drift sediments (Barton et al., 1993). The entire succession of the Orange Basin was therefore originally deposited in a basin under predominantly extensional tectonics followed by passive margin subsidence. The basin is subsequently subjected to a rift-related heat flow history with maximum heat flow during the development of the spreading centres followed by a gradual decrease in heat flow as the margin is subjected to thermal subsidence. Rifting is described by Vail et al. (1989) as a first order tectonic event resulting from thermodynamic processes in the earth's crust and upper mantle followed by a period of flexure subsidence of the shelf and slope region which according to Bott (1980) is controlled by amongst others gravity loading.

The drift succession interval is the main topic of discussion as the study concentrates only on the drift succession of the Orange Basin. The drift succession of the Orange Basin is divided into two subsections, the initial Hauterivian to Lower Aptian succession referred to as the intermediate sequence bounded by unconformities 6At1 and 13At1 and the Early Aptian to present full drift succession (Gerrard & Smith, 1982) bounded by the 13At1 to seafloor (Figure 20). The intermediate sequence was deposited during a transitional period of active to passive spreading, creating restricted marine conditions which according to Brown et al. (1995) allowed for the deposition of characteristic evaporites. Based on the chronostratigraphic classification of the Orange Basin the early drift sequence was first deposited under a transgressive regime followed by an aggradational to a progradational regime (Brown et al., ibid).

This was possibly due to a decrease in new accommodation space and an increased sediment supply as the Orange River delivered sediments at a high rate during the Hauterivian - Lower Aptian (Muntingh and Brown, 1993).

The intermediate, early drift sequence is bounded at the top and base by two very strong reflectors respectively referred to as the13At1 and 6At1 type-1 unconformities that could be traced throughout the basin (Figure 20). The depth map of the intermediate sequence indicated in (Figure 24 (J)) show that the geometry of the succession is still very much influenced by the underlying basement architecture. The thicker sediment package of the intermediate sequence is concentrated in the middle of the section with a trend sub-parallel to the coast depicting the deep underlying grabens that trend sub-parallel to the west coast of South Africa. The section also thins basin-ward as Aghulhas Columbine Arch (basement high) provides a barrier for deeper sedimentation (Figure 24 (J)). Studying the intermediate sequence from the gamma ray of well A-A1 (Figures 30) the general assumption can be made that the sequence is fining upward as the gamma ray response progressively increases indicating a relative subsidence of the basin or rise in sea level. The latter is more acceptable as it can be explained by the final opening of the Atlantic as the African and South American plates finally separated with a major flooding event during the Early Aptian followed by aggrading to prograding sequences possibly due to increased sediment supply (Brown et al., 1995).

The full drift succession of the Orange Basin commenced at the onset of complete open marine drifting that is marked by the 13At1 type 1 erosional unconformity around 112 Ma (Brown et al., 1995) illustrated in the cross section (Figure 20). The succession was deposited under varying accommodation space caused by either rising and falling sea levels and/or tectonic uplift. In general the geometry of the sequence is lens-shaped with a thick mid-section thinning towards the coast and basinward (Figure 20). Supersequence 13, the first of the full drift sequences records a period of regression as sea level fell, causing a basinward shift of the shoreline followed by a period of flooding that resulted in the deposition of prograding sequences (Figure 22) (Brown et al., ibid).

This transition from regression to transgression can be seen in the gamma ray signature of well A-I1 as the regressional, sand rich, low gamma ray profile suddenly changes to a more shale-rich, high gamma ray signature (Figure 31).

Supersequence 14 containing the Ibhubesi gas field in the northern part of the South African section of the Orange Basin can generally be described as third and fourth order sequences with alternating progradational and aggradation character (Brown et al., 1995). The gamma ray signature of this interval is best recorded in well A-L1 for this study (Figure 32). The sequence is predominantly argillaceous with organic rich intervals recorded in well A-L1 where the source intervals show a generally irregular trend, typical of aggradation (Figure 32). This interval is followed by a generally coarsening upward sequence typical of a prograding system.

The supersequence 15 to 16 deposited on the type 1, 15At1 unconformity is generally aggradational becoming slightly progradational (Brown et al., 1995). This interval is best documented in well A-I1 (Figure 33). The gamma ray signature of well A-I1 indicates successive coarsening upward sequences directly above the 15At1 typical of progradation (Figure 33). Supersequences 17-20 cannot be analysed in the study area as there has been no data available but are documented in the literature to record periods of highly progradational and later slightly aggradational sediments (Brown et al., ibid).

Thickness maps of the full drift succession, describes a drift sequence that at the onset of full drift, shifted depocentres towards the north of the study area as indicated on the thickness map 13A (Figure 24 I) as the affect of basement architecture diminishes. Brown et al., (1995) ascribes this phenomenon to the fact that the Orange River did not become the principal drainage until after 103 Ma or at the beginning of Supersequence 14. Amid shifting depocentres throughout the drift succession evolution the affect of the two erosional events during the Tertiaty can be seen on the thickness maps. Thickness maps of the 17A, 18A and 22A (Figure 24 (B) (C) (D)) reveal a thinner sediment package landward of the study area and thicker sediment packages basinward due to the removal of sediments during erosion from the landward side of the basin and redeposited deeper in the basin.

The internal arrangement of the post-rift succession is generally structureless on the shelf but becomes more active along the depositional margin and in the distal regions of the basin, providing evidence of major structural change during the late Cretaceous when regional flooding resulted in highly aggradational deposition, developing into slightly progradational third and fourth order sequences (Brown et al., 1995). This high rate of aggradation along the steep depositional margin resulted in the development of a complex zone of slumps, rollover anticlines and tilted fault blocks visible on the seismic (Figures 22) posing as potential hydrocarbon traps (Brown et al., ibid).

The tectonic activity as described above is synonymous with the thermal regime of a basin be it compressional or extensional. In the case of the Orange Basin which is deposited under extensional tectonics followed by thermal subsidence the crustal heat flow is expected to spike during the period of rifting as the lithosphere is stretched and ultimately broken followed by a decrease in crustal heat flow as active rifting gives way to passive drifting (Figure 44 (A)).

In addition to tectonic activity, erosion is another event affecting the temperature distribution within the basin and is commonly associated with a decrease in basin heat flow (Welte et al., 1997). Two erosional events have been identified and incorporated in this basin model both occurring after the deposition of both source intervals being discussed (Figure 21, 25 (A) (B) (C) and Table 6). The first and more intense of which occurred during the Early Paleogene eroding an estimated thickness of 960 meters down to the 17A sequence (Figure 21, 25 (B) (C)). The second and less intense erosional event of the Early Miocene eroded an estimated thickness of 420 meters of sediments over a much larger area then the preceding erosional event as indicated on the 22A erosion map (Figure 25 (A)).

However, erosion can also have a positive affect on hydrocarbon generation, for example eroded sediments may be removed from the shelf and deposited further basinward (Figure 24 (B)) thus enhancing burial in this area and leading to increased temperature and pressure in the subsurface.

This then leads to the source rock maturing under a renewed temperature and pressure regime. This is the case in the Orange Basin where erosion has removed an estimated 1400 meters of sediment off the shelf to be deposited further basinward with another much younger and well-defined Tertiary package deposited west of the Cretaceous Tertiary shelf break (Figure 21, 23, 25 (A) (B) (C)) which could lead to hydrocarbon generation further offshore.

Two main source rock units are known to occur in the Orange Basin and include the Late Hauterivian synrift source rock and the Barremian - Early Aptian source rock with some indication of a regionally developed Cenomanian - Turonian source rock (Barton et al., 1993). Each of these is respectively related to one of the three main phases of development within the Orange Basin, namely the rift, early drift and complete drift phases. The oldest source rock deposited during the drift is the regionally developed Barremian - Early Aptian source rock deposited above the 13At1 unconformity and is traceable throughout the basin. The source rock is classified as a marine condensed section by Brown et al. (1995) implying the source rock was developed during a period of transgression. Muntingh (1993) characterised the source rock as a kerogen type II source rock.

Van der Spuy. (2003) proposed the Aptian source rock intersected in well A-A1 between 2730 meters and 2830 meters to be an exhausted type II gas prone kerogen based on the total organic carbon content and rock eval analyses. Actual drilling results and the well log data indicate that in well A-L1 there are intermittent source intervals developed between depths of 2335 to 2830 meters with source rock at 2335 meter depth correlating with the 14Ht1 unconformity found above the 14At1 unconformity which are comparable to the source intervals identified in well A-A1. Geochemical analyses though cross plotting the hydrogen indices against Tmax values with the kerogen type overlay (Figure 38), cross plotting the hydrogen indices and oxygen indices (Figure 40 (A), 41 (A)), as well as calculating average values for the hydrogen and oxygen indices, TOC's and Tmax values over the source intervals (Table 7) in well A-L1 and A-A1 indicate a Type III kerogen in the study area.

Elsewhere in the offshore basins of South Africa the Barremian - Early Aptian source rock are well documented. Along the southern margin of South Africa the Oribi oilfield is sourced from the Barremian - Early Aptian source intervals occuring in the Bredasdorp basin in the Southern Outeniqua.

On the west coast of South Africa the Barremian - Early Aptian source interval has been intersected by several wells including well P-A1 to the south of the study area, recording TOC values of 4 percent, A-C1 to 3 recording TOC's ranging from 2 to 4 percent and DSDP 361 with TOC's ranging from 3 to 15 percent for the Barremian - Early Aptian source interval (van der Spuy, 2003).

Source intervals recorded in well K-F1 and K-H1 above the 15At1 unconformity (Figure 36 (B)) correlate with the postulated Cenomanian - Turonian source rock which has been classified by Muntingh (1993) to be of predominantly terrestrial nature with mixed type II and type III kerogen improving from a gas prone source rock on the shelf to oil prone source rock further basinward beyond the shelf break.

Ben-Avraham et al., (2002) also suggest the Cenomanian - Turonian source rock is of terrestrial origin, wet-gas prone, but immature for gas generation with a possibility of becoming more oil prone farther basinward. Aldrich et al. (2003) based on paleo-climate models proposed that the development of the Cenomanian - Turonian source rock is related to the Cenomanian - Turonian upwelling near the shelf/slope and is typically oil prone. Geochemical analyses though cross plotting the hydrogen indices against Tmax values with the kerogen type overlay (Figure 39), cross plotting the hydrogen indices and oxygen indices (Figure 42 (A), 43 (A)), as well as calculating average values for the hydrogen and oxygen indices, TOC's and Tmax values over the source intervals (Table 7) in well K-F1 and K-H1 indicate a Type III kerogen in the study area.

The source rock is recorded in wells further north in the Namibian section of the Orange Basin with TOC's reaching 5 percent in well 2012/13 – 1 (Bray, 1998) and in the Bredasdorp basin along the south coast of South Africa the source interval is described as having potential for wet gas or oil generation (Davies, 1997).

Studying the evolution of the two source rock intervals through time and under the influence of both constant and rift related heat flow (Figure 44 (A) (B), 45 (A) (B)) the study scrutinize the burial history diagrams of a distal well K-H1 and a more proximal well A-I1 relative to the study areas (Figure 47 (A) (B), 50 (A) (B), 53 (A) (B), 56 (A) (B)). The distal burial history (under the rift related heat flow) reveals that the Barremian to Early Aptian source rock, entered the thermal mature window for oil during the Lower Cretaceous and became over mature for oil within the Upper Cretaceous where after the source rock produced mainly gas (Figure 47 (A) (B), 50 (A) (B)). The model assumes that source rock is thermally mature for oil within the temperature window of 60 to 120 degrees Celsius.

At well location A-I1 the Barremian - Early Aptian source rock also entered the thermally mature window for oil during the Lower Cretaceous but has not been subjected to the high burial compared to the source rock deeper in the basin and therefore has not been subjected to such high temperatures and pressures (Figure 47 (A) (B), 50 (A) (B)). The map view with the transformation overlay show that the older Barremian - Early Aptian source rock is presently overmature, producing mainly gas especially in the central study area where 100% transformation has been reached with potential for oil in the distal parts of the study area (Figure 49 (B). The modeling results for the Barremian - Early Aptian source rock are comparable with previous maturation studies of this source rock such as the study conducted by Jungslager (1999) (Figure 64 (A) (B)). The study shows that the Barremian - Early Aptian source rock exhibit a centrally mature, gas prone area becoming progressively more oil prone westward a similar result to the this study. This source rock has also been described by Muntingh, (1993) to exhibit a “rapid transition from gas prone on the shelf to a good quality oil-prone source basinward”.

Burial history for younger postulated Cenomanian - Turonian source rock show that the source rock in the deeper part of the basin (well K-H1) entered the thermally mature zone for oil during the Upper Cretaceous and has remained within this phase till present (Figure 47 (A) (B), 50 (A) (B)). At well A-I1, closer to shore the source rock also entered the thermally mature zone for oil during the Upper Cretaceous but has in general been subjected to lower temperatures compared to the deeper parts of the source rock (Figure 47 (A) (B), 50 (A) (B))

The source rock shows a modest degree of hydrocarbon transformation when studying the transformation ratio overlay onto the source rock depicting a largely immature source rock. However the source rock still contains a centrally mature section (Figure 46 (B))

Several possibilities may explain this outcome of a central mature region and they are outlined below. The model demonstrating the basin architecture indicates the general geometry of the Orange Basin to be lens-shaped with the thickest sediment pile in the mid section and thinning basinward and landward (Figure 20). This thicker sediment sequence in the midsection of the basin would likely have led to increased temperature and pressure over this area resulting in extended maturation of the source rock in this region for both source rocks. This affected the older Barremian to Early Aptian source rock more because it has been subjected to the higher temperature and burial regime for a much longer time compared to the Cenomanian to Turonian source rock.

Taking into account that the model assumed a flow of 80 mW during the period of rifting, decaying to a present day 60mW and that the Barremian - Early Aptian source rock was deposited more or less 30 Ma after the initiation of rifting, the source rock was not subjected to the height of the heat flux during rifting.

Timing of burial in combination with the crustal heat flow history therefore plays a major role in maturation of the source rock. In order to test the effect of temperature and heat flow on the maturation of source rock another model with a constant heat flow history was integrated. This model assumed a constant heat flow of 55mW (Figure 45 (A) (B)) implying that the source rocks, when deposited was only ever subjected to a constant heat flow of 55 mW throughout time.

Burial history diagrams indicate that the deeper (well K-H1) Barremian - Early Aptian source rock in the constant heat flow model (Figure 53 (A) (B), 56 (A) (B)) matures more gradually compared to the same source rock in the rift-drift model. The constant heat flow regime incorporated in the model reduces the rate at which temperature increase with depth therefore delaying maturity. This also applies to the younger Cenomanian - Turonian source rock in the deep section of the basin (K-H1) (Figure 53 (A) (B), 56 (A) (B)).

Results from the geological time extractions taken on the shelf and in the depocentre for both the constant and rift related heat flow also indicate the source rock to be more mature in midsection compared to the shelfal areas (Figure 58 (A) (B), 59 (A) (B), 60 (A) (B), 61 (A) (B)). The time extractions of the Barremian - Early Aptian source rock also indicate that maximum temperature and peak hydrocarbon generation coincide and were reached towards the end of the Cretaceous for the source rock sequence in the centre of the basin for both heat flow models (Figure 59 (A) (B), 61 (A) (B)).

Peak hydrocarbon generation for the Cenomanian - Turonian source rock based on the model was also reached towards the end of the Cretaceous (Figure 58 (A) (B), 60 (A) (B)). This is similar to the evolution of the Barremian - Early Aptian source rock, although these conditions were met only in a small area located in the midsection of the basin.

Based on the chronostratigraphy of the Orange Basin major uplift of the margin occurred towards the end of the Cretaceous leading to erosion of the drift succession of the Orange Basin. Based on these observations it is apparent that this major uplift event stopped the maturation of both source rocks on the shelf but subsequently led to an increase in the rate of maturation for source rocks in the deeper parts of the basin off the shelf break where the sediment load increased (Figure 23).

To compare how accurate the maturity results are with regards to the source rock maturity one can refer to the well calibration panels showing the calibration of the modeled temperature and vitrinite reflectance to the actual measured temperature and vitrinite reflectance (Figure 48 (A) (B), 51 (A) (B), 54 (A) (B), 57 (A) (B)).

The calibration of the model with temperature and vitrinite reflectance shows that the model parameters follow a trend that can be closely correlated to the actual evolution of the Orange Basin sediments. The constant heat flow model show a better fit in vitrinite reflectance at well K-H1 and A-I1 compared to the rift – drift model (Figure 48 (A) (B), 51 (A) (B), 54 (A) (B), 57 (A) (B)).

CHAPTER SIX

CONCLUSION

The process of geologically modeling a defined area of a basin such as attempted by this study aims at incorporating all the relevant geological, geophysical and geochemical data available to aid in the reconstruction and simulation of the basin geological evolution and its effect on the petroleum systems. Nine type one unconformities were identified and mapped throughout the post rift succession of the Orange Basin to provide the framework to classify the various sequences, which in turn provided the evidence for postulating the dominant depositional environment at the time. Various stacking patterns and structures were identified including amongst others the prograding late Cretaceous succession and the large growth faults and associated thrust faults along the shelf break. The effect of these dynamic changes in depositional patterns on the evolution of the source rock was the outcome of this study. The study noted that when comparing the maturity of the two source rocks, the older Barremian to early Aptian source rock and the younger postulated Cenomanian to Turonian source rock in this study share similarities in the regional distribution of their present day maturity. Both source rocks have a centrally mature region mainly controlled by the thick depocentre over the central Orange Basin section with decreasing maturity towards the margins,

The initial aims and objectives of this study have indeed been met with a more comprehensive understanding of the geological processes that resulted in the formation of the Orange Basin and the influence this had on the source rock evolution. Despite shortcoming on the depth conversion the study still proved to simulate the source rock evolution sufficiently to be accurately compared with previous basin modeling studies such as the basin modeling study conducted by Jungslager (1999). These comparisons is illustrated when comparing the present data maturity results of the Barremian to early Aptian source rock with the maturity result of the same source rock by Jungslager (ibid).

The study also provides indications that progradation of Tertiary sediments over the shelf break and into the deepwater portion of the basin leads to enhanced burial and ensuing maturation of the distal and possibly more oil prone Cenomanian Turonian source rock sequence. Accordingly this area should be the most prospective part of the Orange Basin.

Suggestions to further enhance this basin modeling study includes making use of a range of different heat flows to test the affect on the source rock maturation, incorporating more wells that penetrate source rocks to better constrain the their character and possibly conducting a basin modelling exercise on the adjacent South American basins and the evolution of their source rocks to corroborate findings on both sides of the Atlantic margins.

REFERENCES LIST

Aizawa, M., Bluck, B., Cartwright, J., Milner, S., Swart, R., and Ward, J, (2000). Constraints on the Geomorphological evolution of Namibia from the offshore stratigraphic record, Communs Geol. Surv. Namibia, 12, 337 – 346.

Ala, M.A., Selley, R.C., (1997). The West African Coastal Basins. In: African Basins. Sedimentary Basins of the world, 3 edited by R.C Selley, Elsevier Science B.V., Amsterdam, 173-186.

Aldrich, J., Zilinski, R., Edman, J., Leu, W., Berge, T., and Corbett, K. (2003). Documentation of a new petroleum system in the South Atlantic. AAPG Annual Convention, May 11 – 14 2003, Abstract.

Andreoli, M.A.G., Doucoure', J., Van Bever Donker, J., Brandt, D and Andersen, N.J.B., (1996), Neotectonics of southern Africa – a review. Africa Geoscience Review, Vol. 3, No. 1, 1-16.

Barton, K.R., Muntingh, A and Noble, R.D.P., (1993). Geophysical and Geological studies applied to hydrocarbon exploration on the West Coast Margin of South Africa. Extended abstract of the third International Congress of the Brazilian Geophysical Society, Rio de Janeiro, Brazil, Nov. 7-11, 1993.

Bauer, K., S. Neben, B. Schreckenberger, R. Emmermann, K. Hinz, N. Fechner, K. Gohl, A. Schulze, R.B. Trumbull, and K. Weber., (2000). Deep structure of the Namibian continental margin as derived from integrated geophysical studies. Journal of Geophysical Research, Volume 105, No. (B11), 25,829-25,853.

Ben-Avraham, Z., Hartnady, C.J.H and Malan, J.A., (1993). Early tectonic extension between the Aghulhas Bank and the Falkland Plateau due to the rotation of the Lafonia microplate. Earth and Planetary Science Letters, 117 (1993) 43-58, Elsevier Science Publishers B.V., Amsterdam.

Ben-Avraham, Z., Smith, G., Reshef, M and Jungslager, E. (2002). Gas hydrate and mud volcanoes on the southwest African continental margin off South Africa. Geology, Volume 30, No. 10, 927-930.

Birch, G.F. (1977). Surficial sediments on the Continental Margin off the West Coast of South Africa, Marine Geology, 23, 305 – 337.

Bluck, B.J., Ward, J.D., Cartwright, J., and Swart, R., (2007). The Orange River, Southern Africa: An extreme example of a wave-dominated sediment dispersal system in the South Atlantic Ocean, Journal of the Geological Society, London, 164, 341 – 351.

Bott, M.H.P. (1980). Problems of passive margins from the viewpoint of the geodynamics project: a review. Philosophical Transactions of the Royal Society of London. A 294, 5-16.

Bray, R., Swart, R., and Lawrence, S., (1998). Source rock, maturity data indicate potential off Namibia, National petroleum corporation of Namibia (Pty.) Ltd. Windhoek, Oil and Gas Journal, 84 – 89.

Broad, D.S., Jungslager, E.H.A., McLachlan, I.R., Roux, J. (2006). Offshore Mesozoic Basins. In: Johnson, M.R., Anhaeusser, C.R and Thomas, R.J. (Eds), The Geology of South Africa. Geological Society of South Africa, Johannesburg/Council for Geoscience, Pretoria, 553 – 569.

Brooks, J. and Fleet, A.J. (eds) (1987). Marine Petroleum Source Rocks Geological Society Special Publication No, 26, 271 – 286.

Brown, L.F. and Fisher, W.L., (1977). Seismic stratigraphic interpretation of depositional systems: examples from Brazil rift and pull-apart basins. Am. Assoc. Petrol. Geol. Memoir, 26, 231-248.

Brown, L.F., Jr., R.F. Solis-Iriarte, and D.A. Johns, (1990). Regional depositional systems tract, paleogeography, and sequence stratigraphy, Upper Pennsylvanian and Lower Permian strata, North and West-Central Texas: University of Texas, Austin, Bureau of Economin Geology Report of Investigations no 197, 166 p.

Brown, L.F., Benson, Jr.J.M., Brink, G.J., Doherty, S., Jollands, A., Jungslager, E.H.A., Keenan, J.H.G., Muntingh, A., and van Wyk, N.J.S., (1995). Sequence Stratigraphy in Offshore South African Divergent Basins. In: American Association of Petroleum Geologists, Tulsa, Oklahoma, Studies in Geology, 41, An Atlas on Exploration for Cretaceous Lowstand Traps by Soekor (Pty) Ltd. 139-182.

Chapman, R.E., (1976). Petroleum Geology (A Concise Study), Elsevier Scientific Publishing Company, Amsterdam.

Corner, B., Cartwright, J and Swart, R., (2002). Volcanic passive margin of Namibia: A potential fields perspective, In: Menzie, M.A., Klemperer, S.L., Ebinger, C.J., and Baker, J., eds., Volcanic Rifted Margins: Boulder, Colorado, Geological Society of America Special Paper 362, 203-220.

Cubitt, J.M., England, W.A. and Larter, S. (eds) (2004). Understanding Petroleum Reservoirs: towards an Intergrated Reservoir Engineering and Geochemical Approach. Geological Society, London, Special Publications, 237, 133 – 155 © The geological Society of London 2004.

Curtis, M.L. and Hyam, D.M., (1998). Late Paleozoic to Mesozoic structural evolution of the Falkland Islands: a displaced segment of the Cape Fold Belt. Journal of the Geological Society, London, Vol. 155, 1998, 115-129. printed in Great Britain.

Davies, C. P. N., (1997). Hydrocarbon Evolution of the Bredasdorp Basin, Offshore South Africa: From Source to Reservoir. Phd, thesis, University of Stellenbosch.

Dingle, R.V., Siesser, W.G and Newton, A.R., (1983). Mesozoic and Tertiary Geology of Southern Africa, Balkema A.A., Rotterdam, Netherlands, MBS, Salem, USA.

Dingle, R.V., (1992). Structural and sedimentary development of the continental margin off Southwestern Africa.

Emery, D. and Myers., K.J., (1996). Sequence Stratigraphy, Blackwell Science Ltd, BP Exploration, Stockley Park Uxbridge, London.

Fairhead, J.D., (1988). Mesozoic plate tectonic reconstructions of the central South Atlantic ocean: the role of the West and Central African rift systems. Tectonophysics, 155, 181-191.

Fisher, W.L. and McGowen, J.H., (1967). Depositional systems in the Wilcox Group of Texas and their relationship to the occurrence of oil and gas. Gulf Coast Assoc. Geol. Soc. Trans., 17, 105-125.

Gallagher, K. and Brown, R., (1999). The Mesozoic denudation history of the Atlantic margins of southern Africa and southern brazil and the relationship to offshore sedimentation. In: Cameron, N.R., Bate, R.H and Clure, V.S. (eds) The oil and gas habitats of the South Atlantic. Geological Society, London, Special Publication, 153, 41 – 53.

Gerrard, I and Smith,G.C., (1982). Post-Paleozoic Succession and Structure of the Southwestern Africa Continental Margin. In: Watkins, J.S. & Drake, C.L. (eds) Studies in Continental Margin Geology. AAPG Memoir, 34, 49 – 74.

Gladczenko, T.P., Hinz, K., Eldholm, O., Meyer, H., Neben, S. and Skogseid, J. (1997). South Atlantic volcanic margins, Journal of the Geological Society. London, Vol. 154, 465 - 470.

Gluyas, J and Swarbrick, R., (2004). Petroleum Geoscience, Blackwell Publishing

Gradstein, F.M., Ogg, J.G., Smith, A.G., et al. (2004). A Geologic Time Scale 2004, with Cambridge University Press, and the official website of the International Commission on Stratigraphy (ICS) under www.stratigraphy.org.

Greenlee, S.M., and T.C. Moore, (1988). Recognition and interpretation of depositional sequences and calculations of sea-level changes from stratigrpahic data-offshore New Jersey and Alabama Tertiary, in C.K. Wilgus et al., eds., Sea-level changes: an intergrated approach: SEPM Special Publication 42, p. 329-353.

Hoyt, J.H., Oostdam, B.L., and Smith, D.D. (1969). Offshore sediments and valleys of the Orange River (South and South West Africa), Marine Geology, 7, 69 - 84.

Hyam, D.M., (1998). Structural Evidence for the fit of the Falkland Islands in pre break-up Gondwana, Geoscientist, 4 – 7.

Jervey, M.T., (1988). Quantitative geological modelling of siliciclastic rock sequences and their seismic expressions. In: Sea-level Changes: An Integrated Approach (ed. by C.K. Wilgus, B.S. Hastings, C.G. St Kendall, H.W. Posamentier, C.A. Ross & J.C. Van Wagoner). Special Publication, Society of Economic Paleontologists and Mineralogists, Tulsa, 42, 47-69.

Jungslager, E.H.A., (1999 a). Petroleum habitats of the Atlantic margin of South Africa. In: Cameron, N.R., Bate, R.H & Clure, V.S. (eds), The oil and Gas Habitats of the South Atlantic, Geological Society, London, Special Publication, 153, 153 – 168.

Jungslager, E.H.A., (1999 b). New geological insight gained from geophysical imaging along South Africa's western margin, South African Geophysical Association, 6th Biennual Conference & Exhibition, 28th September – 01 October 1999, Cape Town, Extended Abstract, paper 14.4.

Katz, B.J., and Mello, M.R., (2000). Petroleum Systems of the South Atlantic Marginal Basins-An Overview, In: M.R. Mello and B.J. Katz, eds., Petroleum systems of South Atlantic margins: AAPG Memoir 73,1 – 13.

Kroeger, K.F., Ondrak, R., di Primio, R., Horsfield, B., (2008). A three-dimensional insight into the Mackenzie Basin (Canada): Implications for the thermal history and hydrocarbon generation potential of Tertiary deltaic sequences, AAPG Bulletin, V. 92, No. 2, 225 – 247.

Lawrence S. R., (1989). Prospects for Petroleum in Late Proterozoic/Early Palaeozoic Basins of Southern-Central Africa, Journal of Petroleum Geology, 12(2), 231-242.

Loutit, T.S., Hardenbol, J., Vail, P.R and Baum, G.R. (1988). Condensed sections: the key to age determination and correlation of continental margin sequences. In: Sea-level Changes: An Integrated Approach (ed. By C.K. Wilgus, B.S. Hastings, C.G. Kendall, H.W. Posamentier, C.A. Ross & J.C. Van Wagoner). Special Publication, Society of Economic Paleontologists and Mineralogists, Tulsa, 42, 183-213.

Madyibi, L., van der Spuy, D and Zhao, B., (2005). Identification of gas chimneys and intrusives using seismic data offshore West Coast, South Africa. Geo2005, Extended Abstract Volume, University of the KwaZulu-Natal, Durban.

McKenzie, D.P., (1978). Some remarks on the development of sedimentary basins. Earth Planet. Sci. Lett., 40, 25 – 32.

Miles, J.A., (1994), Illustrated glossary of Petroleum Geochemistry, Claredon Press, Oxford

Mitchum, R.M., Jr., Vail, P.R and Thompson III, S., (1977), Seismic stratigraphy and global changes in sea level. Part 2: the depositional sequence as a basic unit for seismic stratigraphic analyses, in C.E. Payton, ed., Seismic stratigraphy-applications to hydrocarbon exploration: AAPG Memoir 26, 53-62.

Muntingh, A., (1991). Sequence Stratigraphy of the Orange Basin, Western offshore South Africa. Soekor (pty) Ltd.

Muntingh, A., (1993), Geology, prospects in Orange basin offshore western South Africa, Oil and Gas Journal, Jan 25, Exploration, 06 - 110, Penn Well Publishing Company.

Muntingh, A., and Brown, L. F., Jr., (1993). Chapter 4, Sequence stratigraphy of petroleum plays, post-rift Cretaceous rocks (Lower Aptian to Upper Maastrichtian), Orange Basin, western offshore, South Africa. In: Weimer, P., and Posamentier, Henry, eds., Siliciclastic sequence stratigraphy: recent developments and applications: AAPG Memoir 58, 71–98.

Naeth, J., di Primio, R., Horsfield, B., Schaefer, R.G., Shannon, P.M., Bailey, W.R., and Henriet, J.P. (2005). Hydrocarbon seepage and carbonate mound formation: A basin modelling study from the Porcupine Basin (Offshore Ireland), Journal of Petroleum Geology, Vol. 28, No 2, 147 – 166.

Paton., D.A., Van der Spuy., D., di Promio., R., and Horsfield., B. (2008). Tectonically induced adjustment of passive-margin accommodation space; influence on the hydrocarbon potential of the Orange Basin, South Africa, AAPG Bulletin, V.92, No. 5, 589 – 609.

Paton., D.A., di Primio, R., Kuhlmann, G., van der Spuy, D., and Horsfield, B. (2007). Insight into Petroleum System Evolution of teh Southern Orange Basin, South Africa, South African Journal of Geology, 110, 261 – 274.

Peters, K. E., (1986). Guidelines for Evaluating Petroleum Source Rock Using Programmed Pyrolysis, American Association of Petroleum Geologist Bulletin, v.70, p. 329

Peacock, D.N., (1992). Geological snapshot of offshore Namibia, Chevron Overseas petroleum Inc.

Promotional pamphlet, Petroleum Agency SA, 2007, Petroleum Exploration Information and Opportunities Brochure

Posamentier, H.W and Vail, P.R. (1988). Eustatic controls on clastic deposition I – sequence and systems track models. In: Sea-level Changes: An Integrated Approach (ed. By C.K. Wilgus, B.S. Hastings, C.G. St C. Kendall, H.W. Posamentier, C.A. Ross & J.C. Van Wagoner). Special Publication, Society of Economic Paleontologists and Mineralogists, Tulsa, USA, 42, 109-124.

Rider, M., (1996). The Geological Interpretation of Well Logs, Second Edition, Blackie, Glasgow.

Ruble, T.E., Lewan, M.D and Philp, R.P., (2001). New insights on the Green River petroleum system in the Uinta basin from hydrous pyrolysis experiments, AAPG Bulletin, V. 85, No 8,1333 -1371.

Rust, D.J. and Summerfield, M.A., (1990). Isopach and borehole data as indicators of rifted margin evolution in southwestern Africa. Marine and Petroleum Geology, Vol. 7, 277-287.

Schlanger, S.O., and Jenkyns, H.C. (1976). Cretaceous oceanic anoxic events causes and consequences: Geology Mijnsonn, 55, 179-184.

Schmidt, S., (2004). The Petroleum Potential of the Passive Continental Margin of South – Western Africa – A Basin Modelling Study.

Selley, R.C., (1985). Elements of Petroleum Geology, W.H. Freeman and Company.

S`eranne, M and Anka, Z., (2005). South Atlantic continental margins of Africa: A comparison of the tectonic vs climatic interplay on the evolution of equatorial West Africa and SW African margins, Journal of African Earth Sciences 43, 283 – 300.

Southern Orange Basin Exploration opportunities offshore South Africa's West Coast, Promotional pamphlet, Petroleum Agency SA.

Stevenson, I.R and McMillan, I.K., (2004). Incised valley fill stratigraphy of the Upper Cretaceous succession, proximal Orange Basin, Atlantic margin of southern Africa, Journal of the Geological Society, London, Vol. 161, 185-208.

Sweeney, J.J and Burnham, A.K. (1990). Evaluation of a simple model of vitrinite reflectance based on chemical kinetics. AAPG Bulletin 74 (10), 1559-1570.

Tankard, A.J., Hobday, D.K., Jackson, M.P.A., Hunter D.R., Eriksson, K.A., Minter, W.E.L., (1982). Crustal Evolution of Southern Africa "3.8 Billion Years of Earth History", Springer-Verlag New York, Inc.

Tissot, B.P. and Welte D.H. (1978). Petroleum formation and occurrence, A new approach to oil and gas exploration. Springer-Verlag, Berlin.

Tulcholke, B.E., Houtz, R.E. and Barret, D.M. (1981). Continental crust beneath the Agulhas Plateau, southwest Indian Ocean. J. Geophys. Res., 86, 3791-3806.

Turner, S., Kelley, S., Hawkesworth, C.J. and Mantovani, M. (1994). Magmatism and continental break-up in the South Atlantic: high precision ^{40}Ar-^{39} geochronology. Earth and Planetary Science Letters, 121, 333-348.

Vail, P.R., (1987). Seismic stratigraphy interpretation using sequence stratigraphy. Part I: seismic stratigraphy interpretation procedure, in A.W.. Bally, ed., Atlas of seismic stratigraphy, v. 1: AAPG Studies in Geology 27, p.1-10.

Vail, P.R., Audemard, F., Eisner, P.N and Perez-Cruz, C. (1989). The new Global Stratigraphy, Rice University, Houston, Texas.

Vail, P.R., Audemard, F. Bowman, S.A., Eisner, P.N and Perez-Cruz, C (1991). The stratigraphic signatures of tectonics, eustasy and sedimentology-and overview, in G. Einsele et el., eds., Cycles and events in stratigraphy, part II: larger cycles and sequences: Berlin, Springer-Verslag, p. 617-659.

Van der Spuy, D., (2003). Aptain source rocks in some South African Cretaceous basins. In: Arthur,T.J., MacGregor, D.S & Cameron, N.R. (eds), Petroleum Geology of Africa: New Themes and Developing Technologies. Geological Society, London, Special Publication, 207, 185-202, The Geological Society of London.

Van der Spuy, D., Jikelo, N.A., Ziegler, T and Bowyer, M., (2003). Deepwater 2D data reveal Orange basin objectives off western South Africa, Penn Well Corporation, Oil and Gas Journal, 2003, Exploration & Development.

Van der Spuy, D., (2007). Republic of South Africa 2007 Licence round. Area B Southern Orange Basin.

Van Wagoner, J.C., (1985). Reservoir facies distribution as controlled by sea level changes: Abstract with Programs, Society of Economic Paleontologists and Mineralogists, mid-year meeting, Golden, Colorado, 91-92.

Van Wagoner, J.C., Posamentier, H.W., Mitchum, R.M., Vail, P.R., Sarg, J.F., Loutit, T.S. and Hardendol, J. (1988). An overview of the fundamentals of sequence stratigraphy and key definitions. In: Sea-level Changes: An Integrated Approach (ed. By C.K. Wilgus, B.S. Hastings, C.G. St C. Kendall, H.W. Posamentier, C.A. Ross & J.C. Van Wagoner). Special Publication, Society of Economic Paleontologists and Mineralogists, Tulsa, 42, 39-45.

Van Wagoner, J.C., Mitchum, R.M., Jr., Campion, K.M. and Rahmanian, V.D. (1990). Siliciclastic Sequence Stratigraphy in Well Logs, Core and Outcrop: Concepts for High Resolution Correlation of Time and Facies. American Association of Petroleum Geologists Methods in Exploration Series, Tulsa, 7, 55.

Viola, G., Andreoli, M., Ben-Avraham, Z., Stengel, I., Reshef, M., (2004). Offshore mud volcanoes and onland faulting in Southwestern Africa: Neotectonic implications and constraints on the regional stress field, Earth and Planetary Science Letters 231, 147 – 160.

Visser, D.J.L., (1998). The Geotectonic Evolution of South Africa and offshore areas, Council for Geoscience, Geological Survey of South Africa, Geological Survey, Pretoria, 230-257.

Watkeys., M.K. (2006). Gondwana Break-Up: A South African Perspective. In: Johnson, M.R., Anhaeusser, C.R and Thomas, R.J. (Eds), The Geology of South Africa. Geological Society of South Africa, Johannesburg/Council for Geoscience, Pretoria, 531 – 537.

Welte, D.H., Horsfield, B and Baker, D.R. (Eds). (1997). Petroleum and Basin Evolution, Insights from Petroleum Geochemistry, Geology and Basin Modelling, Springer.

Weigelt, E and Uenzelmann-Neben, G., (2004). Sediment deposits in the Cape Basin: Indications for shifting ocean currents?, AAPG Bulletin, V. 88, No. 6, 765 – 780.

Wright, J.B., (1968). South Atlantic continental drift and the Benue trough, Tectonophysics, Vol 6, No. 4, 301 – 310.

Wygrala, B.P., (1989). Integrated study of an oil field in the southern Po basin, northern Italy. Dissertation, University of Köln.

INTERNET REFERENCES

Beardsmore, G.R and Cull, J.P., (2001). Crustal Heat Flow: A Guide to Measurements and Modeling, Cambridge University Press
http://www.geosci.monash.edu.au/heatflow/index.html

Dow, W.G., 1977, Kerogen studies and geological interpretations: Journal of geochemical exploration, v. 7, p. 79-99, Wikipedia the free encyclopedia, http://en.wikipedia.org/wiki/Vitrinite

Pedersen, J.H., (2007), oilandgasgeology.com
http://www.oilandgasgeology.com/oil_gas_window.jpg,

Pimmel, A., and Claypool, G., 2001, Introduction to shipboard organic geochemistry on the JOIDES Resolution. ODP Tech. Note, 30
http://www-odp.tamu.edu/publications/tnotes/tn30/

USC Sequence Stratigraphy Web, 2005, University of South Carolina, Geology Department.
http://strata.geol.sc.edu/terminology/accommodation.html

Van Wagoner, J.C., Posamentier, H.W., Mitchum, R.M., Vail, P.R., Sarg, J.F., Loutit, T.S., Hardenbol, J., (1988). An overview of sequence stratigraphy and key definitions. In: Wilgus, C.K., Hastings, B.S., Kendall, C.G.St.C., Posamentier, H.W., Ross, C.A., Van Wagoner, J.C. (Eds.), Sea Level Changes—An Integrated Approach, vol. 42. SEPM Special Publication, pp. 39–45. http://strata.geol.sc.edu/terminology/prog-para-set.html, http://strata.geol.sc.edu/terminology/retro-para-set.html, http://strata.geol.sc.edu/terminology/aggr-para-set.html

C.G. St. C. Kendall, 2004 (modified from Malcolm Rider 1999 & Jerry Baum) USC Sequence Stratigraphy Web, (2005). University of South Carolina, Geology Department, http://strata.geol.sc.edu/log-stacking.html

C.G. St. C. Kendall, 2003 (modified from Malcolm Rider 1999 & Jerry Baum) USC Sequence Stratigraphy Web, (2005). University of South Carolina, Geology Department, http://strata.geol.sc.edu/log-stacking.html